

# POLITECNICO DI TORINO

Corso di Laurea Magistrale

in Ingegneria Meccanica

Tesi di Laurea Magistrale

**Numerical models and experimental measurements for  
parametric dynamic analyses on an RC vehicle in scale 1:5**



Relatori:

Prof. Alessandro Vigliani

Prof. Elvio Bonisoli

PhD. Angelo Domenico Vella

Candidata:

Flora Pesacane

Anno accademico 2019/2020

# Numerical models and experimental measurements for parametric dynamic analyses on a vehicle in scale 1:5

Flora Pesacane

Politecnico di Torino, Department of Mechanical and Aerospace Engineering  
Corso Duca degli Abruzzi, 24 – 10129 Torino, Italy

## Index

Index.....	1
Abstract.....	3
Introduction.....	4
1. Normal-scale vehicle - dynamics overview.....	6
1.1 Basic notions.....	6
1.2 Inertial parameters.....	8
1.3 Suspensions components.....	11
1.4 Tires.....	16
2. Springs.....	18
2.1 Spring numerical model.....	18
2.2 Convergence analysis on the number of elements per spire.....	20
2.3 Linear static analysis on a reference spring.....	22
2.4 Measured stiffnesses.....	23
2.5 Stiffnesses comparison.....	30
2.6 Evaluation of material density.....	31
3. Numerical vehicle model.....	33
3.1 Data and considerations.....	34
3.2 Model description.....	37
3.3 Addition of the Body.....	44
3.4 Addition of the Anti-roll bars.....	46
4. Numerical Real Modal Analysis.....	51
4.1 Basics on Real Modal Analysis.....	51
4.2 Chassis case without Anti-roll bars.....	53
4.3 Body case without Anti-roll bars.....	58
4.4 Chassis case with Front Anti-roll bar.....	60
4.5 Chassis case with Rear Anti-roll bar.....	63
4.6 Chassis case with both Anti-roll bars.....	66
4.7 Body case with Front Anti-roll bar.....	69
4.8 Body case with Rear Anti-roll bar.....	72
4.9 Body case with both Anti-roll bars.....	75
5. Experimental Modal Analysis.....	79
5.1 Setup for the measurement.....	79
5.2 Data acquisition system.....	83
5.3 Measurements and considerations.....	87
5.3.1 Test 1: Point 9.....	87

5.3.2 Test 2: Point 10 ..... 94  
5.3.3 Test 3: Point 10 + new accelerometers setup ..... 100  
5.3.4 Test 4: Point 10 + shaker fixed ..... 104  
Conclusions ..... 110  
Reference ..... 111

## **Abstract**

The purpose of this Thesis report is to collect the activities carried out on a vehicle in scale 1:5. The main aim of this project is to build a numerical model of the scaled vehicle with which is possible to perform several dynamic analyses. In particular, here the focus is on the suspension system, so real Modal Analysis are obtained varying the stiffness of the suspension springs for different configurations. Then, experimental modal analysis is performed on the real vehicle and the results are compared with those obtained numerically in order to validate the numerical model. In Chapter 1 an overview on vehicle dynamics is done, in Chapter 2 the activities to validate the nominal stiffness of the springs are summarized, in Chapter 3 the numerical vehicle model is described, in Chapter 4 several simulations of the model are run, in Chapter 5 the experimental modal tests on the real scaled vehicle are reported.

## Introduction

The object of this thesis activity is a radio-controlled car model in scale 1:5, Losi 5ive-T 2.0. It represents the main tool to conduct several dynamical analyses. The choice to use a scale model is mainly linked to time and cost reasons. In fact, changing the configuration of a normal vehicle would take too long; just think of the disassembly-reassembly of a damper-spring assembly, it would be unwieldy, while on a scale vehicle it would be manageable even by a single person thanks to the low weights. The high cost is related to supply of many spare parts necessary to carry out parametric analyses, in addition to the management and disassembly-reassembly fees.



Figure 1 – Losi 5ive-T 2.0.

In particular, the aim of the thesis work is to build a numerical model of the vehicle then carry out a parametric experimental modal analysis, by varying the stiffness of the suspensions in several configurations, and compare the results with those obtained numerically. For this purpose, preliminary analyses are carried out on the stiffness of the springs, comparing the stiffnesses provided by the catalogue with those calculated theoretically using laboratory-measured geometric data, those measured experimentally and those obtained by computer. Once the stiffness of the springs has been validated, they can be inserted in the model in terms of suspension taking into account the inclination of the suspension and the point of application.



Figure 2 – Suspension.

The 4 available springs are classified according to their stiffness:

- Blue (nominal);
- Gold (soft);
- Red (hard);
- Orange (extra hard).

The stiffness values of the same kind of spring are different between front and rear; Gold type spring is also not available for the rear.

The numerical model created to simulate the dynamic behaviour of the vehicle is called “Losi\_5ive\_7dofs”, it has been built using the tool “LUPOS” in Matlab, and it allows to analyse different cases, for example adding the Body or the Anti-roll bars and choosing different parameters for the Dampers and the Tires. Finally, experimental modal analyses are performed for specific case in order to compare the results with the numerical ones.

# 1. Normal-scale vehicle - dynamics overview

In this chapter, an overview about the dynamics of vehicle is presented, focusing on inertial parameters, suspension components (spring and damper) and tire (unsprung mass). In particular, characteristic values of these essential parts for normal-scale vehicle can be useful to critically compare the ones for the scaled vehicle.

## 1.1 Basic notions

Vehicle Dynamics is a powerful tool to understand the behaviour of a vehicle, and to predict how it will act under some conditions. The most important parts of the system are: vehicle body (sprung mass), the suspension components (spring and damper) and tires (unsprung mass). The models used to study the dynamic of vehicles evolved from the lumped parameter models to the FEM and the multi-body models, from linear to non-linear models.

The lumped parameter modelling method of a vehicle system includes mass, spring and damper elements. In the Figure 1.1.1, some typical vehicle models are shown, like a quarter vehicle model with 2 DOF, half vehicle model with 4 or 5 DOF and full vehicle model with 7 DOF.

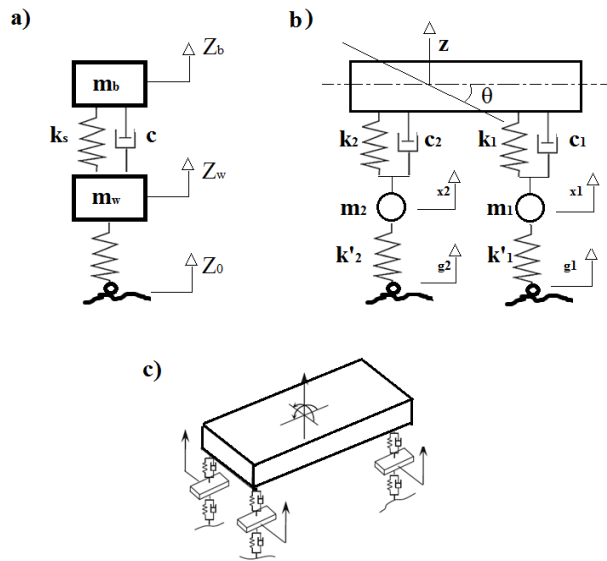


Figure 1.1.1 – Lumped models. **a** 1-D model - **b** 2-D model (4 DOFs), **c** 3-D model (7 DOF) [1].

These lumped models are easier and require less calculation time than finite element models, anyway they can get the vibration characteristics but are less suitable for the complex components (engine, vehicle body, etc), for these reason nowadays they are often combined each other and computerized.[1]

According to the conventions, for the vehicle axis system the  $x$ -axis is a longitudinal axis passing through the center of gravity (CG) and directed forward, the  $y$ -axis goes laterally, and the  $z$ -axis makes the coordinate system a right-hand triad.

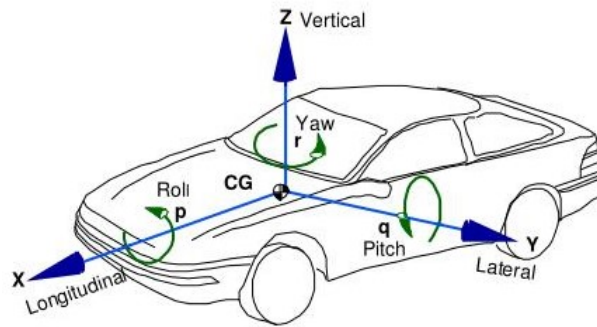


Figure 1.1.2 – Vehicle reference system.

The rotations about the longitudinal (x), lateral (y) and vertical (z) axis are known, respectively as: roll, pitch and yaw motions.

- **Roll:** it is the rotation around the x-axis and it affects the way in which the weight of the vehicle is laterally distributed. This type of motion is caused by the actions of the inertia forces when the car changes direction. This mass displacement in curves can cause instability, for this reason anti-roll bars are introduced, they stiffen the structure, by playing with the stiffness of these bars at the front and rear, understeer or oversteer phenomena can be managed.

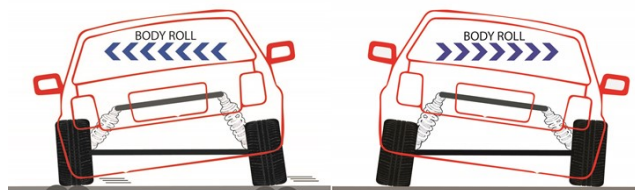


Figure 1.1.3 – Roll rotation of a vehicle.

- **Pitch:** it is the rotation around the y-axis and it affects the way in which the weight is longitudinally distributed. It occurs mainly during acceleration and braking phases. In particular, as a result of a prompt acceleration the front-end of the car tends to rise while the rear-end tends to lower (squat). Contrary, for a prompt braking, the front-end goes down and the rear-end goes up (dive). The pitch depends on various factors, including the stiffness of the suspension (the lower the stiffness, the greater the propensity to pitch), the size of the front and rear overhangs of the car in relation to the overall length of the vehicle (the greater the size, the greater is the possibility of having an accentuated pitch) and the fact that the car is front or rear wheel drive.

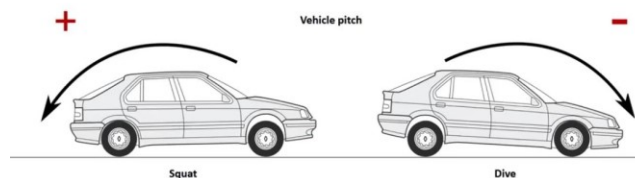
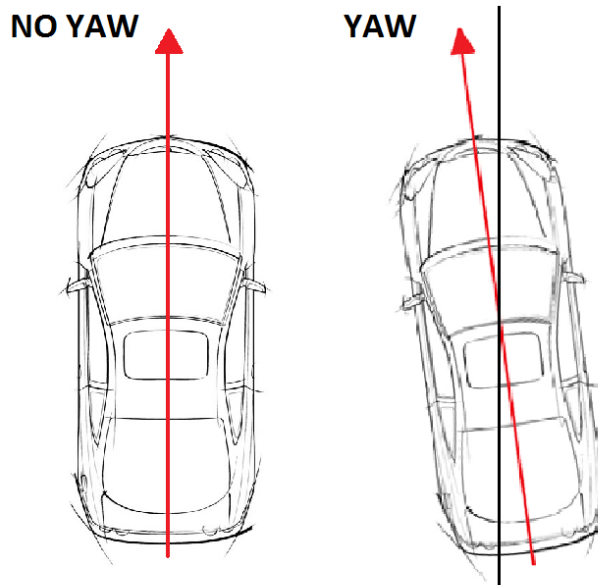


Figure 1.1.4 – Pitch rotation of a vehicle.

- **Yaw:** it is the rotation around z-axis. This motion generally describes the oversteering, i.e. the car turns more abruptly than planned and could get into a spin, this is mainly related to the grip of the tires and the characteristic dimensions of the vehicle: wheelbase and track. As

for the roll, yaw is due to the relocation of weight following an impact. Yaw happens easily on slippery roads with both low-traction rear tires, so that the backside of the vehicle deviates.



• Figure 1.1.5 – Roll rotation of a vehicle.

## 1.2 Inertial parameters

For a reliable dynamic simulation of complex systems such as vehicles, an accurate knowledge of the mass properties (mass, centre of gravity location and inertia tensor) is required. The determination of a vehicle’s weight and lateral and longitudinal coordinates of its center of gravity needs special, but widely available, equipment. Unfortunately, accurate measurement of several important parameters (vehicle center of gravity height, and pitch, roll, and yaw moments of inertia about the vehicle’s center of gravity) requires highly specialized test devices.

A research paper reports a list of mass properties of vehicles, these properties refer mostly to vehicles from the USA market up to the 1998. This research was performed by the National Highway Traffic Safety Administration (NHTSA), that collected the inertial parameters of 32 vehicles into a database. These vehicles covered a wide range of vehicle classes and weights: passenger cars, vans, light trucks, and sport utility cars were tested with vehicle masses ranging from roughly 800 to 2700 kg. In the Table 1.2.1 are reported only the data of some of these vehicles to get an idea about the orders of magnitude, those chosen have been tested without any occupant inside and the fuel tank full. [2]

Table 1.2.1 – Vehicles inertial parameters.

Model	Passenger Car	Pickup Truck	Sport Utility	Van
	Honda Civic 1983	Ford Ranger 1985	Toyota 4Runner 1987	Dodge Caravan 1990
Wheel-base [m]	2.235	2.743	2.624	3.026
Track Width Front [m]	1.377	1.391	1.430	1.524
Track Width Rear [m]	1.379	1.375	1.410	1.575
Roof Height [m]	1.34	1.60	1.80	1.68
Mass [kg]	879	1238	1592	1581

CG Location from Front Axle [m]	0.827	1.186	1.226	1.260
CG Location above Ground [m]	0.519	0.633	0.719	0.642
Moment of Inertia – Pitch [kg m <sup>2</sup> ]	1122	2261	2555	3756
Moment of Inertia – Roll [kg m <sup>2</sup> ]	250	441	361	816
Moment of Inertia – Yaw [kg m <sup>2</sup> ]	1216	2119	3331	3736



Figure 1.2.1 – Honda Civic on the Up Left, Ford Ranger on the Up Right, Toyota 4Runner on the Down Left, Dodge Caravan on the Down Right.

A more recent article presents a database of the mass properties of vehicles carried out on European 24 vehicles from 2000 to 2016. The test rig is basically a multi-bar pendulum carrying the body under investigation and oscillating from well-known initial conditions, by means of proper mathematical procedure the mass properties of the body are accurately measured in a very short testing time. Moreover, empirical formulae for the estimation of the mass properties of vehicle are compared with the experimental data. Although the number of considered vehicles is much smaller than in the database used in previous similar work, it contains a great variety of different vehicles produced in much more recent years and makes an interesting population to verify or to propose interpolating formulae.

The vehicle parameters considered in this analysis are vehicle mass, length, width, roof height, wheel-base, track, power and maximum velocity. These parameters are usually easily available for any vehicle. A correlation analysis among these parameters shows that mass and dimension parameters in the x-y plane are quite correlated, despite roof height is not correlated to any other

parameter. If the correlations among the mass properties is considered, the height of the centre of gravity is not correlated to any of the other parameters. Conversely, the three moments of inertia show quite high correlations between themselves. In particular, a very high correlation exists between  $J_{yy}$  and  $J_{zz}$  (correlation coefficient = 0.98). Referring to the correlation between vehicle parameters and mass properties, the centre of gravity height shows a (weak) correlation only with respect to the roof height of the vehicle (correlation coefficient = 0.75). The moments of inertia show a clear correlation with mass (correlation coefficient = 0.91 ÷ 0.98), length (correlation coefficient = 0.82 ÷ 0.93) and width (correlation coefficient = 0.86 ÷ 0.89). [3]

In the following diagrams are shown some correlation between the mentioned parameters, in terms of experimental data and interpolating formulae.

A proposed formula for the centre of gravity height is expressed by Eq. 1.2.1.

$$h_g = c \cdot h_r \quad (1.2.1)$$

where:

- $h_g$  is the height of the centre of gravity [m];
- $h_r$  is the height of the roof [m];
- $c$  is a constant with values between 0.36 and 0.40;

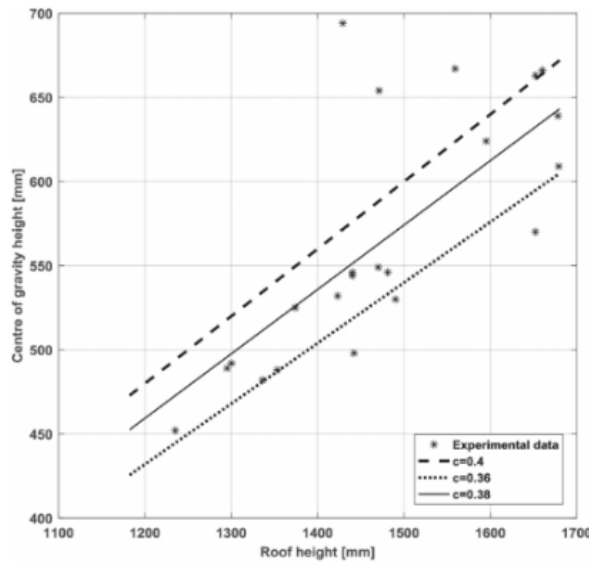


Figure 1.2.2. – Experimental data and interpolating formulae for the height of the centre gravity for different values of the  $c$  constant [3].

Formulae to estimate moments of inertia can take into account only the mass, as shown in Eq.1.2.2 (linear) or in Eq.1.2.3 (no-linear), or also length and width as in Eq.1.2.4, while the roof height does not improve the interpolations.

$$J_{ii} = c_{ii} \cdot m - q_{ii}, \quad i = x, y, z \quad (1.2.2)$$

$$J_{ii} = c_{ii} \cdot m^{q_{ii}}, \quad i = x, y, z \quad (1.2.3)$$

where:

- $J_{ii}$  is the moment of inertia [ $\text{kg m}^2$ ];

- $m$  is the mass of the vehicle [kg];
- $c_{ii}$  and  $q_{ii}$  are coefficients found in the literature, shown in Table 1.2.2;

Table 1.2.2 – Interpolation coefficients for Eq.1.2.2 and Eq.1.2.3.

Case	$c_{xx}$	$q_{xx}$	$c_{yy}$	$q_{yy}$	$c_{zz}$	$q_{zz}$
Linear formula	0.35	34	2.44	-1350	2.58	-1302
No-linear formula	0.45	0.97	0.019	1.59	0.035	1.53

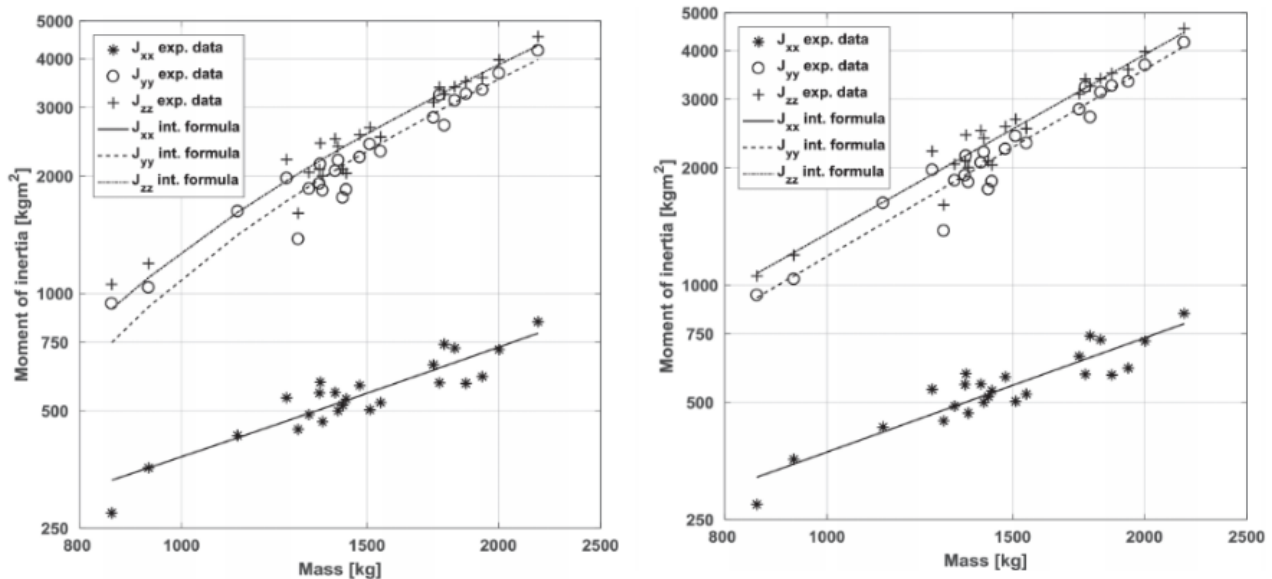


Figure 1.2.3. – Experimental data and interpolating formulae for the moment of inertia as function of mass (Left – linear interpolation, Right – no linear interpolation) [3].

$$J_{ii} = c_{ii} \cdot m^{q_{ii}} \cdot l^{r_{ii}} \cdot w^{s_{ii}}, \quad i = x, y, z \quad (1.2.4)$$

where:

- $J_{ii}$  is the moment of inertia [kg m<sup>2</sup>];
- $m$  is the mass of the vehicle [kg];
- $l$  is the length [m];
- $w$  is the width [m];
- $c_{ii}$ ,  $q_{ii}$ ,  $r_{ii}$ ,  $s_{ii}$  are coefficients shown in Table 1.2.3;

Table 1.2.3 – Interpolation coefficients for Eq.1.2.4.

i	c	q	r	s
x	1.32	0.71	0.25	0.78
y	0.18	1.00	1.54	-0.27
z	0.47	0.85	1.39	0.46

### 1.3 Suspensions components

The suspension system connects the vehicle body (sprung mass) to its wheels (unsprung mass). It is used to observe the vibrations from shock loads due to irregularities of the road surface, it must keep the tires in contact with the road regardless of road surface. The suspension must guarantee good road holding and good comfort, demands that are conflicting with each other, for this reason the suspension becomes a compromise between a soft suspension system capable of absorbing road irregularities and a rigid suspension system that guarantees quick steering responses and high stability. A basic suspension system consists of:

- springs;
- shock absorbers;
- control arms (upper and lower);
- axles;
- ball joints;

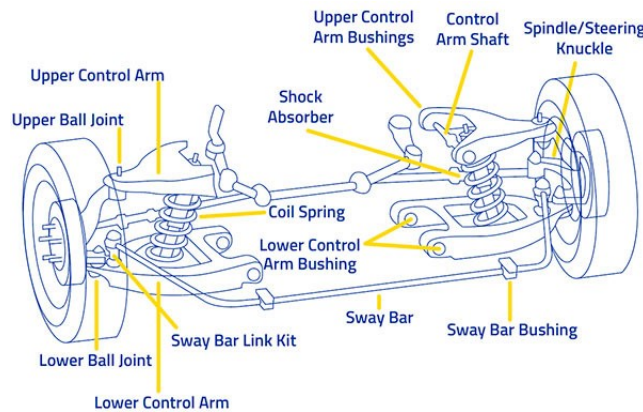


Figure 1.3.1 – Example of a suspension system.

The **spring** is the flexible component of the suspension, it is an elastic object used to store mechanical energy. Different types of elastic elements exist, they must comply with the following requirements: reduced size, low weight, high elastic index, high yield strength, resistance over time. The characteristic of a spring is represented by Eq.1.3.1.

$$k = \frac{F}{x} \quad (1.3.1)$$

Where:

- x is the displacement [mm];
- F is the load [N];
- k is the stiffness [N/mm];

The stiffness depends only on the geometric conditions of the spring and on the elasticity coefficient of the material. Typically, in automotive field, the spring characteristic is not linear, the constant k in fact increases as the spring compression increases, so as to obtain increasing rigidity to have a greater braking capacity of the elastic element as it increases compression in order to withstand high loads, preserving the structure from violent impacts.

Nowadays, four different classes of springs exist:

- **Helical spring:** The most common spring type; consisting of coils that wind around an axis. This absorbs the motion of the vehicle compressing and expanding. The loading capacity of the spring depends on the diameter of the wire, the overall diameter of the spring, its shape,

and the spacing of the coils. This kind of springs are an excellent choice on rutted and rocky off-road trails, while they are not good if you are carrying heavy loads;

- **Leaf spring:** made of *leaves* (metal foils) joined together. Originally designed for coaches, then used on American cars, and now on most trucks and heavy-duty vehicles;



Figure 1.3.2 – Example of a leaf spring.

- **Torsion bar:** it is a bar that takes advantage from the twist, an end is attached to the chassis, while the other end to the suspension arm. In this way, the movement due to road surface irregularities is transferred to the torsion bar, that twists and reacts with a force;

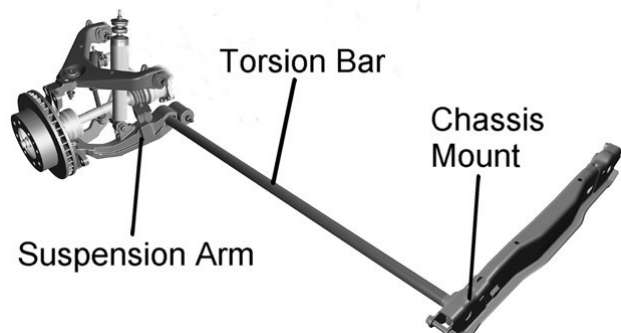


Figure 1.3.2 – Example of a torsion bar spring.

- **Air spring:** it uses the compression of the air to absorb the vibrations, their shape is shown in the following picture.



Figure 1.3.3 – Example of some air springs.

To get an idea about the dimensions of coil springs, some normal models from the brand *Monroe* are reported in the Table 1.3.1.[4]

Table 1.3.1 – Datasheet for some Monroe cylindrical coil spring.

Vehicle	Spring Code	Length [mm]	Weight [kg]	Outer diameter [mm]	Wire diameter [mm]	Number of spires [-]
BMW	SP0069	372	2.70	141.5	11.9	7
Audi	SP0857	476	4.70	180.0	14.2	-
Alfa Romeo	SP0177	335	2.60	174.8	13.3	4.90

Springs are excellent to absorb vibrations, but not at dissipating energy, so it is necessary to couple them with **dampers** (shock absorber), so that the ride is velvety. Dampers act converting the kinetic energy into heat energy, that is then dissipated by a fluid.

The damping force is represented by Eq.1.3.2.

$$F_d = -c \dot{x} \quad (1.3.2)$$

Where:

- $c$  is the damping factor [Ns/m];
- $F_d$  is the damping force [N];
- $\dot{x}$  is the velocity of the piston [m/s];

Evaluation of accurate damping factor is very complex task as damper shows nonlinear behaviour while it operates, the damper has the typical features of non-linearity, non-symmetry and hysteresis. [6]

To understand how this works, we can see the internal structure, Figure 1.3.4.

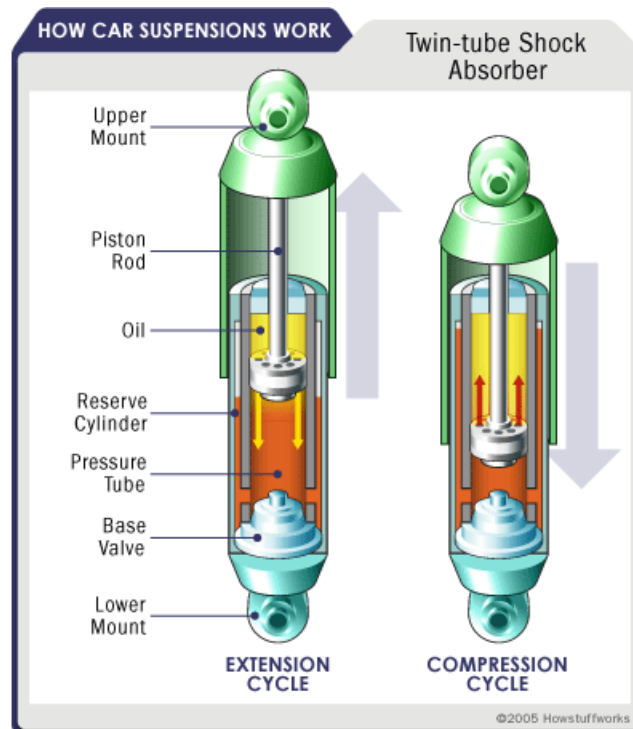


Figure 1.3.4 – Example of a damper [5].

Its working is reported below and is taken from the source linked into the biography. [5]

“A shock absorber is basically an oil pump placed between the frame of the car and the wheels. The upper mount of the shock connects to the frame (i.e., the sprung weight), while the lower mount connects to the axle, near the wheel (i.e., the unsprung weight). In a twin-tube design, one of the most common types of shock absorbers, the upper mount is connected to a piston rod, which in turn is connected to a piston, which in turn sits in a tube filled with hydraulic fluid. The inner tube is known as the pressure tube, and the outer tube is known as the reserve tube. The reserve tube stores excess hydraulic fluid. When the car wheel encounters a bump in the road and causes the spring to coil and uncoil, the energy of the spring is transferred to the shock absorber through the upper mount, down through the piston rod and into the piston. Orifices perforate the piston and allow fluid to leak through as the piston moves up and down in the pressure tube. Because the orifices are relatively tiny, only a small amount of fluid, under great pressure, passes through. This slows down the piston, which in turn slows down the spring.

Shock absorbers work in two cycles: the **compression cycle** and the **extension cycle**. The compression cycle occurs as the piston moves downward, compressing the hydraulic fluid in the chamber below the piston. The extension cycle occurs as the piston moves toward the top of the pressure tube, compressing the fluid in the chamber above the piston. A typical car or light truck will have more resistance during its extension cycle than its compression cycle. With that in mind, the compression cycle controls the motion of the vehicle's unsprung weight, while extension controls the heavier, sprung weight.

All modern shock absorbers are velocity sensitive, the faster the suspension moves, the more resistance the shock absorber provides. This enables shocks to adjust to road conditions and to control all of the unwanted motions that can occur in a moving vehicle, including bounce, sway, brake dive and acceleration squat.

Another common dampening structure is the **strut**, basically a shock absorber mounted inside a coil spring. Struts perform two jobs: They provide a dampening function like shock absorbers, and they provide structural support for the vehicle suspension. That means struts deliver a bit more than

shock absorbers, which don't support vehicle weight, they only control the speed at which weight is transferred in a car, not the weight itself.

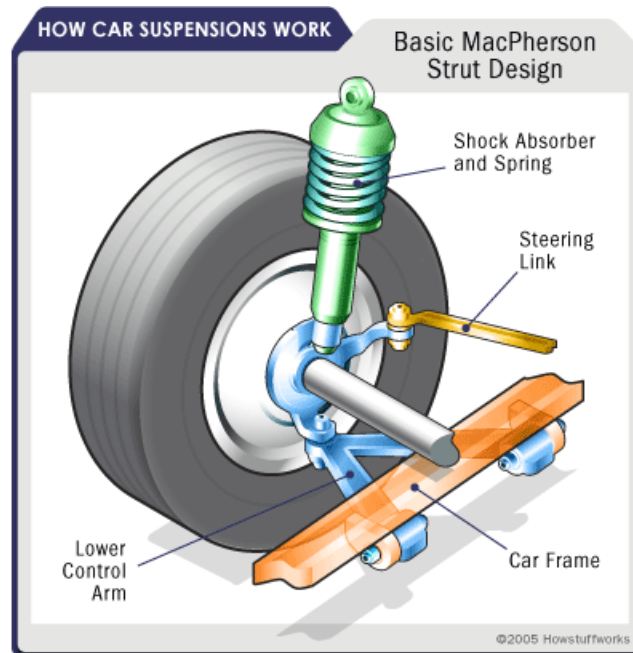


Figure 1.3.5 – Common Strut design [5].

**Anti-sway** bars (also known as anti-roll bars) are used along with shock absorbers or struts to give a moving automobile additional stability. An anti-sway bar is a metal rod that spans the entire axle and effectively joins each side of the suspension together. When the suspension at one wheel moves up and down, the anti-sway bar transfers movement to the other wheel. This creates a more level ride and reduces vehicle sway. In particular, it combats the roll of a car on its suspension as it corners. For this reason, almost all cars today are fitted with anti-sway bars as standard equipment.”

## 1.4 Tires

Tires play a great role in the vehicle performance, in fact they support and link it to the road, they transmit all the forces and attenuates the impact from the irregular road. Tires are very complex, in fact their characteristics are influenced by several factors like material, tread pattern, carcass stiffness, air pressure, and more. The most important factors in tire dynamics are tire forces and torques, slip and turn spin, these quantities allow to describe the characteristics of a tire in all driving situations. Several modelling approaches have been developed to describe the physics of tires so that they can be analysed and evaluates mathematically, according to the article mentioned in the biography [1] “the tire mechanical model can be divided into three categories:

- **pure physical models:** they are theoretical models that see, for example, the tire as a beam, but some aspects are complex to be described analytically, therefore the pure physical model can only serve as the basis for the semi-empirical model;
- **empirical model:** from experimental data of tire an empirical model can be directly built;
- **semi-empirical model:** it based on the tire physical prototype and the experimental data, based on the “Magic Formula” of Pacekja, it is implemented in the commercial software (ADAMS, SIMPACK and MATLAB/Simulink).”

Several studies which try to determine the characteristics of tires exist, the results of an experiment based on semi-empirical models on tractor tires are summarized below:

- The stiffness ( $k$ ) and damping coefficient ( $c$ ) depend on the tire size, inflation pressure ( $p_i$ ) and the load;
- $k$  increase with  $p_i$  while  $c$  decrease;
- $c$  increase with the load, while on  $k$  the load does not have big influence.[7]

The experiment results of this study are reported in the Figure 1.4.1, referring to the test conditions indicated in Table 1.4.1, so that it is possible to get the order of magnitude of these tires parameters.

Table 1.4.1 – Parameters for damping and vertical stiffness tests for the tires.

Tire Code	Code	Tire load [kg]	Tire inflation pressure [kPa]				
			120	150	180	210	240
5.00-16 R1	T1	240	120	150	180	210	240
7.50-20 R1	T2	364	60	90	120	150	180
6.00-12 R1	T3	246	60	90	120	150	180
5.00-16 R1	T4	200	120	150	180	210	240
7.50-20 R1	T5	264	60	90	120	150	180

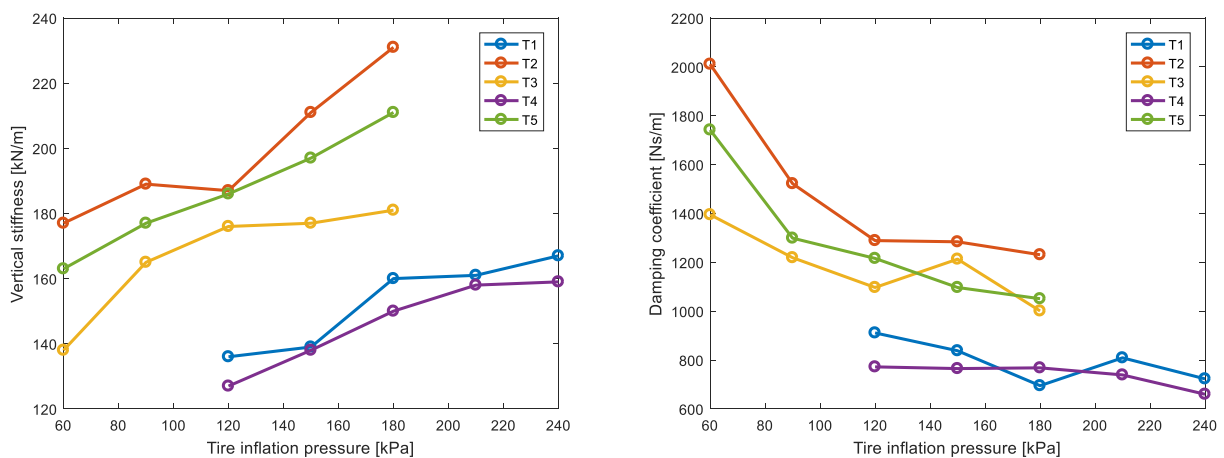


Figure 1.4.1 – Stiffness and damping of tires [7].

## 2. Springs

In this chapter, the activities performed for the springs of the shock-absorbers are described. Since the thesis work is focused on dynamic analysis of the vehicle Losi 5ive-T 2.0 by varying the suspension system setup, it is essential to validate the stiffness values of the springs provided on the technical sheets in order to obtain good modal analysis results. For this purpose, a comparison between the nominal stiffness, the theoretical stiffness, the numerical stiffness, and the measured stiffness is made.

In the following subparagraphs the numerical model of the spring, the experimental procedure to get the stiffness, the stiffness comparison and material density evaluation are reported.

### 2.1 Spring numerical model

In this paragraph, the numerical model which simulate the static behaviour of a spring is described. This model is generated in the Matlab environment using the FEM LUPOS code.

Running the model “Springs.m”, it is possible to choose the front and rear spring by a menu, and then the type of the spring (Blue, Gold, Red, Orange), therefore the values of the geometric properties of the chosen spring are loaded thanks to a text file (diameter, height, number of active spires) and the value of the nominal stiffness taken from the catalogue is loaded too.

The properties of the material, which is a simple spring steel, are added. The spring is built thanks to the Spring.m function [9], it is given like input the coordinates of the two central nodes at the ends, the geometric properties, the direction of the helix (clockwise), the number of nodes per spire (an appropriate analysis will be carried out in the following paragraphs), the identification number of the first node, and the properties of the material.

$$\text{Spring}(\text{Geo}, \text{Rod}, \text{RJs}, \text{dw}, \text{D}, \text{h}, \text{s}, \text{slim}, \text{cw}, \text{nodes\_s}, \text{NodeId1}, \text{NodeId2}, \text{Nodes}, \text{ro}, \text{E}, \text{v}) \quad (2.1.1)$$

Table 2.1.1 –Input and output to the function Spring.

	Symbol	Description	Syntax
Input	Geo	Contains at least the coordinates of the two nodes	[NodeId x y z] (G x 4)
	Rod	Optional initial rod list	[NodeId1 NodeId2 col alpha Dy Dz t ro E v] (R x 10)
	RJs	Optional initial rigid joints list	[NodeId1 NodeId2] (J x 2)
	<i>dw</i>	Wire diameter [m]	-
	<i>D</i>	Helix diameter [m]	-
	<i>h</i>	Helix height [m]	-
	<i>s</i>	Helix active spires [-]	-
	<i>slim</i>	Helix inactive spires [-]	[3/4 or 0]
	<i>nodes_s</i>	Nodes per spire [-]	-
	<i>cw</i>	Helix direction	Clockwise (1) or counter clockwise (2), default 1
	NodeId1	Initial central node	[NodeId1]
	NodeId2	Final central node	[NodeId2]
	Nodes	Starting spring helix node	[NodeId1]

	$\rho$	Material density [kg/m <sup>3</sup> ]	-
	$E$	Material Young modulus [Pa]	-
	$\nu$	Material Poisson ratio [-]	-
Output	Model.Geo	Contains the updated sorted nodes	[NodeId x y z]
	Model.Rod	Contains the updated sorted beams or rods	[NodeId1 NodeId2 col alpha Dy Dz t ro E v]
	Model.RJs	Contains the updated sorted rigid joints	[NodeId1 NodeId2]

Constraints are therefore defined, the translation along the z axis and the rotation around z of the lower end are free, in this way the spring can deform while all degrees of freedom of the upper master node are constrained. The modulus, direction and point of application of the force are defined.

The nominal values of the geometric data of the spring sets measured in the laboratory are reported in Table 2.1.2 and in Table 2.1.3.

Table 2.1.2 – Measured geometric data of the Front springs.

Properties	Code	LOSB2965	LOSB2964	LOSB2966	LOSB2967
	Colour	Blue	Gold	Red	Orange
Wire diameter [m]	$\varnothing_w$	0.0028	0.0027	0.0029	0.003
Inner helix diameter [m]	$\varnothing_{in}$	0.0326	0.0326	0.0326	0.0326
Helix diameter [m]	$\varnothing$	0.0354	0.0353	0.0355	0.0356
Helix height [m]	$h$	0.115	0.1106	0.1119	0.1137
Number of active spires [-]	$s$	6.8	6.75	7	7.25
Number of inactive spires [-]	$ns$	2	2	2	2

Table 2.1.3 – Measured geometric data of the Rear springs.

Properties	Code	LOSB2972	LOSB2971	LOSB2973
	Colour	Blue	Red	Orange
Wire diameter [m]	$\varnothing_w$	0.0026	0.0027	0.0028
Inner helix diameter [m]	$\varnothing_{in}$	0.0326	0.0326	0.0326
Helix diameter [m]	$\varnothing$	0.0352	0.03535	0.0354
Helix height [m]	$h$	0.131	0.1303	0.1325
Number of active spires [-]	$s$	7.5	7.5	7.5
Number of inactive spires [-]	$ns$	2	2	2

Table 2.1.4 – Assumed material properties of the springs.

Property	Symbol	Value
Young modulus [GPa]	$E$	210
Poisson ratio [-]	$\nu$	0.3
Density [kg/m <sup>3</sup> ]	$\rho$	7700

## 2.2 Convergence analysis on the number of elements per spire

This paragraph reports the analysis carried out on the spring model in order to choose the optimal number of elements per spire. “Optimal number of elements” means the number of elements that allows to reach a stiffness value close enough to the one provided in the catalogue with the quickest calculation time. For the choice of the optimal number of elements, refer to the Lupos manual [10]. The analysis is conducted on a reference spring, the "Front Gold (soft)", to which a force of modulus 20 N is applied along the z direction. The properties of this spring are listed in Table 2.1.2 and Table 2.1.4.

Theoretical stiffness is calculated by Eq. 2.2.1.

$$k = \frac{f}{\Delta x} = \frac{1}{8} \frac{G}{s} \frac{\varnothing_w^4}{\varnothing^3} \quad (2.2.1)$$

where:

- $k$  is the stiffness [N/m];
- $f$  is the force along the spring axis [N];
- $\Delta x$  is the displacement [m];
- $G$  is the tangential modulus [Pa];
- $s$  is the number of active spires [-];
- $\varnothing_w$  is the wire diameter [m];
- $\varnothing$  is the helix diameter [m];

As said in the above paragraph, the Spring model is built using the Spring function of LUPOS. Theoretically, we should use an high number of nodes to better approximate the average helix diameter with segments, but the Spring function allows to obtain good results also for a low number of nodes per spire because it optimizes the layout of the nodes with respect to the helix diameter. Basically, when there are few nodes, the octagon edges will be external to the helix circumference of the spring, so to keep the circle circumscribed and inscribed to the octagon, arranged symmetrically to the diameter of the helix required, as shown in Figure 2.2.1.

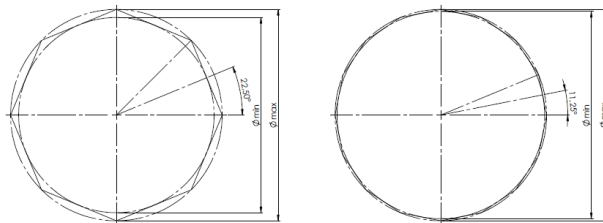


Figure 2.2.1 –Spring function-layout optimization of nodes.

Thanks to the model created for this analysis, the trend of the spring stiffness is obtained as a function of the number of nodes per spire shown in Figure 2.2.2.

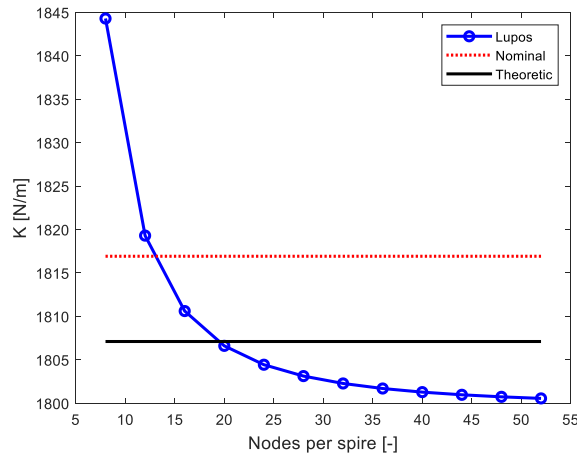


Figure 2.2.2 – Front Gold spring convergence diagram.

The values detected punctually are reported in Table 2.2.1. The percentage error between the nominal catalogue stiffness and the stiffness computed by Lupos is calculated by Eq. 2.2.2.

$$\varepsilon = 100 \frac{k_{Lupos} - k_{nom}}{k_{nom}} \quad (2.2.2)$$

Table 2.2.1 – Spring stiffness “Front Gold (soft)”-convergence analysis. (nominal value of 1816.92 N/m).

Nodes per spire	Lupos stiffness [N/m]	$\varepsilon$ (%)
8	1844.29	1.51
12	1819.30	0.13
16	1810.61	-0.35
20	1806.60	-0.57
24	1804.43	-0.69
28	1803.12	-0.76
32	1802.27	-0.81
36	1801.69	-0.84
40	1801.28	-0.86
44	1800.97	-0.88
48	1800.73	-0.89
52	1800.55	-0.90

As we can notice, the Lupos stiffness curve is not limited to the theoretic computed value. There is a difference between the theoretic value and the asymptote of the curve because the spring model takes into account the boundary conditions, such as the constraint on the end nodes, while the theoretic computed value doesn't.

Based on the data obtained, it follows that a number of optimal nodes, which can be set as default to the model for further analyses, can be 16, with which the error respect to the nominal value provided in the technical spreadsheet is only 0.35% .

## 2.3 Linear static analysis on a reference spring

In this paragraph we want to show how to perform a linear static analysis by using the Lupos code. The first step to perform the analysis is calling up the control panel in the Command Window in Matlab by typing "LUPOS\_Gui", the window shown in Figure 2.3.1 opens.

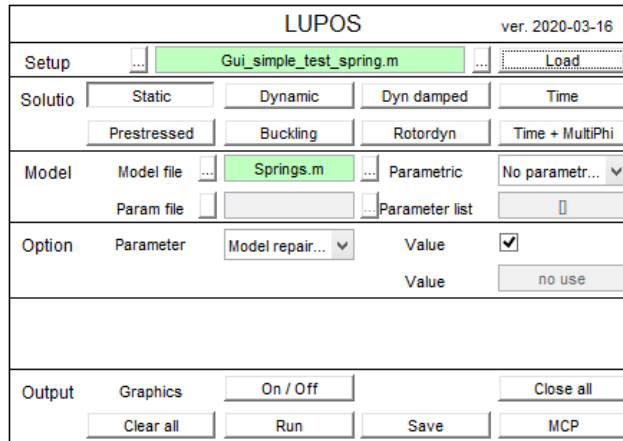


Figure 2.3.1 – Control Panel LUPOS.

In Setup we can upload a file *Gui* containing all the setting options and the location of the model, so as to make the analysis faster. The Setup file has been created for this simple linear static analysis, and another file for the convergence analysis described in the previous paragraph. The type of analysis is selected in Solution (including: Static, Real Modal-Dynamics, Complex Modal-Dynamics). In Model the model to be executed is loaded, and if necessary, the vector/file for a parametric analysis. In Option it is possible to choose a series of useful options for analysis. You can choose to show the output graphs or not, in the latter case the simulation will be faster. Finally, the simulation is performed thanks to the Run command.

The reference spring for this analysis is the "Front Gold (soft)", the force to which it is subject has a modulus of 20 N and the number of nodes per spire is equal to 16.

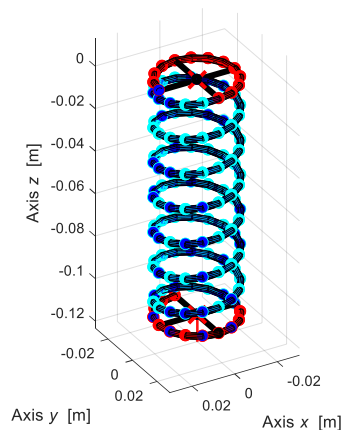


Figure 2.3.2 – Deformed shape amp factor 1 on Front Gold (soft) spring.

After that, the *postprocessing.m* file can be run to obtain the value of the displacement through the LUPOS function *Simul.Xstat(1,1)* and so to compute the numerical stiffness.

## 2.4 Measured stiffnesses

In this paragraph, the experimental procedure to get the stiffness is described. This activity has been conducted in the laboratory “*Meccanica del veicolo*” at the DIMEAS. The aim is to obtain the stiffness values of 7 springs, 4 front and 3 rear, these are shown in the Figure 2.4.1.

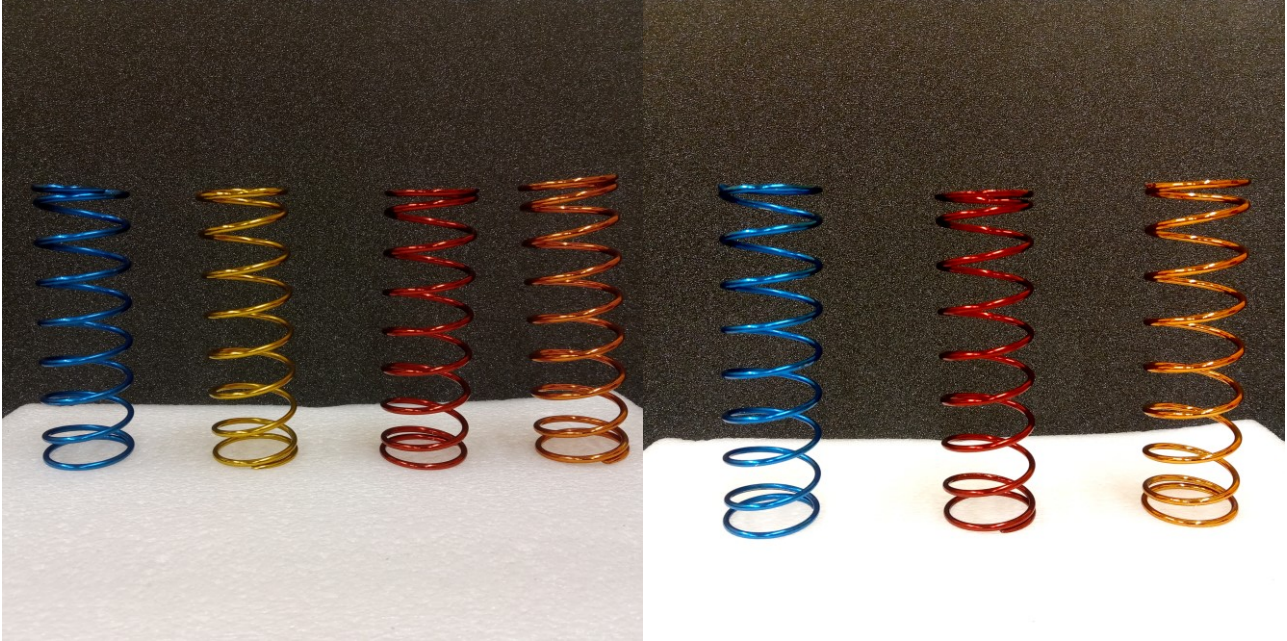


Figure 2.4.1 – Front springs (left) and Rear springs (right).

The main idea is to put under tension the spring by some known weights and then measure the elongation, and so get a data cloud. The traction has been preferred to the compression to avoid the buckling effect, this exchange is possible thanks to a linear elastic behaviour. The ideal scheme which we want to replicate is shown in Figure 2.4.2.

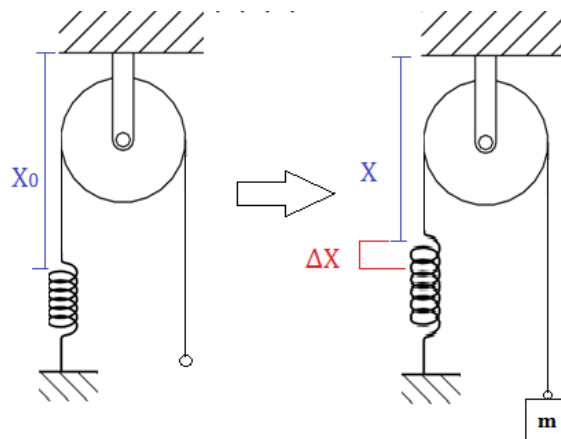


Figure 2.4.2 – Scheme of measurement.

The first operation is to understand what is the step of the weight useful to appreciate the elongation through a simple meter, for this purpose an easy calculation is done considering the lowest available weight ( $m = 0.5$  kg) and the highest nominal stiffness ( $k$  Front Orange) by Eq.2.4.1.

$$f = \frac{mg}{k} \quad (2.4.1)$$

The result of Eq.2.4.1 is around 2 mm, this is a readable value on a meter, so it is possible to use the 0.5 kg weight as step.

The available weights are shown in the Figure 2.4.3, they are linked to the setup system by a chain and a carabiner, although the value of the weights is written above, it is a good practise to weigh them using a precision balance, the values are reported in Table 2.4.1.



Figure 2.4.3 – Weights and chain-carabiner.

Table 2.4.1 – Weights values.

Weight	Nominal [kg]	Measured [kg]
A	0.5	0.4765
B	1	1.0136
C	2	1.9950
D	2	1.9771
Chain+Carabiner	-	0.0603

At this point, it is possible to build the setup. The spring must be well fixed and in a vertical position, to reach this goal the inactive low spire is blocked by coupling an endless screw, 2 locknuts and 2 washers to a perforated rigid bar which is in turn blocked thanks to a clamp, as shown in Figure 2.4.4. Locking inactive coils is right as they play no role in elongation.



Figure 2.4.4 – Setup – clamp and low-end spring detail.

The spring must not lean during the test, to prevent it, the pulling force must be orthogonal to both support base and upper base and it must be applied in the centre of the spire. Also for the upper inactive spire we can use the coupling endless screw with 2 locknuts and 2 washers, the endless screw goes through the centre and it has been positioned as much coaxial as possible with respect to the lower endless screw. Next, a rope (not elastic) is knotted to the endless screw and blocked by nut and locknut, the rope runs on the pulley, Figure 2.4.5

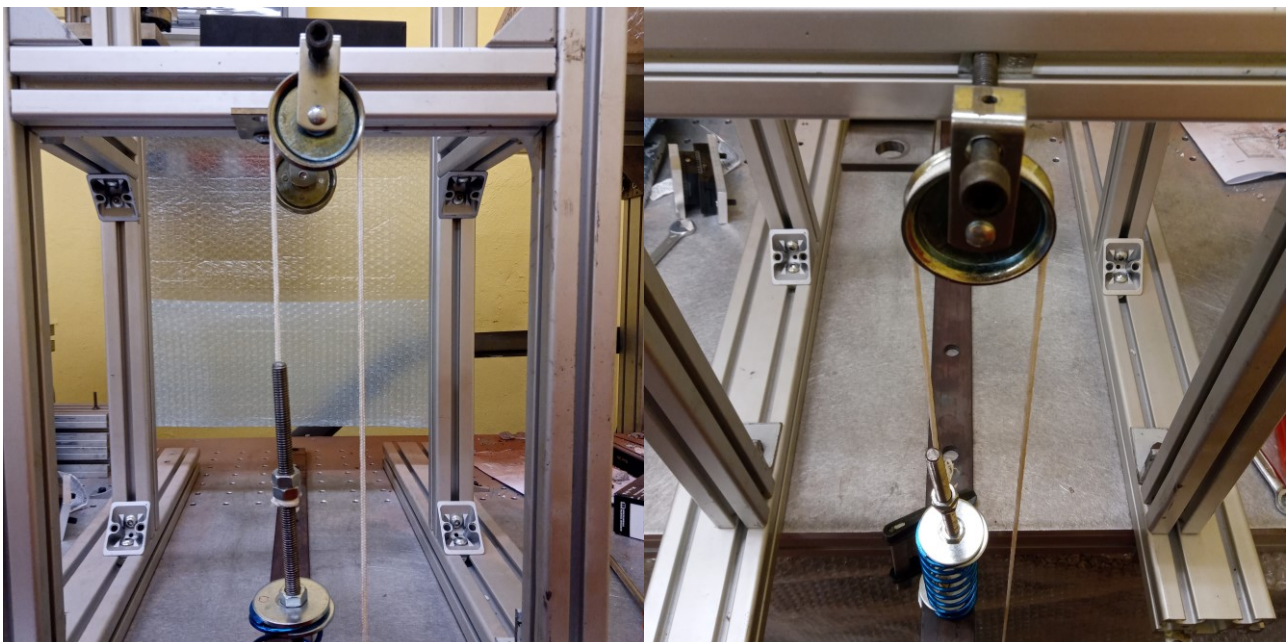


Figure 2.4.5 – Setup – upper-end spring and pulley detail.

As written before, the spring must not lean, so we can control that is in the right position using a level (horizontal bubble) as shown in Figure 2.4.6.

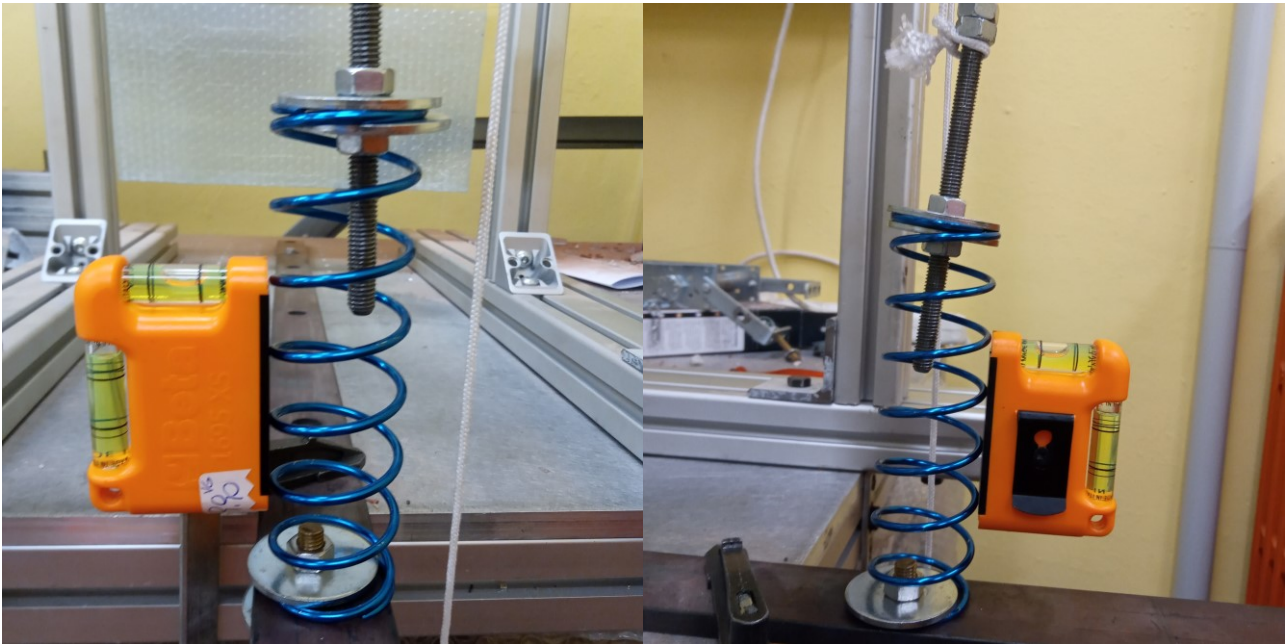


Figure 2.4.6 – Setup – level, control the vertical position of the spring.

The assemblage procedure described till now takes around 6 minutes.

Then a hook knot is made on the end of the rope and here it is possible to attach the weight by a carabiner and a chain. The complete setup is shown in Figure 2.4.7.

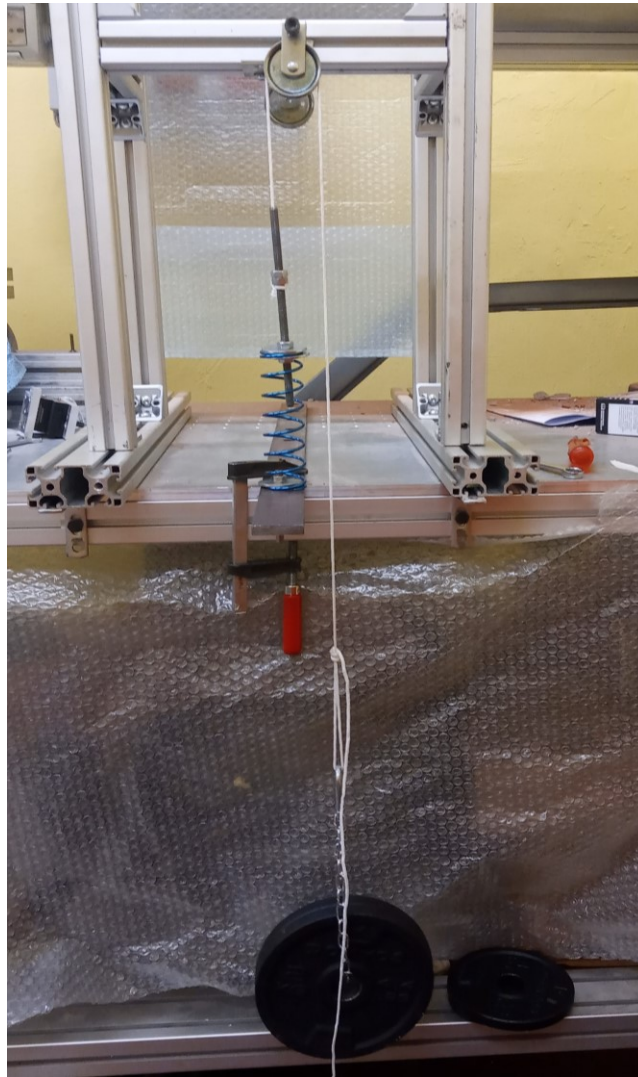


Figure 2.4.7 – Setup.

The measures of the distances  $X_0$  and  $X$  (Figure 2.4.1) are taken by a meter from a fixed point to the upper washer, paying attention to bring it down vertically, as shown in Figure 2.4.8.



Figure 2.4.8 – Measuring the distances.

At this point, the setup is configured. Now, for each spring, we measure the offset  $X_0$  without any weights and then the displacement  $X$  changing the weights from 0.5 kg to 4 kg by a step of 0.5 kg. The data are collected in the Table 2.4.2 and Table 2.4.3. The measuring procedure takes around 20 minutes for each spring, while the disassembling of the setup for changing spring takes around 2 minutes.

Table 2.4.2 – Displacement values- Front springs.

Measure	Weights	Front springs			
		Blue	Gold	Red	Orange
$X_0$ [m] (offset)	No weights	0.268	0.268	0.269	0.265
X [m] (at 0.5 kg)	A+chain+carabiner	0.267	0.265	0.266	0.264
X [m] (at 1.0 kg)	B+chain+carabiner	0.265	0.263	0.263	0.261
X [m] (at 1.5 kg)	A+B+chain+carabiner	0.263	0.259	0.261	0.26
X [m] (at 2.0 kg)	C+chain+carabiner	0.259	0.258	0.259	0.257
X [m] (at 2.5 kg)	A+C+chain+carabiner	0.256	0.257	0.258	0.256
X [m] (at 3.0 kg)	B+C+chain+carabiner	0.253	0.252	0.256	0.253
X [m] (at 3.5 kg)	A+B+C+chain+carabiner	0.250	0.25	0.254	0.25
X [m] (at 4.0 kg)	C+D+chain+carabiner	0.249	0.246	0.252	0.248

Table 2.4.3 – Displacement values- Rear springs.

Measure	Weights	Rear springs		
		Blue	Red	Orange
$X_0$ [m] (offset)	No weights	0.251	0.253	0.251
X [m] (at 0.5 kg)	A+chain+carabiner	0.247	0.25	0.247
X [m] (at 1.0 kg)	B+chain+carabiner	0.243	0.246	0.243
X [m] (at 1.5 kg)	A+B+chain+carabiner	0.239	0.243	0.242

X [m] (at 2.0 kg)	C+chain+carabiner	0.236	0.24	0.24
X [m] (at 2.5 kg)	A+C+chain+carabiner	0.232	0.238	0.237
X [m] (at 3.0 kg)	B+C+chain+carabiner	0.23	0.236	0.235
X [m] (at 3.5 kg)	A+B+C+chain+carabiner	0.226	0.233	0.233
X [m] (at 4.0 kg)	C+D+chain+carabiner	0.225	0.229	0.231

Then the data are elaborated in a Matlab script, the force is computed as shown in Eq.2.4.2 while the elongation as shown in Eq.2.4.3. Then, using the *polyfit* function it is possible to fit a polynomial to data, giving in input the elongation  $\Delta X$  and the force  $F$  vectors, in this case the chosen polynomial degree is 1, in this way we can obtain the regression line which represents the characteristic of the spring and so get its coefficient that represents the stiffness.

$$F = (m_w + m_c)g \quad (2.4.2)$$

Where:

- $F$  is the force applied on the spring [N];
- $m_w$  is the mass of the current weight [kg];
- $m_c$  is the mass of the chain and the carabiner [kg];
- $g$  is the gravity acceleration [ $m/s^2$ ].

$$\Delta X = X_0 - X \quad (2.4.3)$$

Where:

- $\Delta X$  is the elongation [m];
- $X_0$  is the offset [m];
- $X$  is the distance measured with the weights [m];

The plot of the data points and the relative regression line is shown in Figure 2.4.9

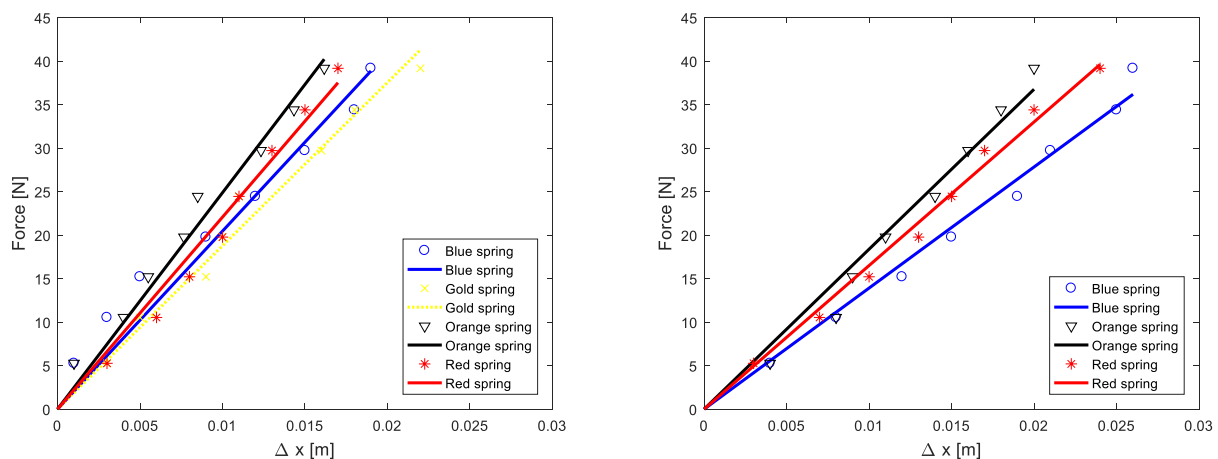


Figure 2.4.9 – Springs characteristics – Front (left) and Rear (right).

As we can notice from the springs characteristics, the front orange spring is the stiffest of all the front springs in fact the slope is the highest, then in descending order: the red, the blue and the gold, the same consideration is for the rear springs. The coefficients of the fitting lines are the stiffnesses, they are reported in the Table 2.4.4, together with the coefficient of determination  $R^2$  computed by Matlab function *fitlm(x,y)* according to the Eq.2.4.4.

$$R^2 = 1 - \frac{n-1}{n-p} \frac{SSE}{SST} \quad (2.4.4)$$

Where:

- SSE is the sum of squared error;
- SST is the sum of the squared total;
- n is the number of observations;
- p is the number of regression coefficients.

In regression, the  $R^2$  coefficient of determination is a statistical measure of how well the regression predictions approximate the real data points.

Table 2.4.4 –Experimental results.

Springs		Stiffness [N/m]	$R^2$
Front	Blue	2045.31	0.986
	Gold	1877.13	0.973
	Orange	2487.40	0.989
	Red	2206.50	0.991
Rear	Blue	1391.39	0.984
	Orange	1837.88	0.989
	Red	1650.07	0.989

The  $R^2$  coefficient is very close to 1 for every spring, this means that the regression fits well the data, and the measurement is reliable.

## 2.5 Stiffnesses comparison

We must compare the different values obtained by distinct ways to validate the nominal values. These values are reported in Table 2.5.1, the Theoretic stiffness is calculated as shown in Eq. 2.2.1 while the percentage errors are computed likewise the Eq. 2.2.2.

Table 2.5.1 – Stiffnesses comparison.

Springs		Stiffness [N/m]				$\varepsilon$ (%)		
		Nominal	Theoretic	Lupos	Measured	Theoretic vs Nominal	Lupos vs Nominal	Measured vs Nominal
Front	Blue	2046.24	2057.16	2060.32	2045.31	+0.53	+0.69	-0.05
	Gold	1816.92	1807.10	1810.61	1877.13	-0.54	-0.35	+3.31
	Red	2275.56	2280.16	2287.23	2206.50	+0.20	+0.51	-3.03
	Orange	2504.88	2500.07	2501.60	2487.40	-0.19	-0.13	-0.69
Rear	Blue	1411.2	1410.46	1408.28	1391.39	-0.053	-0.21	-1.40
	Red	1640.52	1626.39	1623.70	1650.07	-0.86	-1.03	0.58
	Orange	1887.48	1865.16	1861.30	1837.88	-1.18	-1.39	-2.63

As it possible to notice from the previous Table, the percentage errors are quite low, in fact the maximum error stands at +3.31%. Anyway, some considerations must be done; it can be observed, for example, that for the rear orange spring the stiffness values obtained theoretically, numerically and experimentally are all lower (by at least 1.18%) than the nominal one, this could cause results in the numerical modal analysis discordant with those of the experimental modal analysis, as in the numerical model of the vehicle the nominal stiffness value is used while in the experimental analysis the real spring will be added, the same consideration can also be extended to other springs. Another observation is that the relative errors of a certain spring have the same sign for both Theoretic and LUPOS stiffness and their values are really close to each other, while the measured one has mostly opposite sign and slightly different value, this can be justified by saying that the theoretical and numerical results both derive from formulas, while with the experimental results it is necessary to take into account the chain of errors, such as inaccurate measuring instruments, human errors, non-ideal support elements, springs that are not perfectly in a vertical position.

## 2.6 Evaluation of material density

In the following paragraph we want to estimate the material density of the spring. As said at the beginning of the chapter, the material is a simple spring steel, but there is not any information about it on the spring technical spreadsheet, so till now we have assumed plausible properties value. In order to get a right density value, the theoretical mass and the numerical mass have to be equal to the measured one.

The springs' masses are measured in the laboratory by a weighing machine; the theoretic masses are calculated thanks to the Eq.2.6.1 and the numerical masses are computed in Lupos thanks to the "CheckVolMass.m" function, as shown in Table 2.6.1.

$$m = \rho \frac{\pi}{4} \varnothing_w^2 \left[ (ns \varnothing \pi) + \left( s \sqrt{p^2 + (\varnothing \pi)^2} \right) \right] \quad (2.6.1)$$

where the data are taken from Table 2.1.2 and Table 2.1.3, while the step  $p$  is given by the Eq.2.3.2.

$$p = \frac{h}{s} \quad (2.6.2)$$

- $m$  is the mass of the spring [kg];
- $\rho$  is the material density [kg/m<sup>3</sup>];
- $s$  is the number of active spires [-];
- $ns$  is the number of inactive spires [-];
- $\varnothing_w$  is the wire diameter [m];
- $\varnothing$  is the helix diameter [m];
- $p$  is the step [m];
- $h$  is the helix height [m];

Table 2.6.1 –Input and output to the function CheckVolMass.m.

Symbol		Description	Syntax
Input	Geo	Matrix of geometric position of nodes	[NodeId x y z] (G x 4)
	Lks	Matrix of beam links	[NodeId1 NodeId2 colour alpha b h t ro E v] (L x 10)

	Rod	Matrix of beam link	[NodeId1 NodeId2 colour alpha Dy Dz t ro E v] (R x 10)
Output	Vol	Total volume of links and rods used in the structure	-
	Mass [kg]	Total mass of the structure	-

Table 2.6.2 – Masses comparison, density 7700 kg/m<sup>3</sup>.

Springs		Mass [kg]			ε (%)	
		Theoretic	Lupos	Measured	Theoretic vs Measured	Lupos vs Measured
Front	Blue	0.046814	0.03638	0.0465	+0.67	-21.757
	Gold	0.043138	0.03347	0.04315	-0.027	-22.43
	Red	0.051456	0.04024	0.05125	+0.40	-21.48
	Orange	0.056739	0.04471	0.0568	-0.11	-21.28
Rear	Blue	0.043368	0.03444	0.0434	-0.073	-20.66
	Red	0.046894	0.03723	0.04585	+2.27	-18.79
	Orange	0.050588	0.04017	0.05035	+0.47	-20.22

As you can see from the Table 2.6.2, the mass computed by LUPOS is always lower than the measured one, this because in the *Spring function* is not possible to insert the right number of inactive spires, but only 3/4 or 0 (here, 0 is set). For this reason, it is possible to correct the mass obtained in LUPOS, adding the contribution of the inactive spires, Eq.2.6.3, Table 2.6.3.

$$m_{ns} = \rho \frac{\pi}{4} \varnothing_w^2 (ns \varnothing \pi) \quad (2.6.3)$$

Table 2.6.3 – Contribution of inactive spires to LUPOS masses.

Springs		Mass [kg]			ε (%)
		Contribution inactive spires	Lupos	Modified LUPOS	Modified LUPOS vs Measured
Front	Blue	0.010546	0.036383	0.046929	+0.92
	Gold	0.0097783	0.03347	0.043248	+0.23
	Red	0.011344	0.04024	0.051584	+0.65
	Orange	0.012175	0.04471	0.056885	+0.15
Rear	Blue	0.0090417	0.034435	0.043477	+0.18
	Red	0.0097783	0.03723	0.047011	+2.53
	Orange	0.010546	0.04017	0.050715	+0.72

The percentage errors are very low, this means that the assumed material properties can be used.

### 3. Numerical vehicle model

In this chapter, the numerical model created to simulate the dynamic behaviour of the vehicle is described. Having a numerical model available is very useful to complement the next experimental measurements, so that it will be easier to verify the accuracy of the tests, already knowing what to expect.

This model is generated in the Matlab environment using the FEM LUPOS code [11].

The model "Losi\_5ive\_7dofs" contains the vehicle's inertial and geometric data, stiffness and damping of the suspension, stiffness and damping of the tyres.

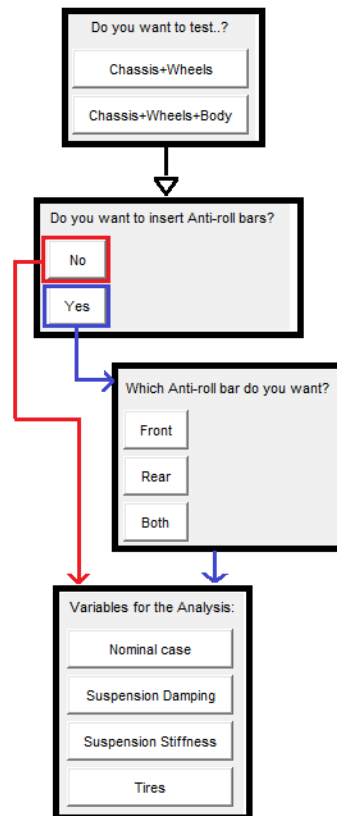


Figure 3.1 – Flowchart for the simulation.

A pop-up menu has been built which allows you to choose what to test. The first possible selection concerns the insertion of the body, so you can choose between these two cases:

- **Chassis case:** the sprung mass is constituted by aluminium plate, the suspensions and the propulsion/braking systems, and the unsprung mass is the set of the four wheels;
- **Body case:** the body is represented by several circular plastic rod whose aim is to support the plastic shell cover of the vehicle and it is added to the sprung mass of the Chassis case, and the unsprung mass is the set of the four wheels;



Figure 3.2 – Chassis case (left) and Body case (right).

Then, you can choose whether to enrich the model by inserting the anti-roll bars, and you can also select which bars to add between:

- Front anti-roll bar;
- Rear anti-roll bar;
- Both front and rear anti-roll bars;

Finally, it is possible to select the parameters for the analysis, switching the nominal case values with the other stiffnesses and damping.

### 3.1 Data and considerations

In “Losi\_5ive\_7dofs”, the geometry of the vehicle is defined through the coordinates of the nodes, the connection between the nodes are made by different type of elements, then lumped mass, stiffness and damping matrices are set out, and finally the boundary conditions are defined.

The origin of the reference system is placed on the axis of symmetry of the vehicle, located in the middle of front suspension and at the height of the wheel centre.

The inertial and geometric data of the vehicle have been obtained from previous experimental research activity [8]. The geometric data are measured in the nominal condition, i.e. all the blue springs are mounted on the vehicle and the ring-nut that tightens them is in the highest position, in this way the springs are as relaxed (extended) as possible and the low arms recline making minimum the height of the barycentre. When the ring-nut will be screwed, the barycentre height will increase and the low arms will recline, the increased height depends from the stiffness of the spring and from the entity of the screwing, so the model will be enhanced taking into account this aspect.

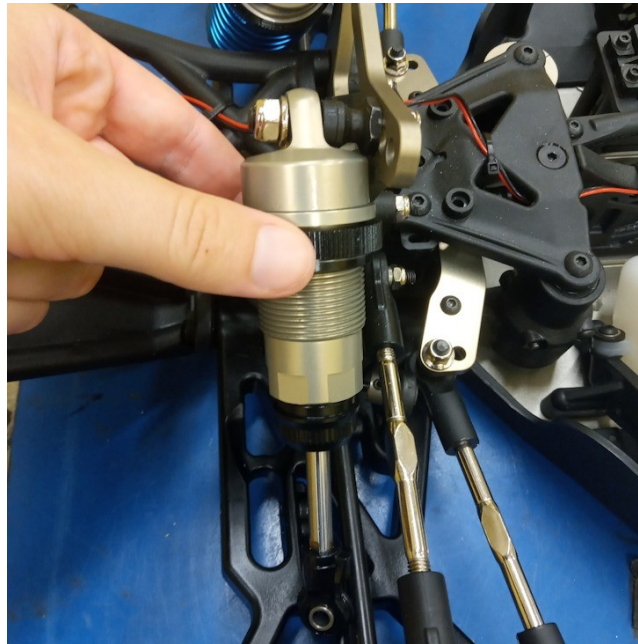


Figure 3.1.1 – Ring-nut that tightens the spring.

The data values of the “Chassis case”, which represents the base case, are reported in the following tables.

Table 3.1.1 – Inertial Properties - Chassis case.

<b>Symbol</b>	<b>Value</b>	<b>Description</b>
Car.m	11.95	Sprung mass - chassis[kg]
Car.Ix	0.10929	Car moment of inertia around x [kg m <sup>2</sup> ]
Car.Iy	0.725	Car moment of inertia around y [kg m <sup>2</sup> ]
Car.Iz	0.74771	Car moment of inertia around z [kg m <sup>2</sup> ]
Car.m1	0.6237	Unsprung mass of a single front wheel [kg]
Car.m2	0.6237	Unsprung mass of a single front wheel [kg]

Table 3.1.2 – Geometrical Data.

<b>Symbol</b>	<b>Value</b>	<b>Description</b>
Car.L	0.965	Car length [m]
Car.B	0.527	Car width [m]
Car.H	0.311	Car height [m]
Car.TyreL	0.071	Tyre width [m]
Car.TyreH	Car.TyreL·0.55	Side tire height [m]
Car.TyreD	0.181	Tyre external diameter [m]

Table 3.1.3 – Chassis Barycentre location.

<b>Symbol</b>	<b>Value</b>	<b>Description</b>
Car.a	0.61	Car wheelbase [m]
Car.a1	0.305	Car front semi-wheelbase [m]
Car.a2	0.305	Car rear semi-wheelbase [m]
Car.t	0.456	Car track [m]

Car.h	0.04	Ground clearance of the upper surface of the plate
Car.hG	0.054+Car.h	Car barycentre height [m]

Table 3.1.4 – Suspension connection locations.

Description	x [mm]	y [mm]	z [mm]
Front up	22	40	130
Front low	33.5	112	-12
Rear up	-640	75	123
Rear low	-655	150	-12

Table 3.1.5 – Top arm connections locations.

Description	x [mm]	y [mm]	z [mm]
Front - chassis side	-7	35	80
Front – wheel side	-10	171	70
Rear – chassis side	-612.5	60	60
Rear – wheel side	-612.5	160	60

As stated previously, tuning the rig-nuts the height of the barycentre changes and so the reclination of the low arms; in particular, when the rig-nuts are screwed, the springs are shorten, and so all the nodes of the chassis translate upwards, while the low arms recline and the track will be reduced. For simplicity, the screwing will not be measured instead the barycentre height variation due to this, named  $\Delta h$ . Referring to the Figure 3.1.2, it is possible to calculate the variations that will be added or subtract to the nodes coordinates as function of  $\Delta h$  according to the following equations.

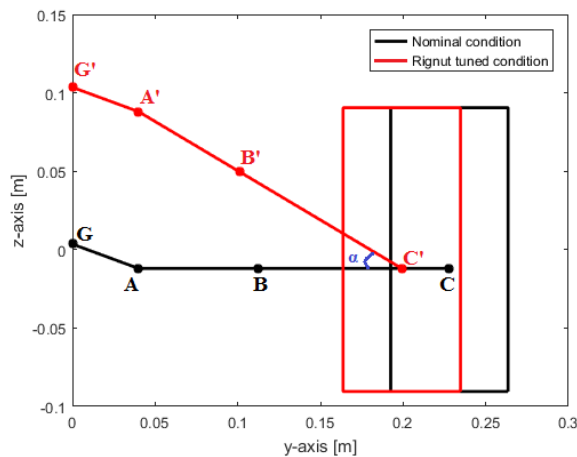


Figure 3.1.2 – Rig-nut tuning scheme, Front Left particular.

$$\Delta y_C = d - \sqrt{d^2 - \Delta h^2} \quad (3.1.1)$$

$$\alpha = \arctan \left( \frac{\Delta h}{\sqrt{d^2 - \Delta h^2}} \right) \quad (3.1.2)$$

$$\Delta z_B = d_2 \sin(\alpha) \quad (3.1.3)$$

$$\Delta y_B = d_1 - d_1 \cos(\alpha) \quad (3.1.4)$$

Where:

- $\Delta h$  is the increment of the barycentre height due to the tuning of the rig-nut;
- $d$  is the length of the low arm AC;
- $d_1$  is the length of the low arm AB;
- $d_2$  is the length of the low arm BC;
- $\alpha$  is the angle between the low arm in the nominal condition and the low arm in the rig-nut tuned configuration;
- $\Delta y_C$  is the decrement of the semi-track;
- $\Delta z_B$  is the increment of the low arm point height;
- $\Delta y_B$  is the decrement of the low arm point along  $y$ -axis.

Since the barycentre height also depends on the stiffness of the springs, when the springs are changed, the rig-nuts will be tightened so that the barycentre has the same height as in nominal condition with the blue springs.

The values for the parametric analysis are reported in the following Tables. The stiffness of the springs are those described into Chapter 2, while the stiffness of the tyres are taken from a previous Thesis work.

The damping of tires and of the shock absorbers are not currently available, as they are the object of another on-going Thesis. Due to the lack of these data, real Modal Analyses will be performed instead of complex Modal Analyses, the latter much more suitable for vehicles since they are among the most damped bodies in mechanics, however the model created provides for the insertion of such data, so it will be sufficient to replace the real data with those hypothesized here to complete the analyses.

Table 3.1.6 – Tyres - stiffness.

Tire type	Stiffness [N/m]
LOS 45023 with insert	18277
LOSB 7240 with insert	18746
LOS 45023 without insert	7368
LOSB 7240 without insert	7078

Table 3.1.7 – Springs - stiffness.

Springs		Nominal stiffness [N/m]
Front	Blue	2046.24
	Gold	1816.92
	Red	2275.56
	Orange	2504.88
Rear	Blue	1411.2
	Red	1640.52
	Orange	1887.48

### 3.2 Model description

In the following paragraph an accurate description of the model is given, in particular the “Chassis case” is examined as it represents the base model. We are interested in evaluating the first 7 vibration modes and the related frequencies; these modes correspond to the sprung mass and unsprung mass main motions: the sprung mass can translate along z-axis (rebound motion) and it can rotate around x-axis (rolling) and y-axis (pitching), while each wheel can translate along z-axis. The syntax of all LUPOS model variables used for the model are summarised into the Table 3.2.1.

Table 3.2.1 –LUPOS model variables.

<b>Variables</b>	<b>Description</b>	<b>Syntax</b>
Model.Geo	Matrix of geometric position of nodes	[NodeId x y z] (G x 4)
Model.Mss	Matrix of lumped masses	[NodeId m Jxx Jyy Jzz Jxy Jxz Jyz] (M x 8)
Model.Bcs	Matrix with dofs to be deleted	[NodeId dof] (V x 2)
Model.RJs	Matrix with rigid joints	[NodeId1 NodeId2] (J x 2)
Model.RBE	Matrix with rigid body elements	[NodeId1 dof1 NodeId2 dof2] (B x 4)
Model.Rod	Matrix of rod links	[NodeId1 NodeId2 col alpha Dy Dz t ro E v c_alpha c_beta N] (R x 13)
Model.Lks	Matrix of beam link	[NodeId1 NodeId2 col alpha b h t ro E v c_alpha c_beta N] (L x 10) or (L x 12) or (L x 13)]
Model.Els	Matrix of lumped springs	[NodeId1 dof1 NodeId2 dof2 k] (K x 5)
Model.Dmp	Matrix of lumped dampers	[NodeId1 dof1 NodeId2 dof2 c] (C x 5)

After writing all the necessary data, the first step to build the vehicle model is to create nodes, they are listed into Model.Geo matrix. The positions of the nodes are derived from the geometrical data of Table 3.1.2, Table 3.1.3, Table 3.1.4 and Table 3.1.5 taking into account the location of the reference system origin, which is located, like said previously, on the axis of symmetry of the vehicle and in the middle of front suspension .

The sprung mass is lumped into the barycentre while the unsprung masses are lumped into the wheel-centres, so in their representative nodes the inertial properties (Table 3.1.1) are assigned thanks to the Model.Mss. These representative nodes are marked as red circle in Figure 3.1.1. The constraints are imposed in Model.Bcs: since the wheels touch the ground, the model is not free-free but constrained, therefore all degrees of freedom are removed at the contact, these points are shown as crosses in Figure 3.2.1; the other removed degree of freedom are the translation of the barycentre along the x-axis and y-axis, the rotation of the barycentre around z-axis, and the rotation of the wheel-centre around z-axis.

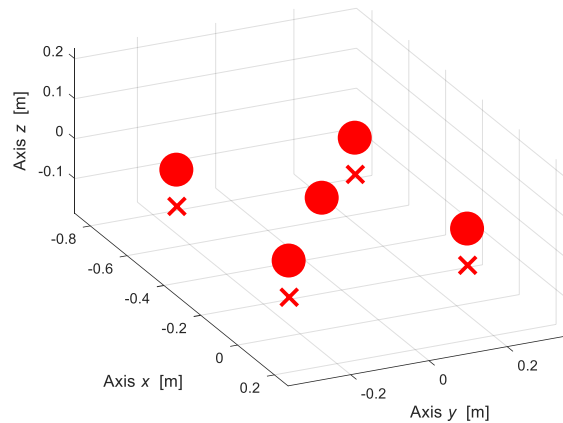


Figure 3.2.1 – Model.Mss and Model.Bcs.

The chassis geometry is simplified, and it is modelled by rigid joints (Model.RJs), rigid body elements (Model.RBE) and rod links (Model.Rod):

- the Rigid Joints elements (RJs) are used to define a relationship between translational and rotational dofs of nodes that have to maintain constant relative distance [12]. In the model they are used to sketch the frame, wheels hub and upper support arms to the suspensions, shown as black lines in Figure 3.2.2;

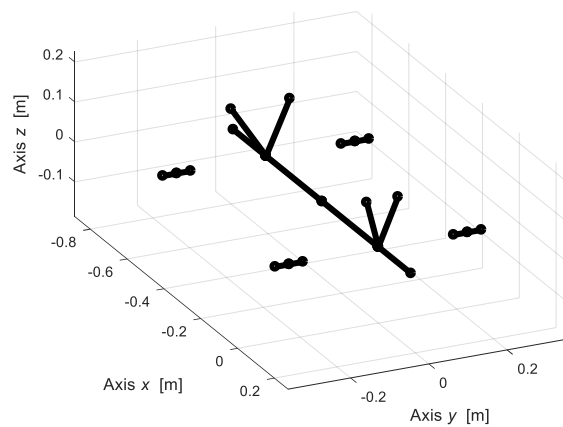


Figure 3.2.2 – Model.RJs

- the rod element (Rod) is defined as a circular or elliptical pipe between two nodes, in the model Timoshenko approach is used. In this model the rod element is used in two different ways; the first way is giving very low density and low Young modulus only to draw wheels sketch, as show on the right side of Figure 3.2.3; the second way is assigning zero density and very high Young modulus to use it like a rigid element, in particular the rod elements have been operated to sketch the joint arms of the suspensions, shown in orange, fuchsia and green lines in Figure 3.2.3, the wheel hubs (red lines) and the supports for the anti-roll bars (fuchsia lines);

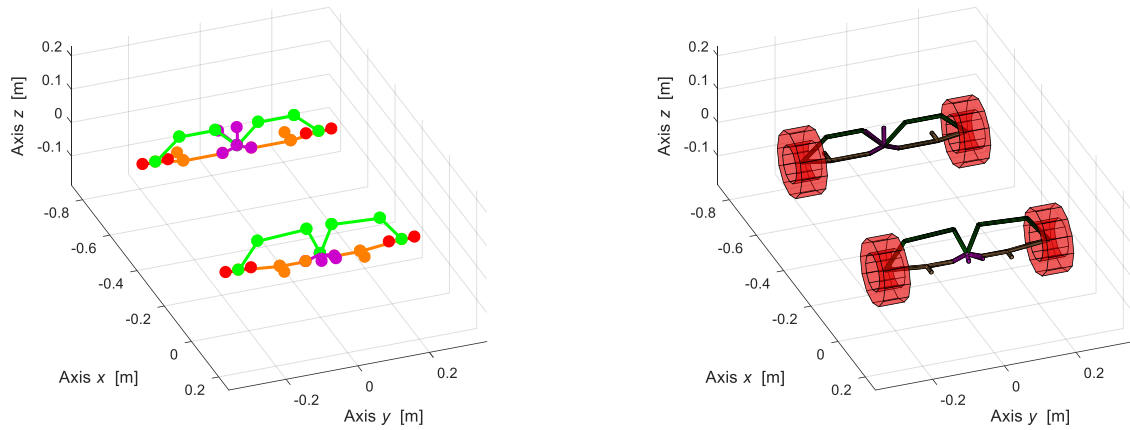


Figure 3.2.3 – Model.Rod, rigid elements (left) and wheels sketch (right).

- Rigid Body Elements (RBE) are used to joint some dofs between independent nodes to represent constraints such as relative sliders, relative pins, spherical hinges, etc [12]. In the model, some coincident nodes belonging to different parts are created and an RBE element is inserted between these to link these parts. In particular, there is an RBE between the barycentre and the middle node of the frame, all the degrees of freedom are removed to guarantee the continuity; then there are RBE elements to simulate the joints that link the arms of the suspensions. The nodes where RBE are applied are show like red points in the Figure 3.2.4;

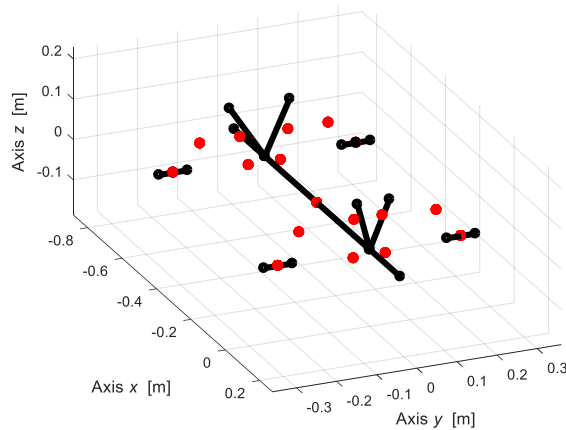


Figure 3.2.4 – Model.RBE

For a better understanding of what has been said, it is possible to refer on Front-Left side since there is a sort of symmetry. A picture of the real car is reported, Figure 3.2.5, in which are highlighted some real elements with the same colour of the simplified model, Figure 3.2.6. The LUPOS model variable used are summarised in Table 3.2.3.

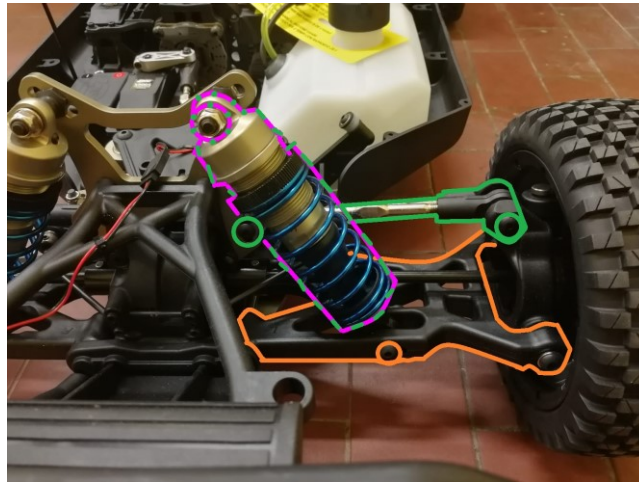


Figure 3.2.5 – Front Left of real car

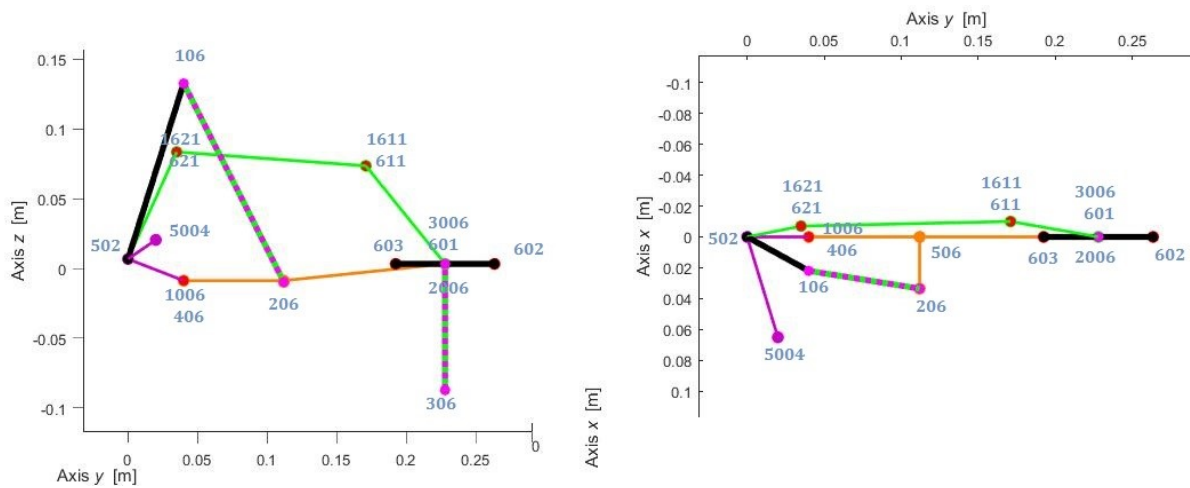


Figure 3.2.6 – Front-Left particular,  $yz$ -section (left),  $xy$ -section (right).

Table 3.2.2 – Front-Left side, nodes description.

Description	Node
Upper attachment damper	106
Lower attachment damper	206
Contact point wheel-ground	306
Suspension arm node	406
Chassis node	502
Suspension arm node	506
Wheel	601
Wheel, left end	602
Wheel, right end	603
Arm node, wheel side	611
Arm node, chassis side	621
Arm joint	1006
Arm joint, wheel side	1611
Arm joint, chassis side	1621
Wheel joint, low arm	2006
Wheel joint, top arm	3006

Table 3.2.3 – Front-Left side, variables description.

Node 1	Node 2	LUPOS variable
206	506	Rod
406	502	Rod
502	1621	Rod
502	5004	Rod
506	1006	Rod
506	2006	Rod
602	603	Rod
611	3006	Rod
621	1611	Rod
106	206	Els+Dmp
306	601	Els+Dmp
502	106	RJs
601	602	RJs
601	603	RJs
406	1006	RBE
601	2006	RBE
601	3006	RBE
611	1611	RBE
621	1621	RBE

As can be notice from Figure 3.2.6, the tyre is perfectly orthogonal to the ground so there is just z-component for its stiffness and damping; contrary the suspension ones are angled, therefore the compression of the spring generates a force not only along the z axis but with components also along x and y, for this reason the nominal stiffnesses of the springs are decomposed along the three main directions x-y-z. The decomposing procedure is described referring to the Front-Left damper, Figure 3.2.7, the equation used for the stiffness are Eq. 3.2.1 to Eq. 3.2.9, the same is done for the damping.

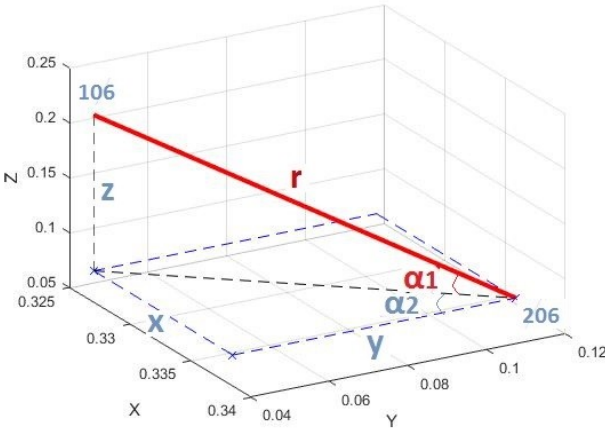


Figure 3.2.7 – Damper decomposing.

$$\Delta x = x_{206} - x_{106} \quad (3.2.1)$$

$$\Delta y = y_{206} - y_{106} \quad (3.2.2)$$

$$\Delta z = z_{206} - z_{106} \quad (3.2.3)$$

$$\Delta r = \sqrt{\Delta x^2 + \Delta y^2 + \Delta z^2} \quad (3.2.4)$$

$$\alpha_1 = \arcsin\left(\frac{\Delta z}{\Delta r}\right) \quad (3.2.5)$$

$$\alpha_2 = \arctan\left(\frac{\Delta x}{\Delta y}\right) \quad (3.2.6)$$

Table 3.2.4 – Geometric computed data for Front damper decomposing.

Geometric data	Value	Description
$\alpha_1$ [°]	62.8	Angle between damper and its projection on $xy$ plane
$\alpha_2$ [°]	9	Angle between damper projections on $xy$ plane and on $y$ -axis
$\Delta x$ [m]	0.0115	Projection of the spring on $x$ -axis
$\Delta y$ [m]	0.0720	Projection of the spring on $y$ -axis
$\Delta z$ [m]	0.1420	Projection of the spring on $z$ -axis
$\Delta r$ [m]	0.1596	Distance between up and low damper attachments

$$k_x = (k \cos(\alpha_1)) \sin(\alpha_2) \quad (3.2.7)$$

$$k_y = (k \cos(\alpha_1)) \cos(\alpha_2) \quad (3.2.8)$$

$$k_z = k \sin(\alpha_1) \quad (3.2.9)$$

Table 3.2.5 – Components of stiffness for Front Blue Damper.

Data	Value	Description
$k$ [N/m]	2046.24	Nominal stiffness
$k_x$ [N/m]	147.42	x-component stiffness
$k_y$ [N/m]	923	y-component stiffness
$k_z$ [N/m]	1820.3	z-component stiffness

Similar procedure has been used to decompose stiffness and damping of Rear springs.

The stiffness components of the suspensions and the stiffness of the tyres are added to the Model.Els matrix, while the damping components of the suspensions and the damping of the tyres are added to Model.Dmp matrix.

The total number of the elements loaded are:

- 70 Geo elements;
- 5 Mss elements;
- 31 BCs elements;
- 36 Rod elements;
- 16 RJs elements;
- 98 RBE elements;
- 16 Els elements;
- 16 Dmp elements;

### 3.3 Addition of the Body

As written into the introduction of the chapter, it is possible to insert the body to the base model. The body is composed by several circular plastic rod whose aim is to support the plastic shell cover of the vehicle; but since this model is a simplification of the real vehicle, the body is inserted as simple lumped mass linked to extreme longitudinal nodes of the chassis, at the front and rear axles. The inertial properties and the barycentre location of the body are reported into the Table 3.3.1 and Table 3.3.2.

Table 3.3.1 – Inertial Properties - Body case.

Symbol	Value	Description
Car.mb	2.2825	Sprung mass – body [kg]
Car.Ixb	0.0273	Body moment of inertia around x [kg m <sup>2</sup> ]
Car.Iyb	0.14033	Body moment of inertia around y [kg m <sup>2</sup> ]
Car.Izb	0.16521	Body moment of inertia around z [kg m <sup>2</sup> ]

Table 3.3.2 – Body Barycentre location.

Symbol	Value	Description
Car.a1b	0.352	Car front semi-wheelbase [m]
Car.a2b	0.257	Car rear semi-wheelbase [m]
Car.hb	0.03	Ground clearance of the upper surface of the plate
Car.hGb	0.212+Car.hb	Car barycentre height [m]

The body is connected to the chassis via 4 points, they are highlighted in the Figure 3.3.1 and their coordinates are taken by a meter and reported in the Table 3.3.3, the *x* and *y* coordinates are measured with respect to the extreme longitudinal nodes (node 501 for the front, and node 505 for the rear) while the *z*-coordinate is taken from the wheel centre.



Figure 3.3.1 – Body attachments- Front (left) and Rear (right).

Table 3.3.3 – Body attachments coordinates.

Node		x [mm]	y [mm]	z [mm]
Front	Left	-60	80	50
	Right	-60	-80	50
Rear	Left	0	132.5	85
	Right	0	-132.5	85

Summing up, if the “Body case” is selected from the pop-up menu, the mass and the moments of inertia are loaded, then new nodes for the barycentre and for the attachment to the chassis are added to the Model.Geo while the inertial properties are added to the Model.Mss.

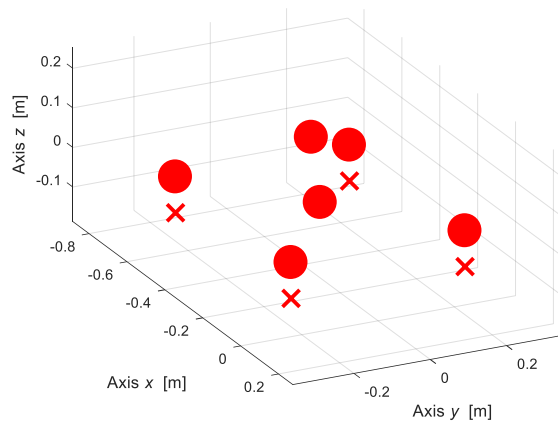


Figure 3.3.2 – Model.Mss - Body case.

Then, some RJs elements are created to extend the front and rear axles and permit the body to attach at the chassis and four rods link the barycentre to these front and rear axles, these rods are used like rigid elements so the density value is very low and the Young modulus high. In the Figure 3.3.3 the Rods are shown as light blue lines. The number of the body parts is 4 and no less because in this way we do not exert a large torque on the hinges.

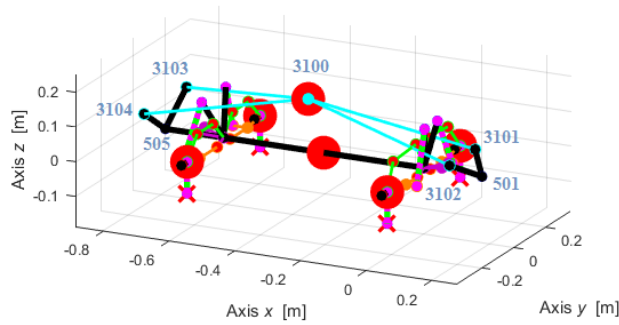


Figure 3.3.3 – Body case.

Table 3.3.4 – Body case, variable description

Node 1	Node 2	LUPOS variable	Description
3100	3101	Rod	Body arm – Front Left
3100	3102	Rod	Body arm – Front Right
3100	3103	Rod	Body arm – Rear Left
3100	3104	Rod	Body arm – Rear Right
501	3101	RJs	Chassis attachment – Front Left
501	3102	RJs	Chassis attachment – Front Right
505	3103	RJs	Chassis attachment – Rear Left
505	3104	RJs	Chassis attachment – Rear Right

The updated entire vehicle presents now:

- 75 Geo elements loaded;
- 6 Mss elements loaded;
- 31 BCs elements loaded;
- 40 Rod elements loaded;
- 20 RJs elements loaded;
- 98 RBE elements loaded;
- 16 Els elements loaded;
- 16 Dmp elements loaded;

### 3.4 Addition of the Anti-roll bars

The scale vehicle Losi 5ive-T 2.0 is equipped with medium (0.35 mm diameter) sway bars on front and rear. Vehicle anti-roll bar (or sway bar) is part of an automobile suspension system which limits body roll angle. This U-shaped metal bar connects opposite wheels trough short lever arms and is clamped to the vehicle chassis with some hooks.

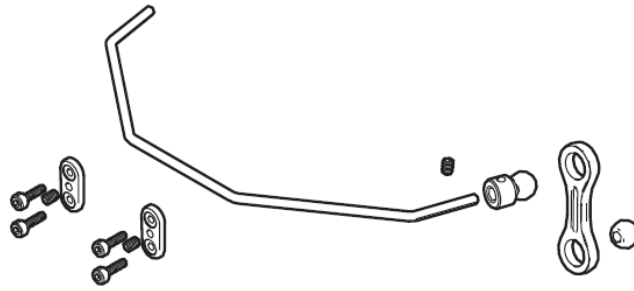


Figure 3.4.1 – Sway bar set and hardware.

The black plastic element circled in Figure 3.4.2 (left side), which we will call “Hardware”, links the metal bar to the low arm. Thanks to a spherical joint all the relative rotations between the Hardware and the metal bar are allowed, so does between the Hardware and the low arm. The Hardware has a prismatic shape with thickness 4 mm and width 8 mm. While the hooks, circled in Figure 3.4.2 (right side), clamp the metal bar to the chassis leaving free the translation along  $y$ -axis and the rotation about  $y$ -axis.



Figure 3.4.2 – Sway bar installation, hardware (left side), hooks (right side).

The materials of the various parts are not given by the Losi 5ive manual, so they are supposed to be the spring steel for the bar and polypropylene for the hardware, the material properties are reported in Table 3.4.1.

Table 3.4.1 – Assumed material properties of the set sway bar.

Property	Symbol	Bar	Hardware
Young modulus [GPa]	$E$	210	1.4
Poisson ratio [-]	$\nu$	0.3	0.45
Density [ $\text{kg/m}^3$ ]	$\rho$	7700	910

For our purpose, the material assumed for the “Hardware” part should be the same of the low arm, so that the properties used are the same of the rigid elements.

The locations of the set nodes are reported in Table 3.4.2, they are measured with respect to the low arm nodes on left side, except for the  $y$ -coordinates of 4<sup>th</sup>s nodes that represent the absolute positions; moreover only the left sides are reported, the right sides is obtained mirroring them.

Table 3.4.2 – Anti-roll set locations, left specular side.

Node		x [mm]	y [mm]	z [mm]
Front	1 <sup>st</sup>	Low arm node left side (node 506)		
	2 <sup>nd</sup>	0	-0.008	+0.027
	3 <sup>rd</sup>	-0.02	-0.012	+0.027
	4 <sup>th</sup>	-0.07	+0.026	+0.027
Rear	1 <sup>st</sup>	Low arm node left side (node 508)		
	2 <sup>nd</sup>	0	-0.008	+0.031
	3 <sup>rd</sup>	+0.025	-0.006	+0.031
	4 <sup>th</sup>	+0.065	+0.02	+0.031

For greater clarity, it is preferred to model firstly the anti-roll bar as subsystem and then add it to the entire vehicle model. Referring to the Figure 3.4.3, in the Table 3.4.3 are shown the LUPOS variables used to model the Front Anti-roll bar, similarly has been done for the Rear Anti-roll bar.

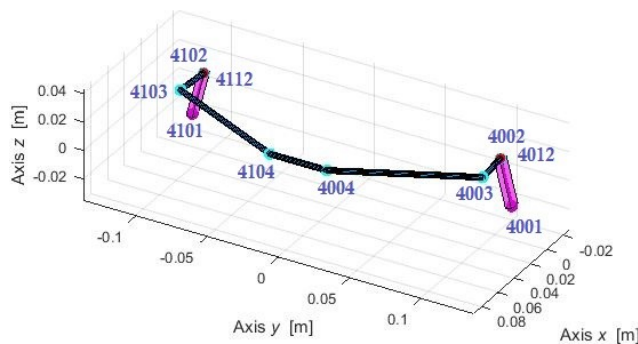


Figure 3.4.3 – Front Anti-roll bar subsystem.

Table 3.4.3 – Front Anti-roll bar subsystem, variable description

Node 1	Node 2	LUPOS variable	Description
4001	4012	Lks	Hardware, left
4002	4003	Rod	Vertical bar arm, left
4003	4004	Rod	Oblique bar arm, left
4004	4104	Rod	Horizontal bar arm
4101	4112	Rod	Hardware, right
4102	4103	Rod	Vertical bar arm, right
4103	4104	Rod	Oblique bar arm, right
4002	4012	RBE	Hardware – Bar joint, DOFs constrained: translations along $x - y - z$ and rotation around $z$

4102	4112	RBE	Hardware – Bar joint, DOFs constrained: translations along $x - y - z$ and rotation around $z$
------	------	-----	---

Then, the Anti-roll bars subsystems are properly insert into the entire vehicle model, paying attention on the constraints. As said previously, between the Hardware and the low arm the rotations are allowed, and between the Hooks and the chassis the translation along  $y - axis$  and the rotation about  $y - axis$  are permitted. The new elements for the Front side are reported in the Table 3.4.4, similarly it has done for the Rear side.

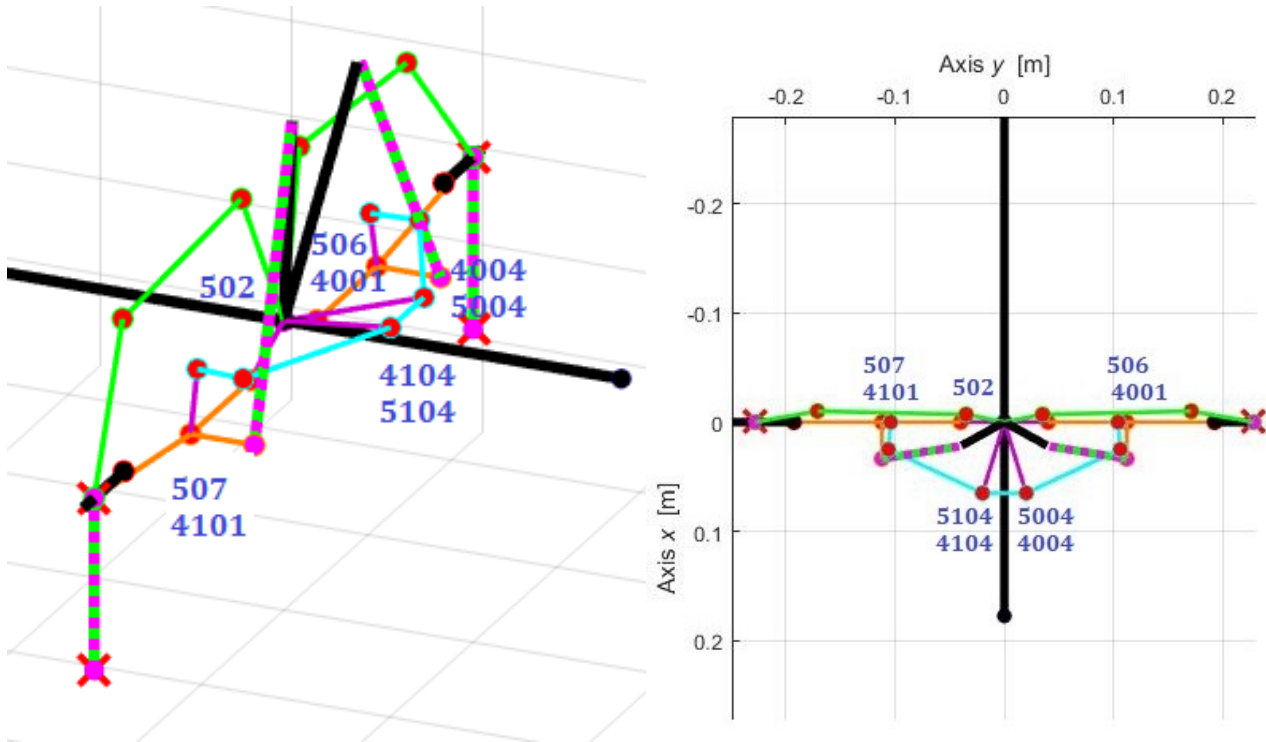


Figure 3.4.4 – Front side of vehicle model with supplement of Anti-roll bar.

Table 3.4.4 – Front Anti-roll bar subsystem, variable description

Node 1	Node 2	LUPOS variable	Description
502	5004	Rod	Chassis
502	5104	Rod	Chassis
506	4001	RBE	Hardware – Low arm joint, DOFs constrained: translations along $x - y$
507	4101	RBE	Hardware – Low arm joint DOFs constrained: translations along $x - y$
4004	5004	RBE	Hook – Chassis, DOFs constrained: translations along $x - z$
4104	5104	RBE	Hook – Chassis, DOFs constrained: translations

			along $x - z$
--	--	--	---------------

The updated entire vehicle, “Chassis case” with both anti-roll bars, presents now:

- 98 Geo elements;
- 5 Mss elements;
- 31 Bcs elements;
- 50 Rod elements;
- 16 RJs elements;
- 186 RBE elements;
- 16 Els elements;
- 16 Dmp elements.

## 4. Numerical Real Modal Analysis

In this chapter several simulations of the vehicle model, described previously, are reported. Real Modal Analysis are carried out on different configurations. At the beginning, some basic notions on Real Modal Analysis are given, then the numerical results obtained are reported and discussed. A new model “Losi\_5ive\_7dofs\_param\_k”, slightly different from the previous, is created to allow an automatic execution of a parametric analysis, using as parameter the stiffness. The new flowchart is showed in the following Figure.

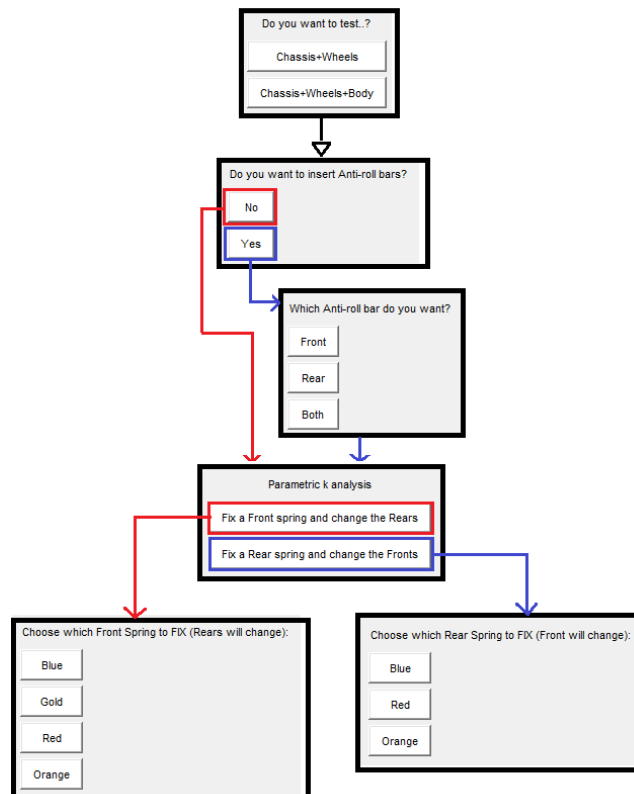


Figure 4.1 – Flowchart for parametric analysis.

### 4.1 Basics on Real Modal Analysis

Modal analysis is an important tool for understanding the vibration characteristics of mechanical structures. The purpose of a modal analysis is to find the shapes and frequencies at which the structure will amplify the effect of a load. Modal analysis embraces both theoretical and experimental techniques. The theoretical modal analysis relies on a physical model of a dynamic system comprising its mass, stiffness and damping properties.

The generic model for a dynamic matrix problem is:

$$[M]\{\ddot{u}\} + [C]\{\dot{u}\} + [K]\{u\} = \{F\} \quad (4.1.1)$$

Where:

- **[M]** is the mass matrix;
- **[C]** is the damping matrix;
- **[K]** is the stiffness matrix.

All three matrices are constant in linear dynamics.

- $\{\ddot{\mathbf{u}}\}$  is the acceleration vector;
- $\{\dot{\mathbf{u}}\}$  is the velocity vector;
- $\{\mathbf{u}\}$  is the displacement vector;
- $\{\mathbf{F}\}$  is the load vector.

For a Real Modal Analysis we do not consider the damping matrix, so the equation becomes:

$$[M]\{\ddot{\mathbf{u}}\} + [K]\{\mathbf{u}\} = \{\mathbf{F}\} \quad (4.1.2)$$

Neglecting static generalized external forces, Eq.4.1.2 results:

$$[M]\{\ddot{\mathbf{u}}\} + [K]\{\mathbf{u}\} = \{\mathbf{0}\} \quad (4.1.3)$$

Solution to the Eq.4.1.3 have the form:

$$\{\mathbf{u}\}(t) = \{\mathbf{U}\} e^{i\omega t} \quad (4.1.4)$$

$$\{\ddot{\mathbf{u}}\}(t) = -\omega^2 \{\mathbf{U}\} e^{i\omega t} \quad (4.1.5)$$

Where:

- $\{\mathbf{U}\}$  is a constant vector;
- $e^{i\omega t}$  represents the time-response which is simply a sine wave;
- $\{\ddot{\mathbf{u}}\}(t)$  is obtained by differentiating  $\{\mathbf{u}\}(t)$  twice

Using this, we obtain:

$$-\omega^2 [M]\{\mathbf{U}\} e^{i\omega t} + [K]\{\mathbf{U}\} e^{i\omega t} = \{\mathbf{0}\} \quad (4.1.6)$$

Dividing by  $e^{i\omega t}$  results in the eigenvalue equation:

$$([K] - \omega^2 [M])\{\mathbf{U}\} = \{\mathbf{0}\} \quad (4.1.7)$$

Apart the trivial solution  $\{\mathbf{U}\} = \mathbf{0}$  that corresponds to the static undeformed condition, Eq.4.1.7 presents non-null solutions, when the rank is not full, hence an eigenproblem is definable.

Eigenvalues and eigenvectors are evaluated, hence:

$$([K] - \omega_r^2 [M])\phi_r = \mathbf{0} \quad (4.1.8)$$

Finding the non-null solutions by means of

$$\det([K] - \omega_r^2 [M]) = 0 \quad (4.1.9)$$

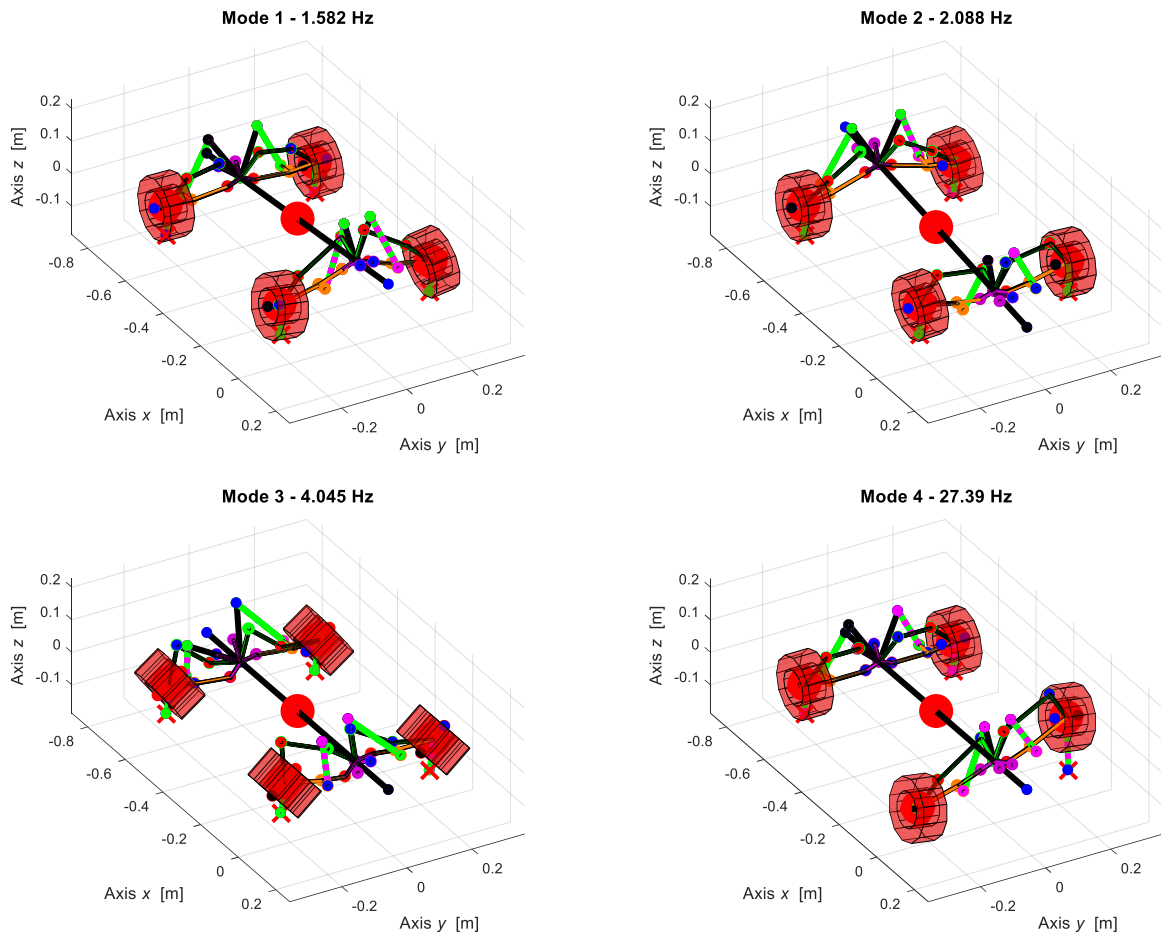
For every eigenvalue  $\omega_r^2$  a non-null corresponding eigenvector  $\phi_r$  can be evaluated through Eq.4.1.8.

## 4.2 Chassis case without Anti-roll bars

The results are for the nominal configuration, so with blues springs both for front and rear and the rig-nut in the highest position. The first 7 vibrations modes and their frequencies are shown in the Figure 4.2.1, the frequencies' values are summarized in the Table 4.2.1.

Table 4.2.1 – Natural frequencies of Chassis case without Anti-roll bars.

Mode	$f_n$ [Hz]	Description
1	1.582	Chassis rebound and pitching
2	2.088	Chassis pitching
3	4.045	Chassis rolling
4	27.39	Front suspensions out-of-phase
5	27.39	Front suspensions in-phase
6	27.50	Rear suspensions out-of-phase
7	27.50	Rear suspensions in-phase



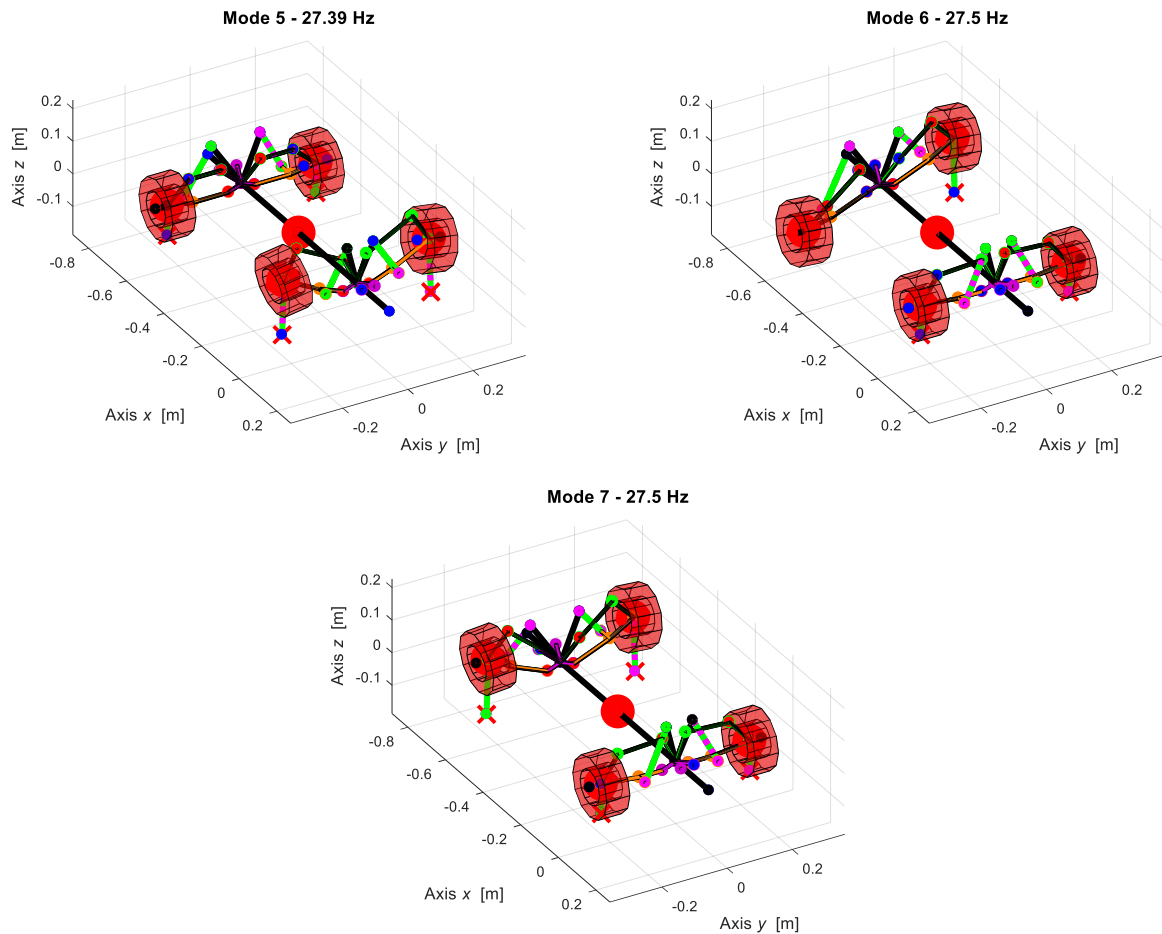


Figure 4.2.1 – Mode shapes.

It is noteworthy that the modes relative to the sprung mass are not so far from a normal scale vehicle, while the modes relative to the unsprung mass occur at frequencies around 2 or 3 times higher with respect to normal scale vehicle. The dynamic behaviour of the scaled vehicle is not so different from the normal vehicle because everything is scaled, such as form factors and stiffnesses values.

It is possible to perform a parametric analysis as shown in the introduction of the chapter. We are interested in understanding the influence of the stiffness on modal results. So, a way to compare the results with different springs is plotting the natural frequencies as function of stiffness. We can fix a type of spring for the fronts dampers and change only the rears, then we can fix a couple of springs for the rears and change the fronts. The results of this parametric analysis are shown in the following figures.

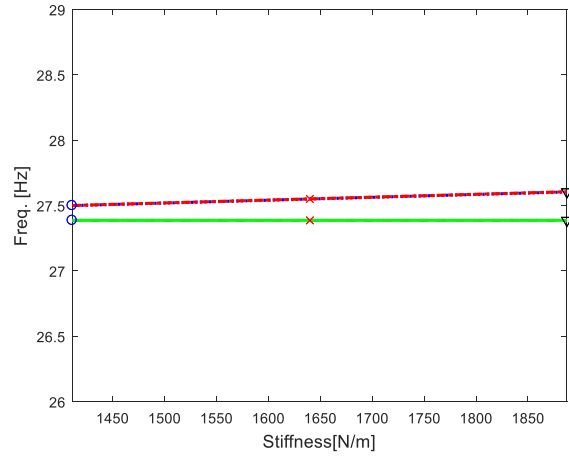
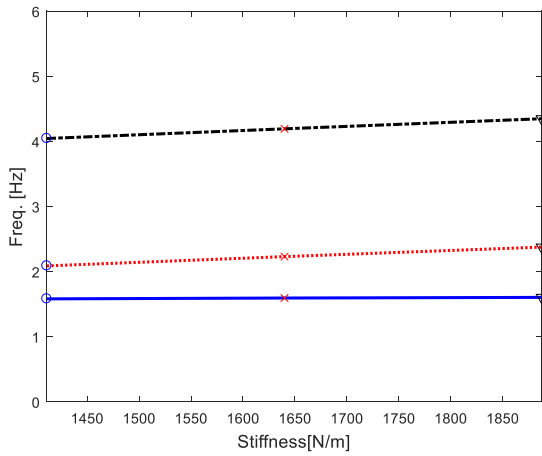


Figure 4.2.2 – Front Blue fixed, changing rears- sprung mass modes (left), unsprung mass modes (right).

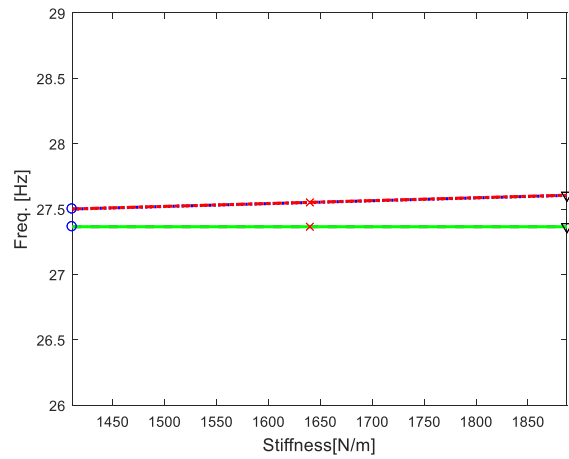
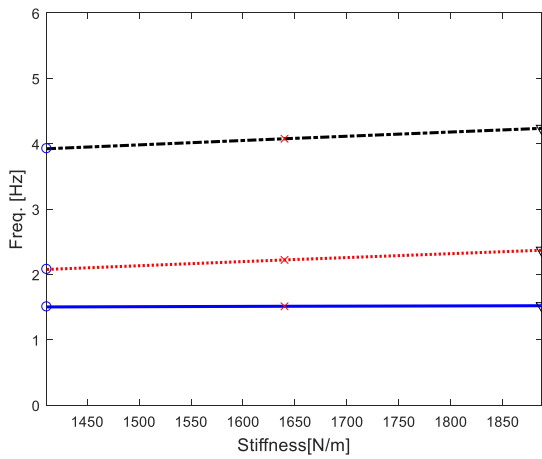


Figure 4.2.3 – Front Gold fixed, changing rears- sprung mass modes (left), unsprung mass modes (right).

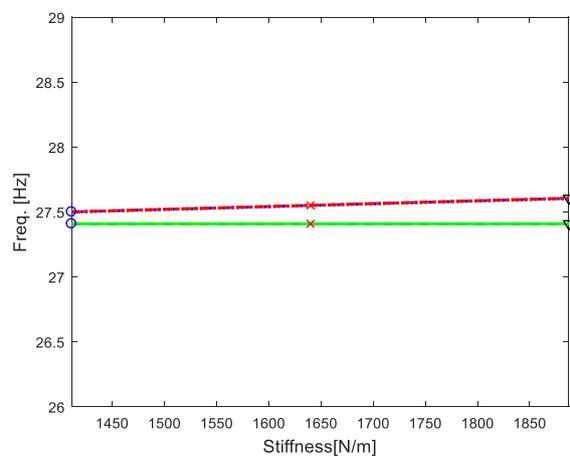
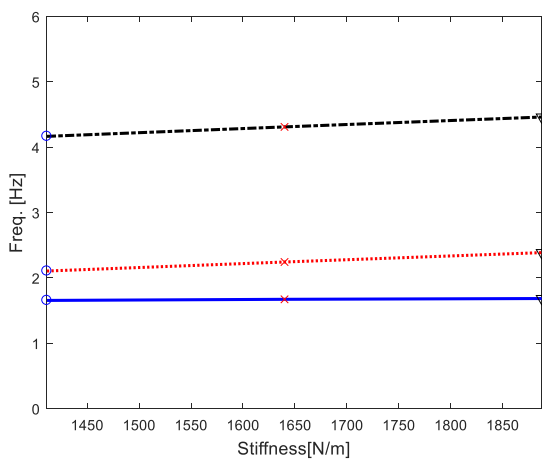


Figure 4.2.4 – Front Red fixed, changing rears- sprung mass modes (left), unsprung mass modes (right).

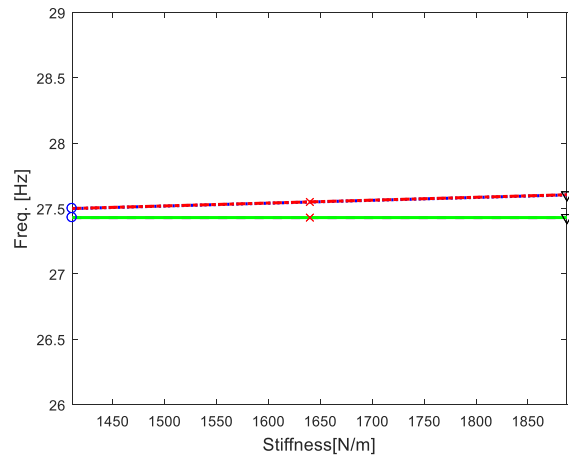
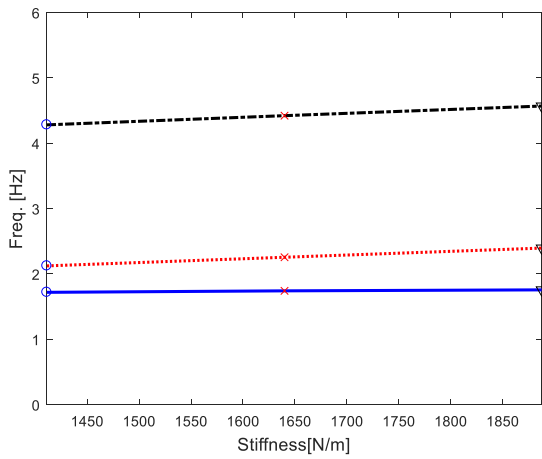


Figure 4.2.5 – Front Orange fixed, changing rears- sprung mass modes (left), unsprung mass modes (right).

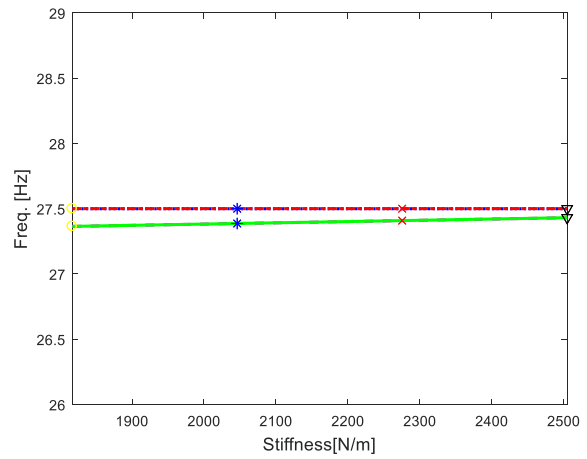
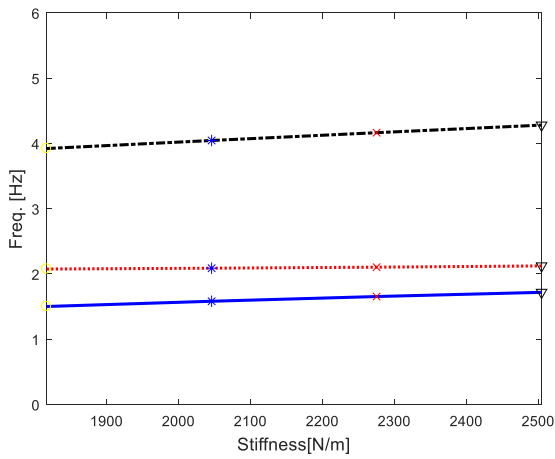


Figure 4.2.6 – Rear Blue fixed, changing fronts- sprung mass modes (left), unsprung mass modes (right).

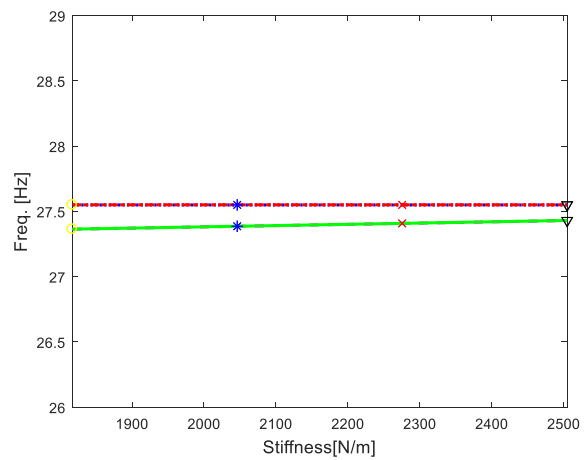
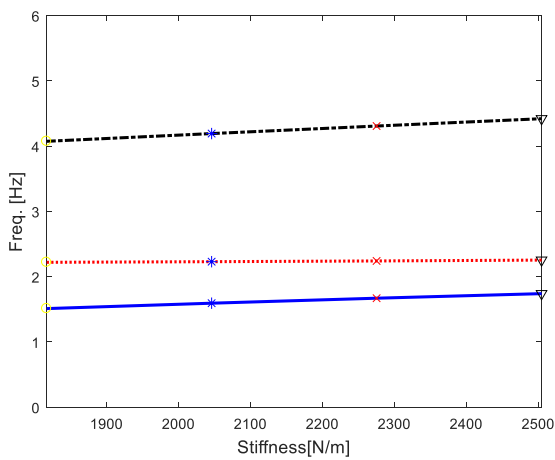


Figure 4.2.7 – Rear Red fixed, changing fronts- sprung mass modes (left), unsprung mass modes (right).

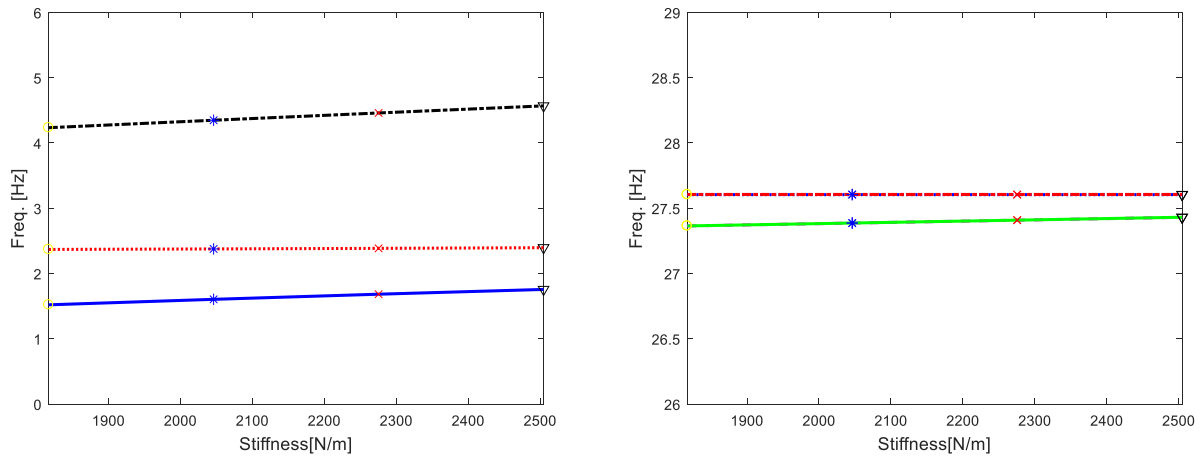


Figure 4.2.8 – Rear Orange fixed, changing fronts- sprung mass modes (left), unsprung mass modes (right).

As it can be notice from the previous graphs, the trends are the same for the different configurations, for this reason in the next analysis there will be reported just the most representative case so as not to be repetitive. The stiffness has not a significant impact on the real modal analysis, in fact the lines are almost flat, there are only little increments of natural frequencies with the increasing the stiffness. In particular, the stiffness has more influence on the roll mode than on the others, while it does not impact on the modes of the unsprung mass. The rear springs have more influence on the rolling with respect to the front springs, while the front springs have more influence on the pitch.

Another way to understand the effect of the stiffness can be considering the following cases, and show the natural frequencies as function of the modes:

- **Gold case:** gold springs on the front and blue springs on the rear;
- **Blue case:** blue springs on the front and on the rear;
- **Red case:** red spring on the front and on the rear;
- **Orange case:** orange spring on the front and on the rear.

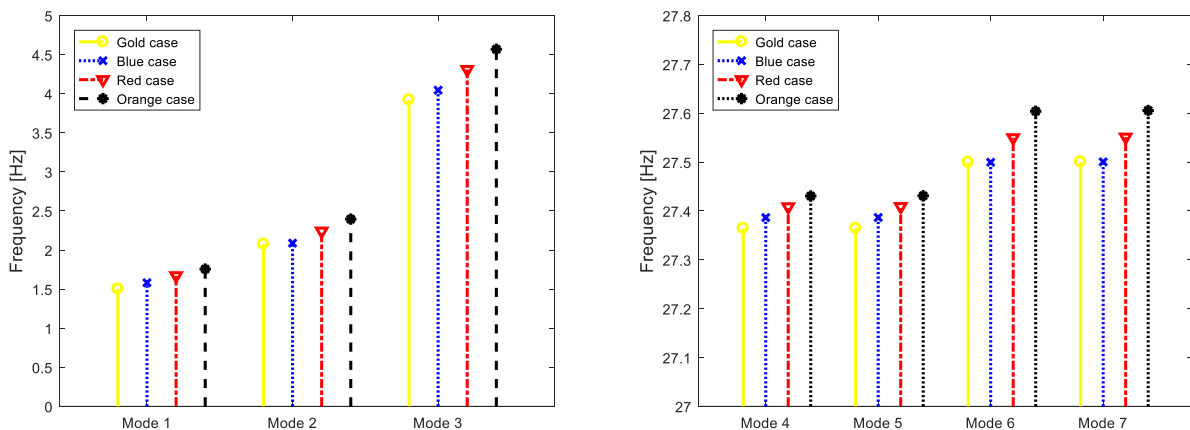


Figure 4.2.9 – Comparing the modes for the different cases.

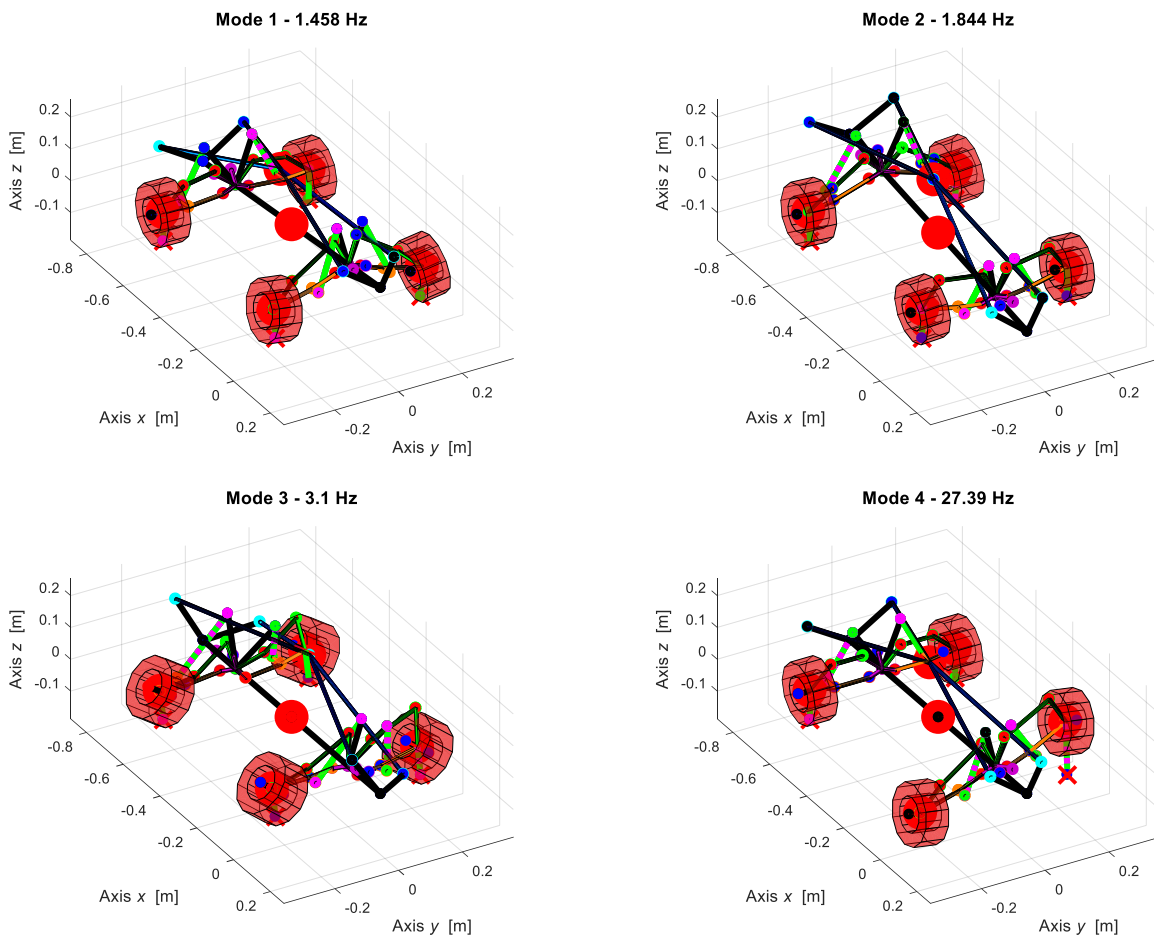
Also in this case, the variation of frequency is not so significant changing the springs, but it is slightly more evident.

### 4.3 Body case without Anti-roll bars

The results are for the nominal configuration, so with blues springs both for front and rear and the rig-nut in the highest position. The first 7 vibrations modes and their frequencies are shown in the Figure 4.3.1, the frequencies' values are summarized in the Table 4.3.1.

Table 4.3.1 – Natural frequencies of Body case without Anti-roll bars.

Mode	$f_n$ [Hz]	Description
1	1.458	Chassis rebound and pitching
2	1.844	Chassis pitching
3	3.1	Chassis rolling
4	27.39	Front suspensions out-of-phase
5	27.39	Front suspensions in-phase
6	27.50	Rear suspensions out-of-phase
7	27.50	Rear suspensions in-phase



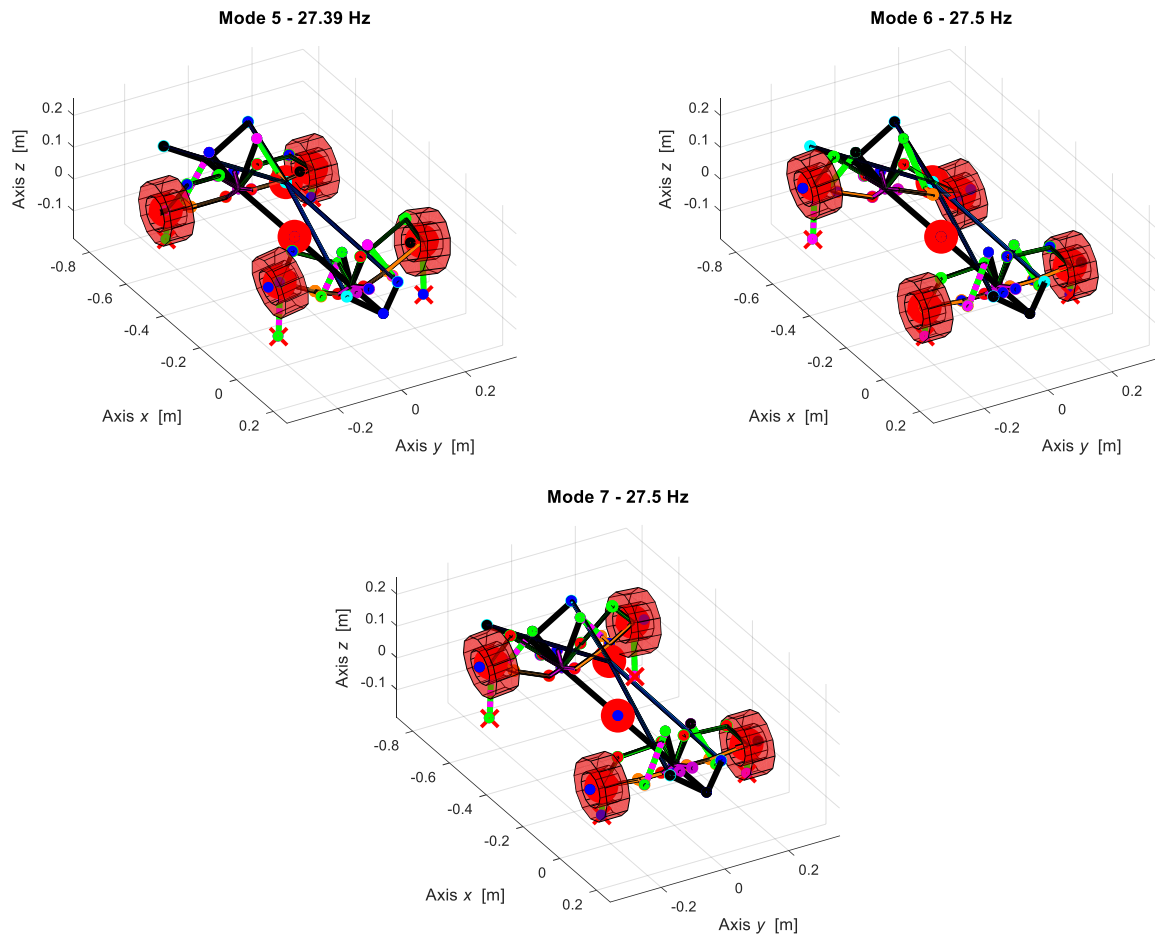


Figure 4.3.1 – Mode shapes

As it is possible to notice from the previous figures, the mode shapes for the body case are almost equal to the mode shapes for the chassis case. The eigenvalues are the same for the unsprung masses modes (last 4 frequencies), while the first 3 frequencies are lower than the chassis case, this can be explained by the increase in mass.

It is possible to perform the parametric analysis as explained in the previous paragraph. The results can be shown as Frequency function of stiffness or as Frequency function of different cases grouped in modes. In both case we can see how the stiffness has little influence on the analysis, exactly as in the Chassis case. Then, to not be repetitive just a trend is reported.

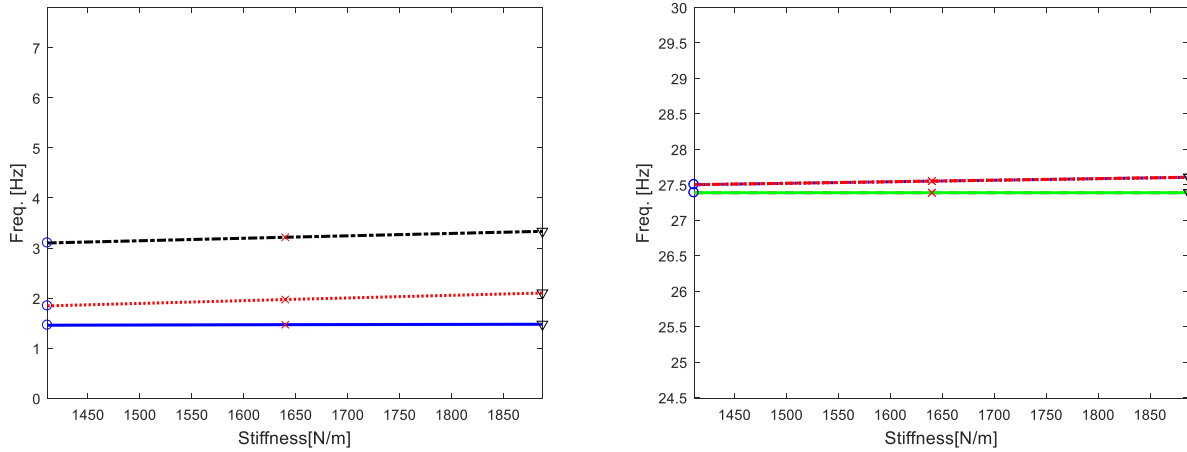


Figure 4.3.2 – Front Blue fixed, rears change (Body case).

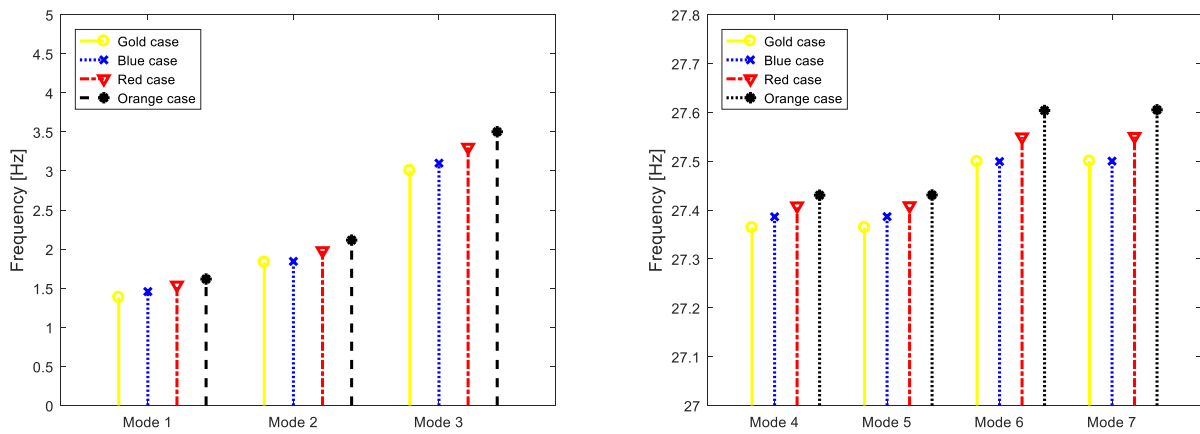


Figure 4.3.3 – Comparing the modes for the different cases (Body case)

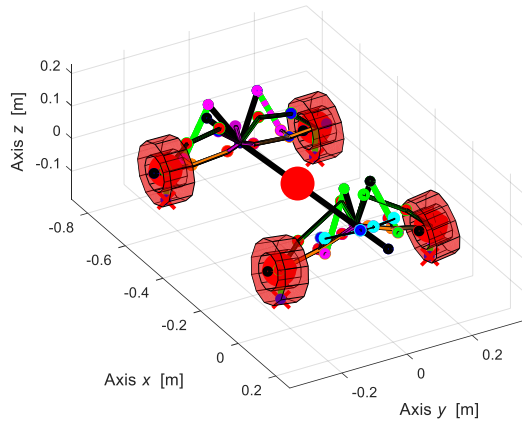
#### 4.4 Chassis case with Front Anti-roll bar

The results are for the nominal configuration, so with blues springs both for front and rear and the rig-nut in the highest position. The first 8 vibrations modes and their frequencies are shown in the Figure 4.4.1, the frequencies' values are summarized in the Table 4.4.1.

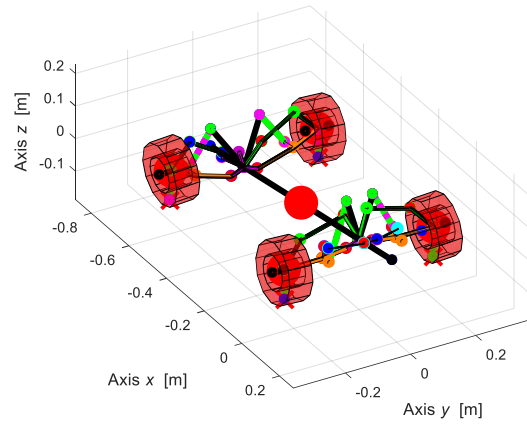
Table 4.4.1 – Natural frequencies of Chassis case with Front Anti-roll bar.

Mode	$f_n$ [Hz]	Description
1	1.579	Chassis rebound and pitching
2	2.087	Chassis pitching
3	4.002	Chassis rolling
4	19.84	Anti-roll bar torsion
5	27.38	Front suspensions in-phase
6	27.50	Rear suspensions out-of-phase
7	27.50	Rear suspensions in-phase
8	27.93	Front suspensions out of-phase

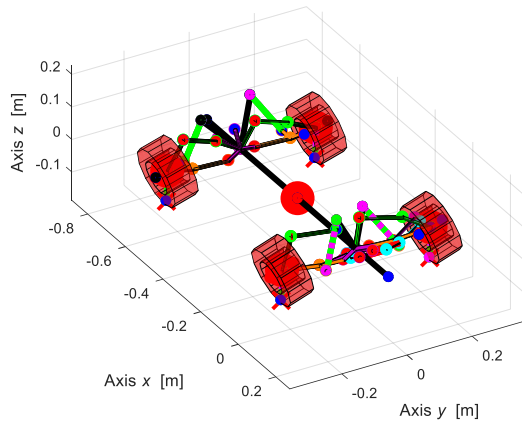
**Mode 1 - 1.579 Hz**



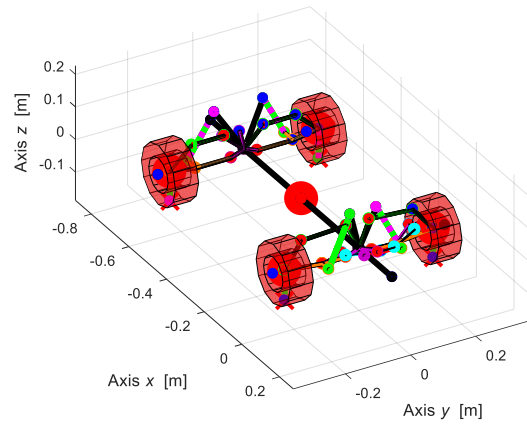
**Mode 2 - 2.087 Hz**



**Mode 3 - 4.002 Hz**



**Mode 4 - 19.84 Hz**



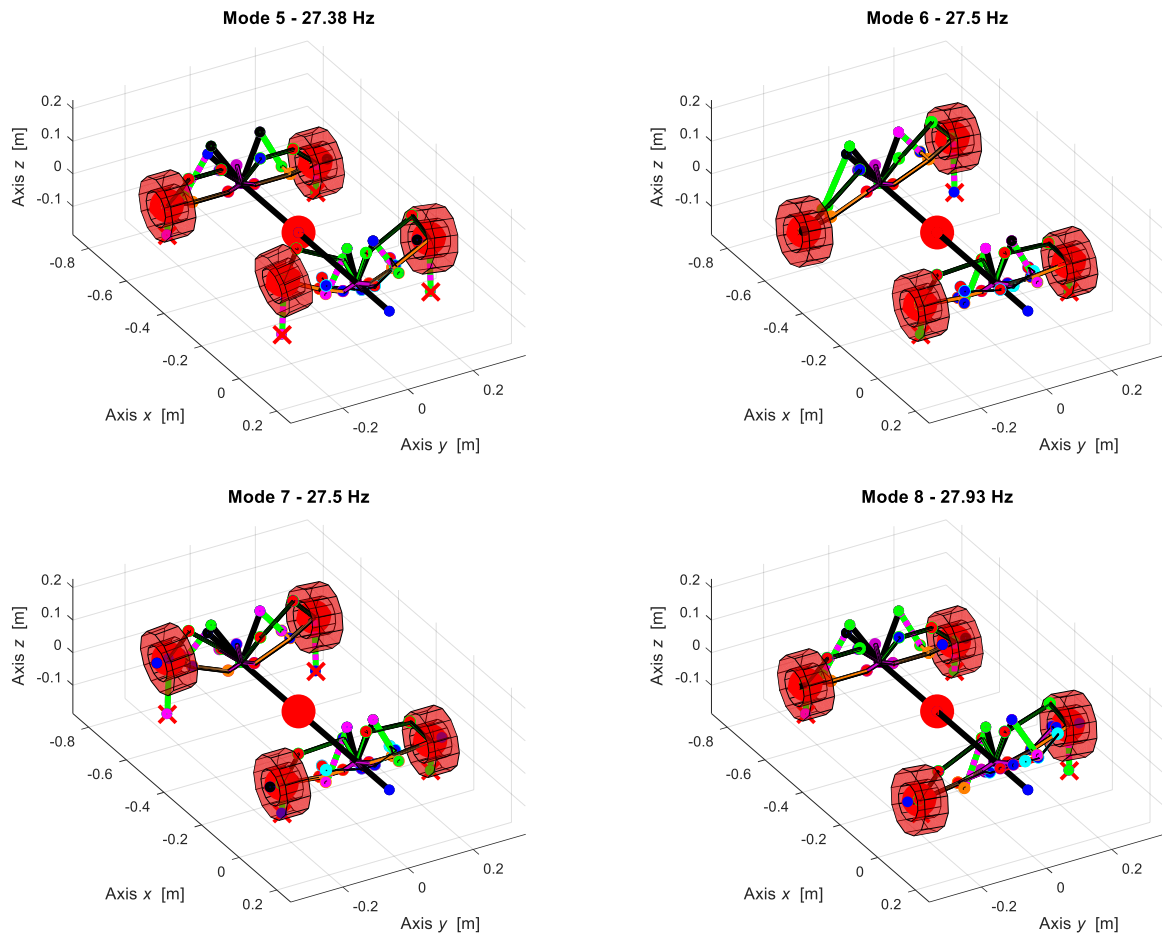


Figure 4.4.1 – Mode shapes.

The anti-roll bar has the scope to reduce the rolling motion, as expected the entity of the rolling is reduced with respect to the case without the anti-roll bar, while the natural frequencies for the suspension modes are the same. Another mode appears, it is related to the torsion of the anti-roll bar. While the mode shapes for the unsprung mass appear in a different order with respect to the previous case, at slightly different frequencies.

The considerations for the parametric analysis are analogue to the case without anti-roll bars, the trend in fact is almost flat.

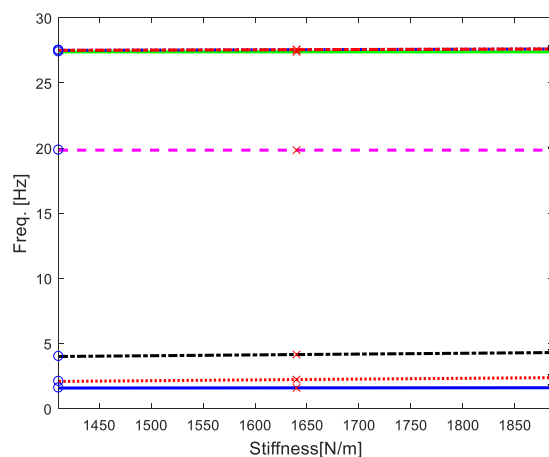


Figure 4.4.2 – Parametric analysis-fronts blue fixed and rears change.

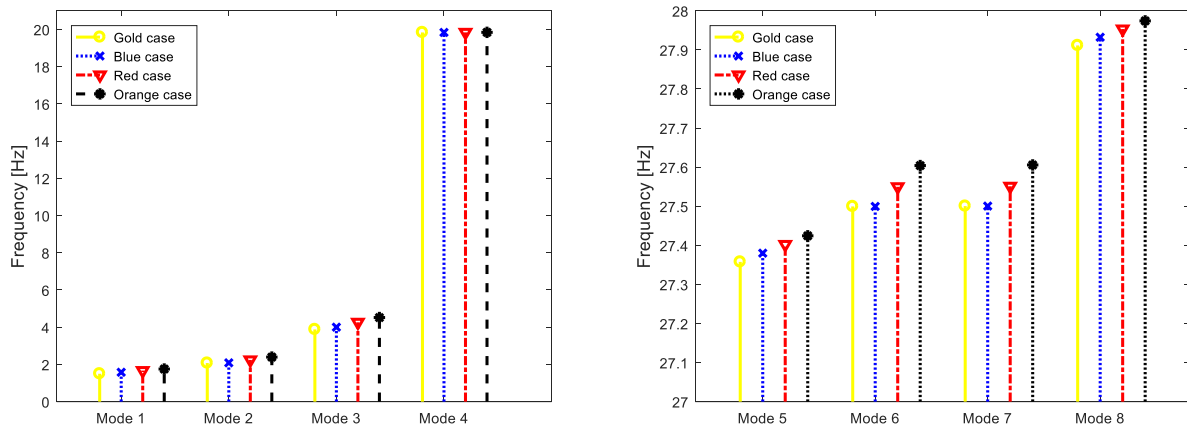


Figure 4.4.3 – Parametric analysis-comparing modes.

The mode related to the torsion of the anti-roll bar is completely independent from the stiffness of the springs, as we can see it does not change with the different configurations.

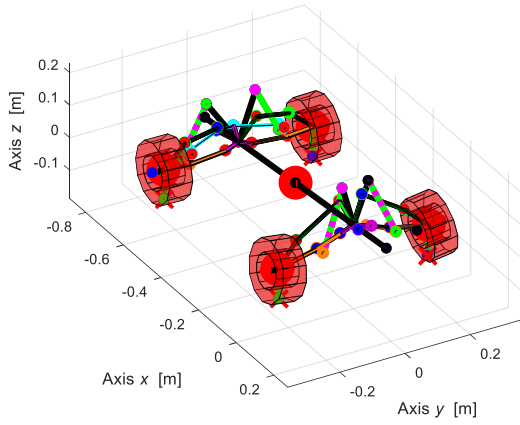
#### 4.5 Chassis case with Rear Anti-roll bar

The results are for the nominal configuration, so with blues springs both for front and rear and the rig-nut in the highest position. The first 8 vibrations modes and their frequencies are shown in the Figure 4.5.1, the frequencies' values are summarized in the Table 4.5.1.

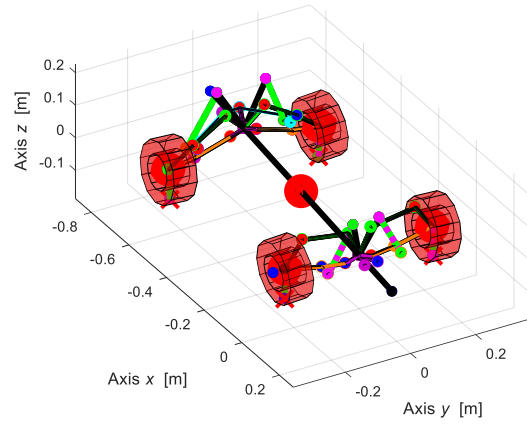
Table 4.5.1 – Natural frequencies of Chassis case with Rear Anti-roll bar.

Mode	$f_n$ [Hz]	Description
1	1.582	Chassis rebound and pitching
2	2.084	Chassis pitching
3	3.950	Chassis rolling
4	15.27	Anti-roll bar torsion
5	27.39	Front suspensions out-of-phase
6	27.39	Front suspensions in-phase
7	27.48	Rear suspensions out-of-phase
8	27.95	Rear suspensions in-phase

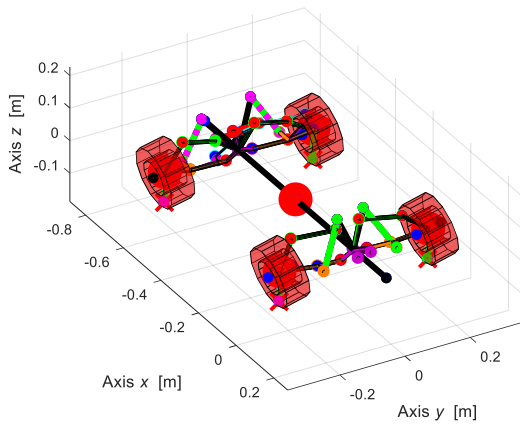
**Mode 1 - 1.582 Hz**



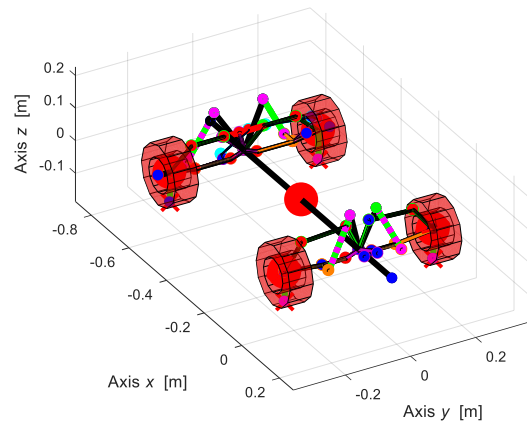
**Mode 2 - 2.084 Hz**



**Mode 3 - 3.95 Hz**



**Mode 4 - 15.27 Hz**



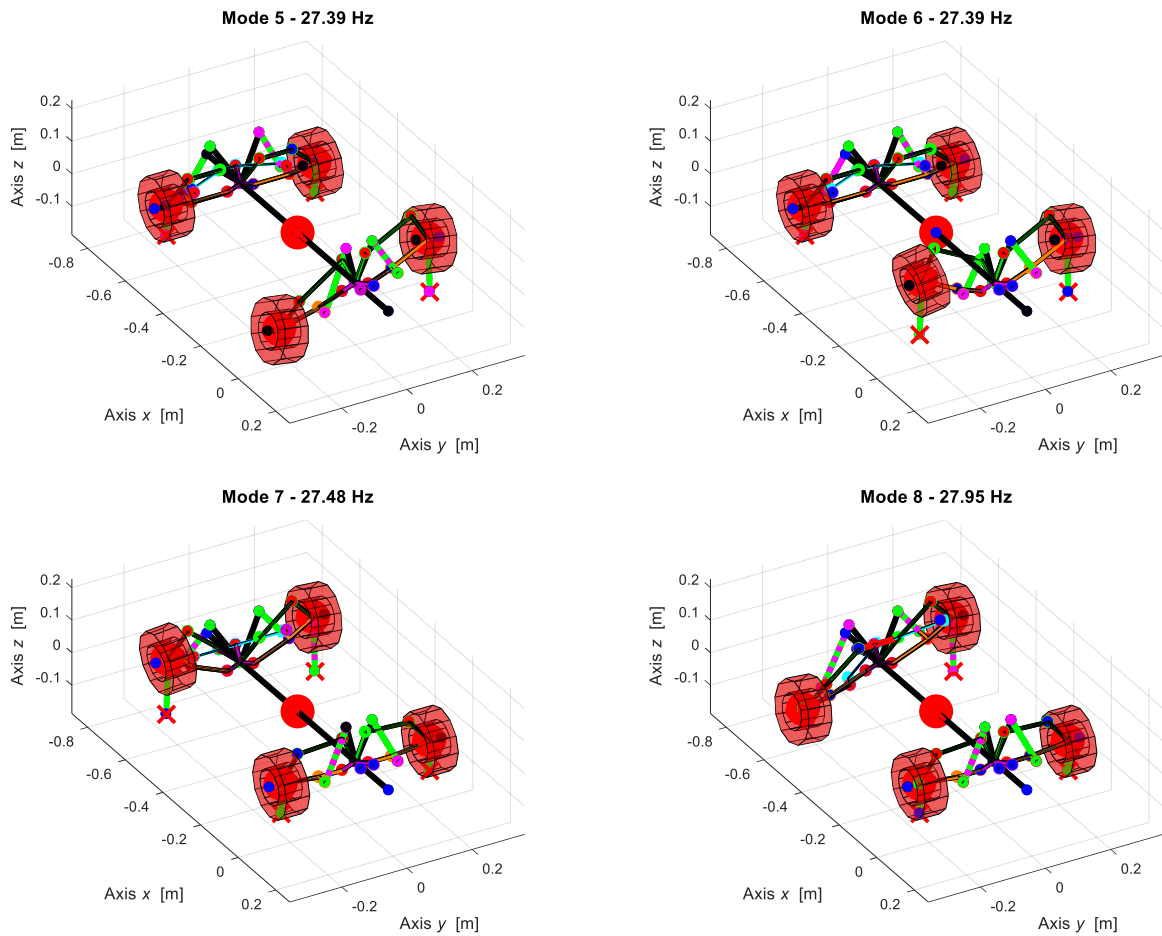


Figure 4.5.1 – Mode shapes

As for the previous case, the anti-roll bar reduces the entity of the rolling motion. In this case, there is also a little changing for the 3<sup>rd</sup> eigenvalue, the roll mode appears at a slightly lower frequency. A 4<sup>th</sup> mode appears for the torsion of the rear anti-roll bar, at a frequency lower than the front anti-roll bar. The modes of the unsprung masses are in the same order of the configuration without the anti-roll bars.

The considerations for the parametric analysis are the same done for to the case with the front anti-roll bars, the trend in fact is almost flat.

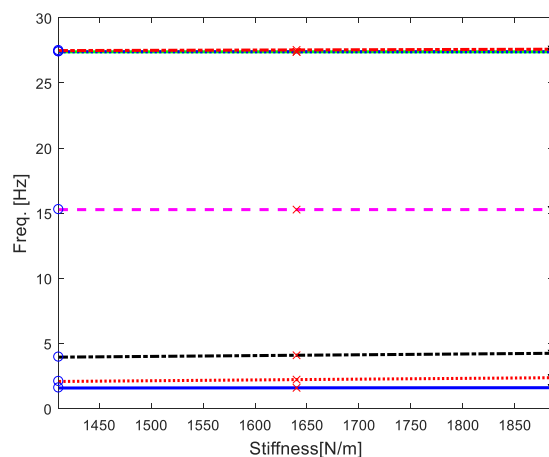


Figure 4.5.2 – Parametric analysis-fixed front blue (rear anti-roll-bar).

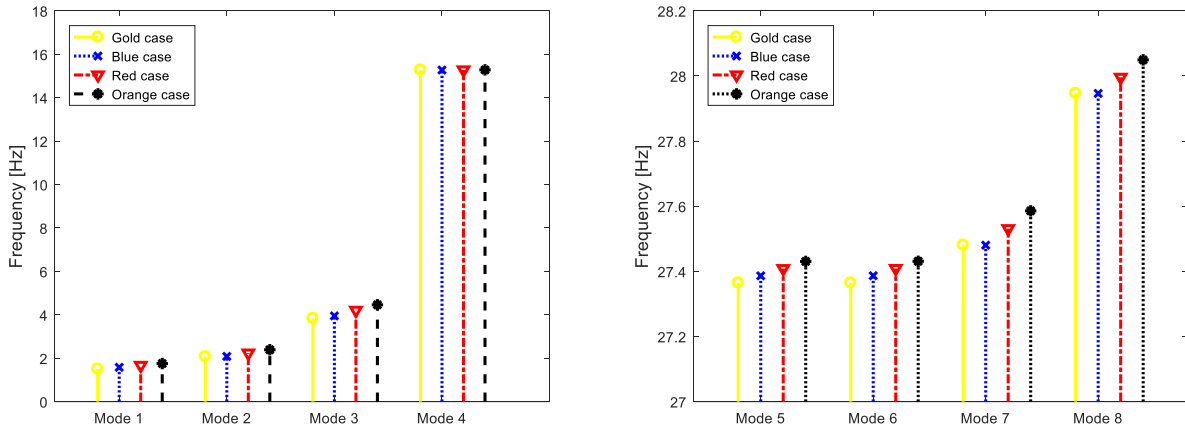


Figure 4.5.3 – Parametric analysis-comparing modes (rear anti-roll-bar).

Also in this case, the mode related to the torsion of the anti-roll bar is completely independent from the stiffness of the springs.

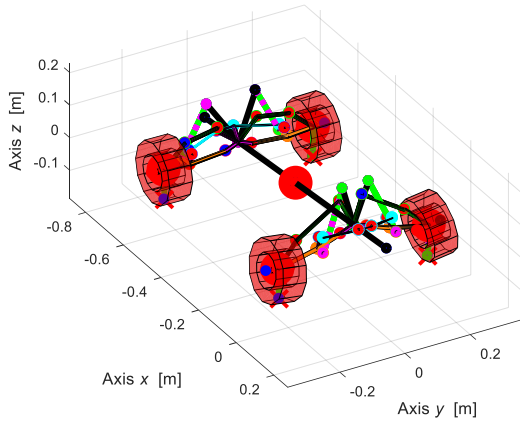
#### 4.6 Chassis case with both Anti-roll bars

The results are for the nominal configuration, so with blues springs both for front and rear and the rig-nut in the highest position. The first 9 vibrations modes and their frequencies are shown in the Figure 4.5.1, the frequencies' values are summarized in the Table 4.5.1.

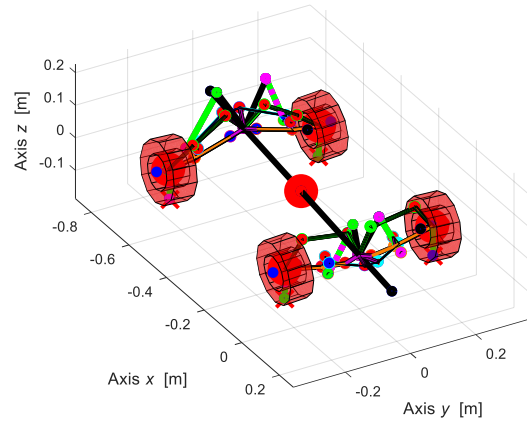
Table 4.5.1 – Natural frequencies of Chassis case with both Anti-roll bars.

Mode	$f_n$ [Hz]	Description
1	1.580	Chassis rebound and pitching
2	2.083	Chassis pitching
3	3.910	Chassis rolling
4	15.34	Rear Anti-roll bar torsion
5	19.97	Front Anti-roll bar torsion
6	27.38	Front suspensions in-phase
7	27.48	Rear suspensions in-phase
8	27.94	Front suspensions out-of-phase
9	27.96	Rear suspensions out of-phase

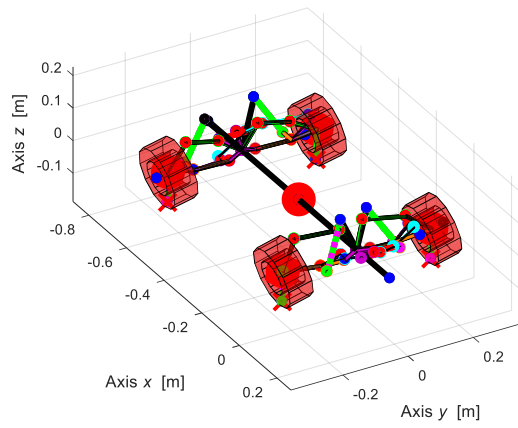
**Mode 1 - 1.579 Hz**



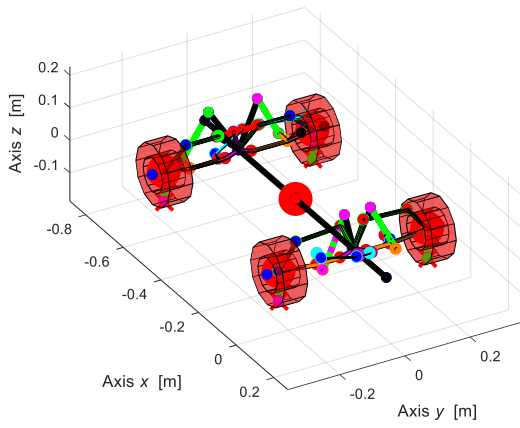
**Mode 2 - 2.083 Hz**



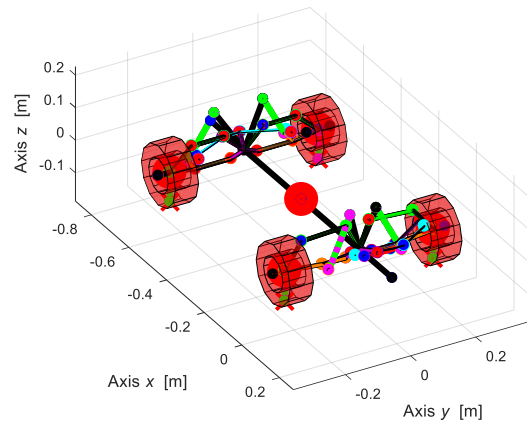
**Mode 3 - 3.91 Hz**



**Mode 4 - 15.34 Hz**



**Mode 5 - 19.97 Hz**



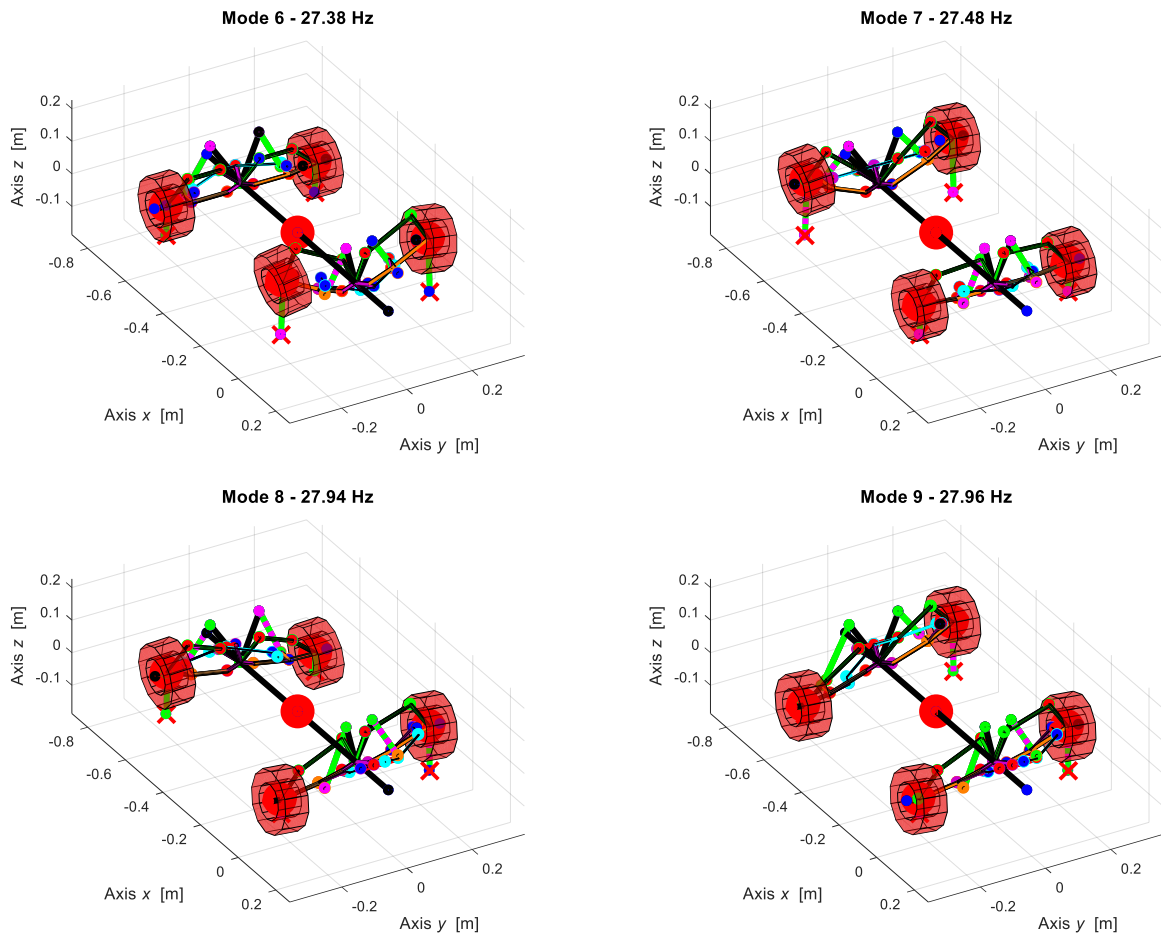


Figure 4.5.1 – Mode shapes

The torsion modes of the anti-roll bars occur at different frequencies values for the rear and the front bar, in particular the natural frequency for the rear one is lower than the front anti-roll bars, this is due to its length which is bigger than the length of the front bar. In fact, the torsional stiffness is inversely proportional to the length, so a big length means a low stiffness and so a low natural frequency.

The considerations for the parametric analysis are the same done for to the case with the front anti-roll bars, the trend in fact is almost flat, and the torsion modes do not depend from the stiffness of the springs.

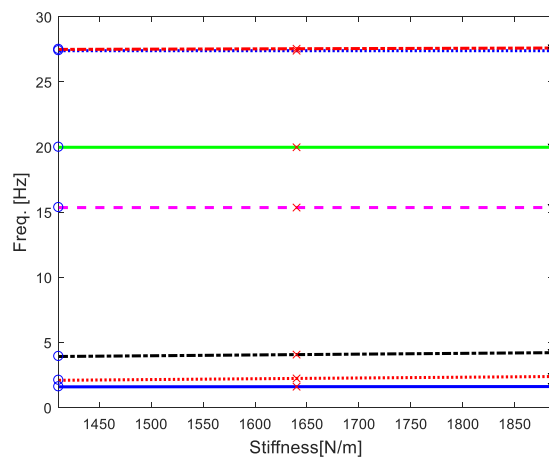


Figure 4.5.2 – Parametric analysis- fixed front blue (both anti-roll bars).

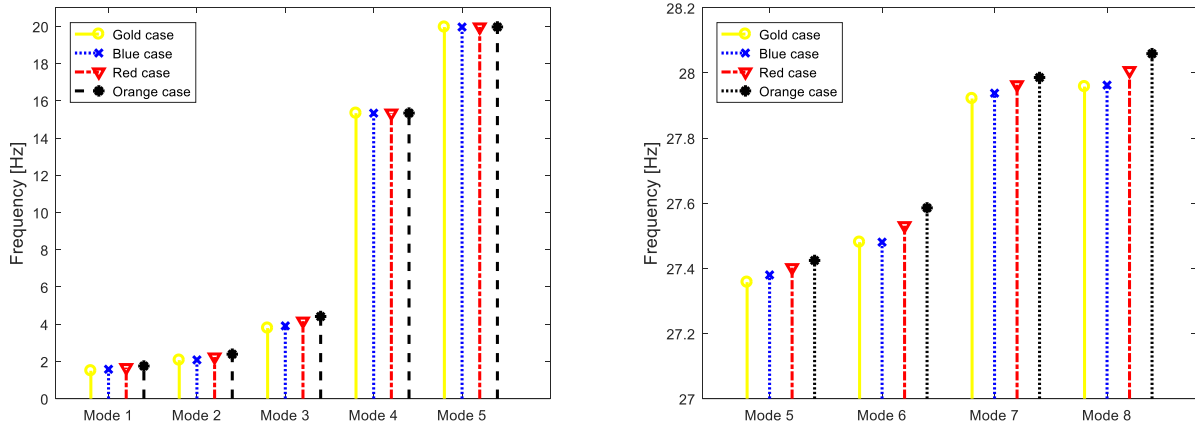


Figure 4.5.3 – Parametric analysis- comparing modes (both anti-roll bars).

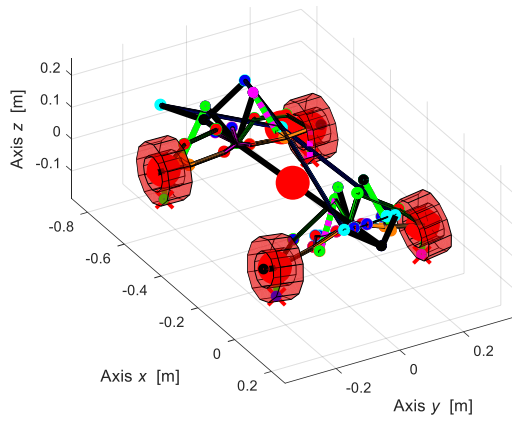
#### 4.7 Body case with Front Anti-roll bar

The results are for the nominal configuration, so with blues springs both for front and rear and the rig-nut in the highest position. The first 8 vibrations modes and their frequencies are shown in the Figure 4.7.1, the frequencies' values are summarized in the Table 4.7.1.

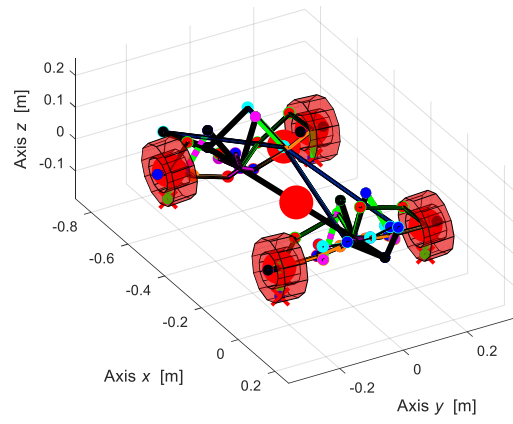
Table 4.7.1 – Natural frequencies of Body case with Front Anti-roll bar.

Mode	$f_n$ [Hz]	Description
1	1.460	Chassis rebound and pitching
2	1.843	Chassis pitching
3	3.081	Chassis rolling
4	19.71	Anti-roll bar torsion
5	27.38	Front suspensions in-phase
6	27.50	Rear suspensions out-of-phase
7	27.50	Rear suspensions in-phase
8	27.93	Front suspensions out-of-phase

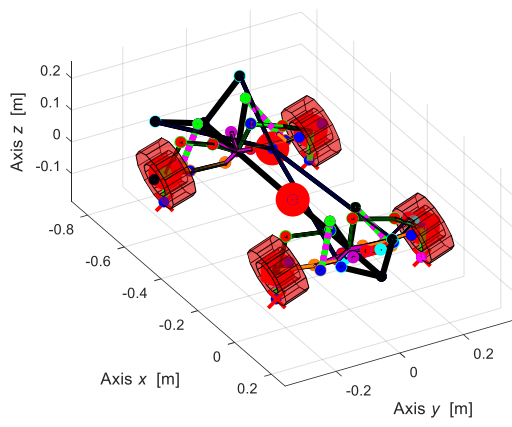
Mode 1 - 1.456 Hz



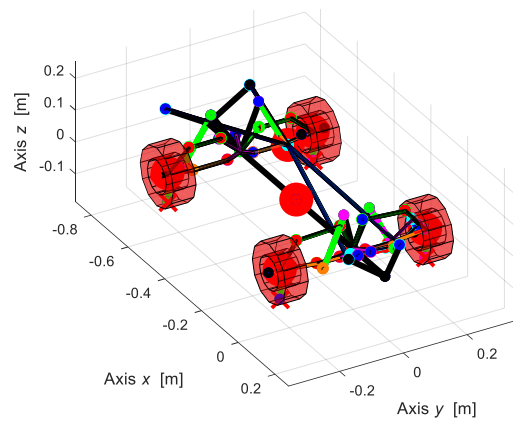
Mode 2 - 1.843 Hz



Mode 3 - 3.081 Hz



Mode 4 - 19.75 Hz



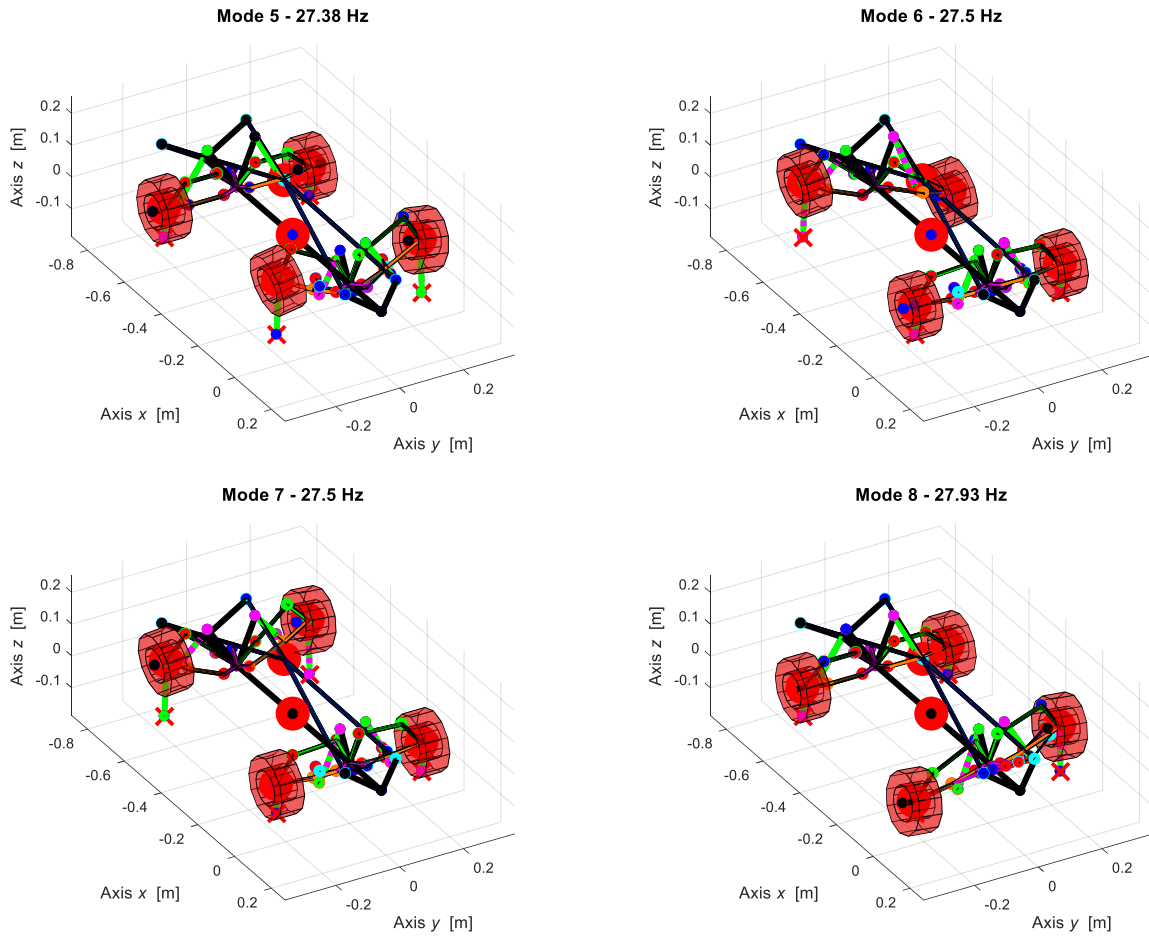


Figure 4.7.1 – Mode shapes.

As said for the chassis case, the entity of the rolling is reduced with respect to the case without the anti-roll bar, as expected, while the natural frequencies for the suspension modes change just a little. There is a 4<sup>th</sup> mode related to the torsion of the front anti-roll bar, at the same frequency of the chassis case, this because it is only inherent to the anti-roll bar. While the mode shapes for the unsprung mass appear in a different order with respect to the body case without anti-roll bars. The considerations for the parametric analysis are analogue to the case without anti-roll bars, the trend in fact is almost flat, and the anti-roll bar mode does not depend from the stiffness.

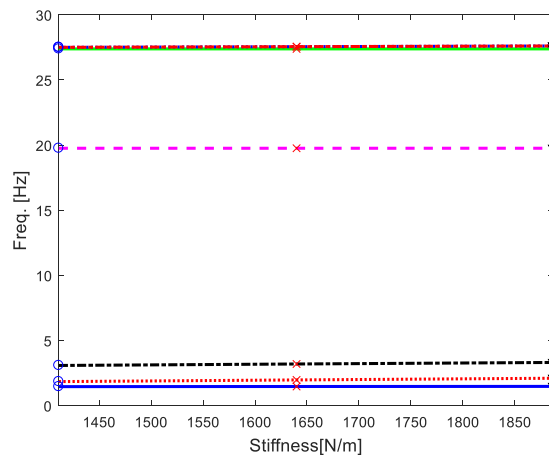


Figure 4.7.2 – Parametric analysis – fixed front blue (body case with front anti-roll).

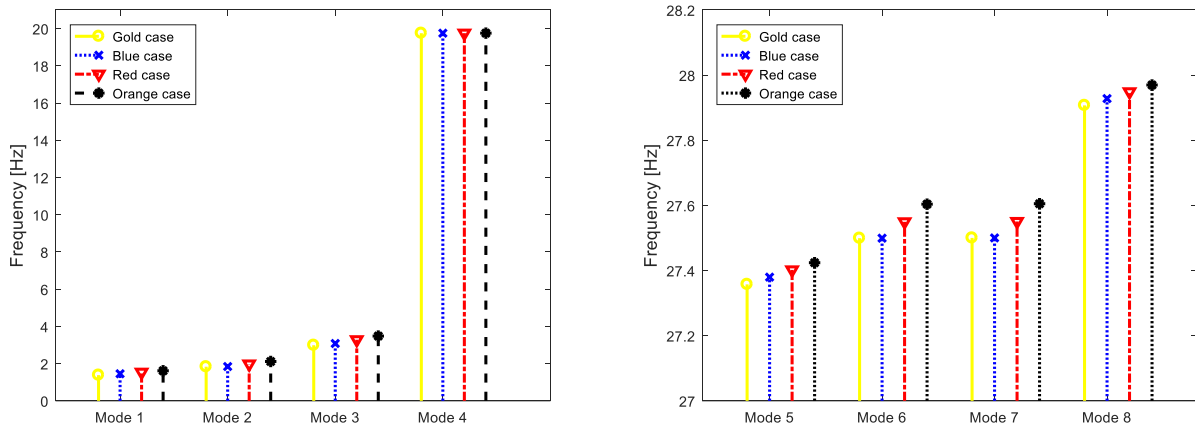


Figure 4.7.3 – Parametric analysis – comparing modes (body case with front anti-roll).

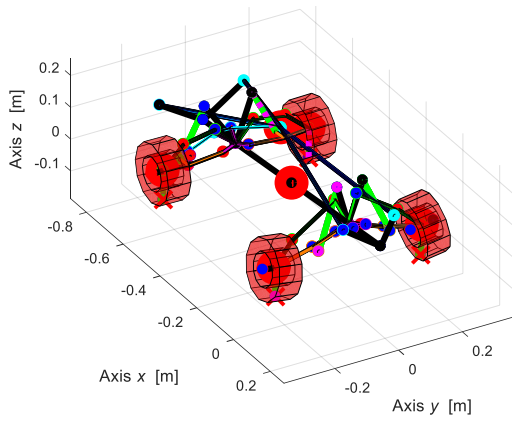
### 4.8 Body case with Rear Anti-roll bar

The results are for the nominal configuration, so with blues springs both for front and rear and the rig-nut in the highest position. The first 8 vibrations modes and their frequencies are shown in the Figure 4.8.1, the frequencies' values are summarized in the Table 4.8.1.

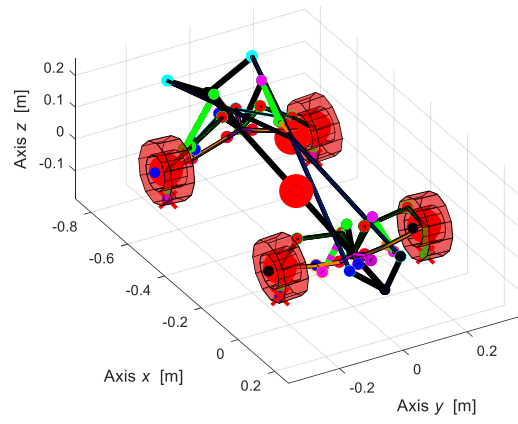
Table 4.8.1 – Natural frequencies of Body case with Rear Anti-roll bar.

Mode	$f_n$ [Hz]	Description
1	1.458	Chassis rebound and pitching
2	1.841	Chassis pitching
3	3.036	Chassis rolling
4	15.05	Anti-roll bar torsion
5	27.39	Front suspensions out-of-phase
6	27.39	Front suspensions in-phase
7	27.48	Rear suspensions out-of-phase
8	27.94	Rear suspensions in-phase

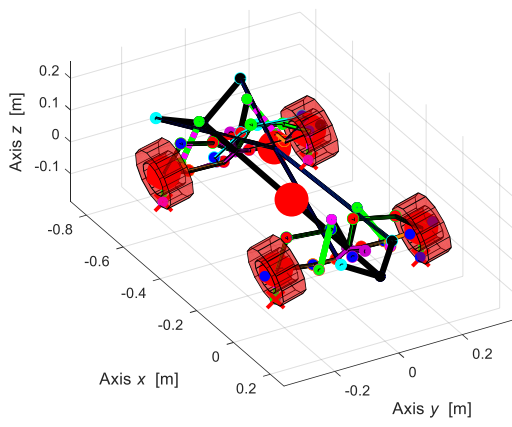
**Mode 1 - 1.458 Hz**



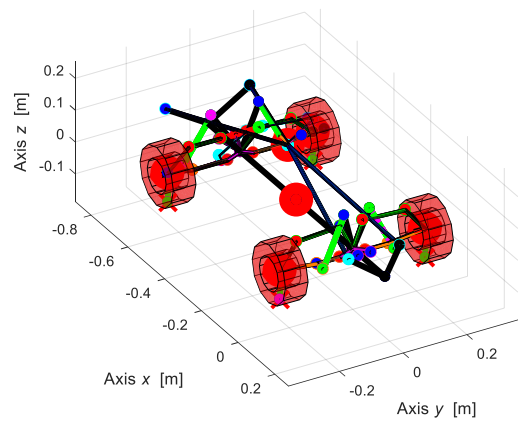
**Mode 2 - 1.841 Hz**



**Mode 3 - 3.058 Hz**



**Mode 4 - 15.12 Hz**



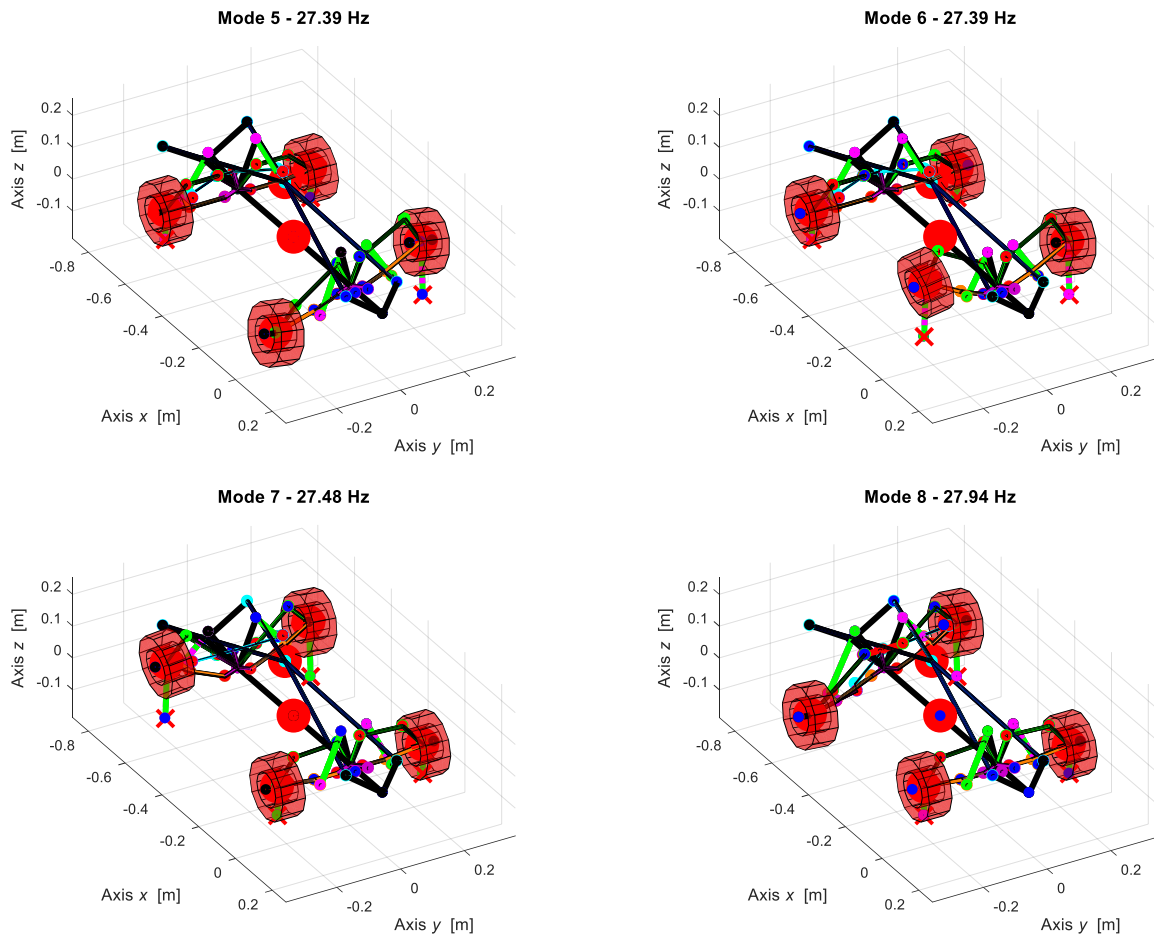


Figure 4.8.1 – Mode shapes.

As before, the entity of the rolling is reduced with respect to the case without the anti-roll bar and the natural frequencies change just a little. There is a 4<sup>th</sup> mode related to the torsion of the rear anti-roll bar, at the same frequency of the chassis case, this because it is only inherent to the anti-roll bar. The considerations for the parametric analysis are analogue to the case without anti-roll bars, the trend in fact is almost flat, and the anti-roll bar mode does not depend from the stiffness.

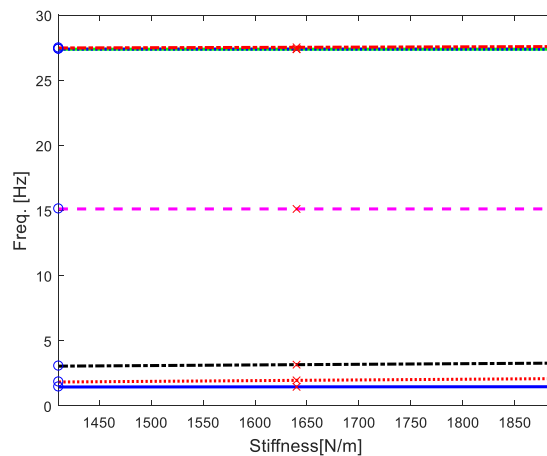


Figure 4.8.2 – Parametric analysis- fixed front blue (body case with rear anti-roll bar).

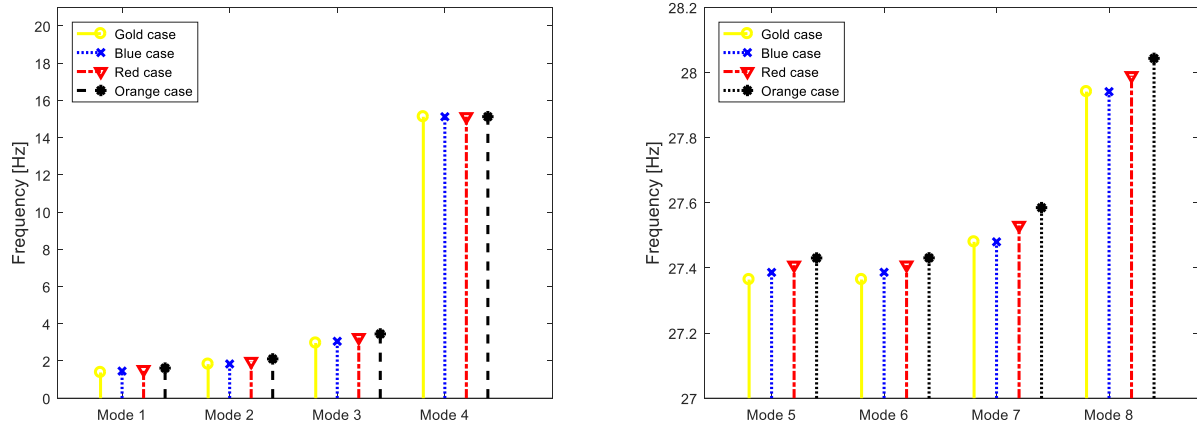


Figure 4.8.3 – Parametric analysis – comparing modes (body case with rear anti-roll).

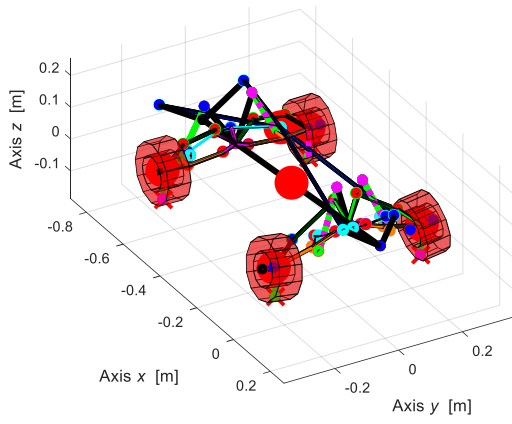
## 4.9 Body case with both Anti-roll bars

The results are for the nominal configuration, so with blues springs both for front and rear and the rig-nut in the highest position. The first 9 vibrations modes and their frequencies are shown in the Figure 4.9.1, the frequencies' values are summarized in the Table 4.9.1.

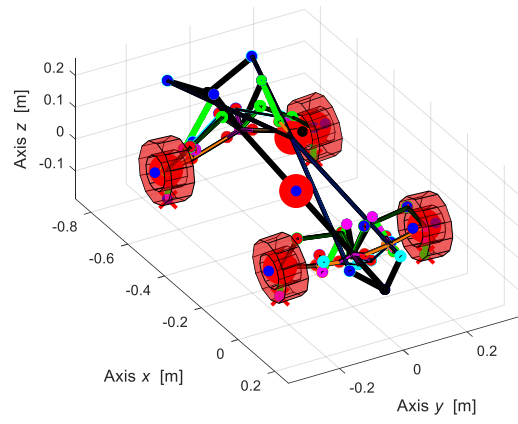
Table 4.9.1 – Natural frequencies of Body case with both Anti-roll bars.

Mode	$f_n$ [Hz]	Description
1	1.456	Chassis rebound and pitching
2	1.840	Chassis pitching
3	3.04	Chassis rolling
4	15.2	Rear Anti-roll bar torsion
5	19.87	Front Anti-roll bar torsion
6	27.38	Front suspensions out-of-phase
7	27.48	Front suspensions in-phase
8	27.94	Rear suspensions out-of-phase
9	27.95	Rear suspensions in-phase

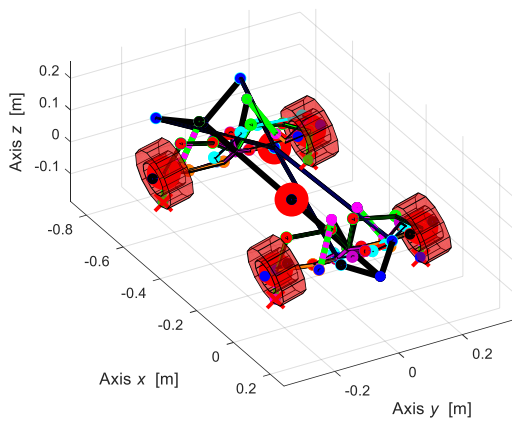
**Mode 1 - 1.456 Hz**



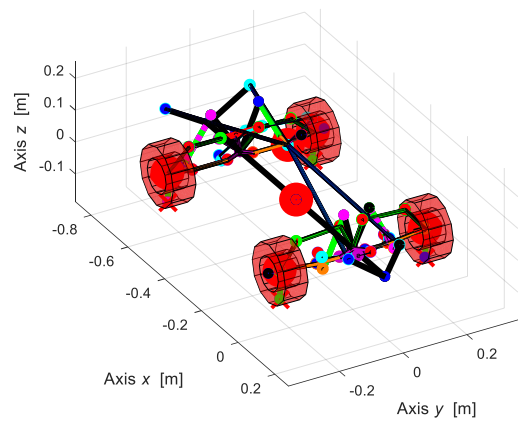
**Mode 2 - 1.84 Hz**



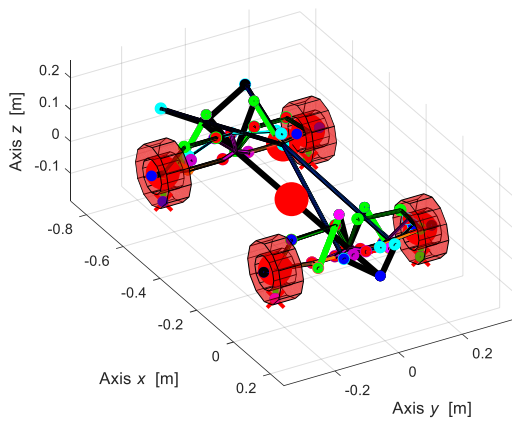
**Mode 3 - 3.04 Hz**



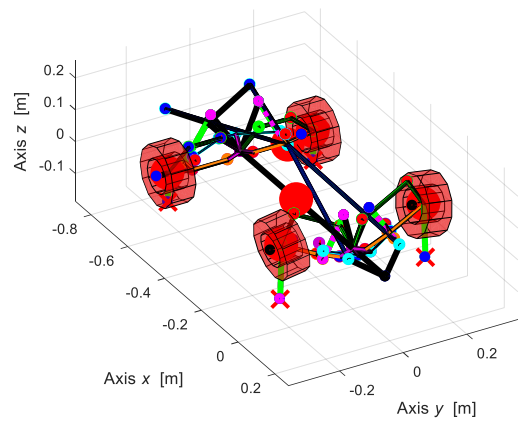
**Mode 4 - 15.2 Hz**



**Mode 5 - 19.87 Hz**



**Mode 6 - 27.38 Hz**



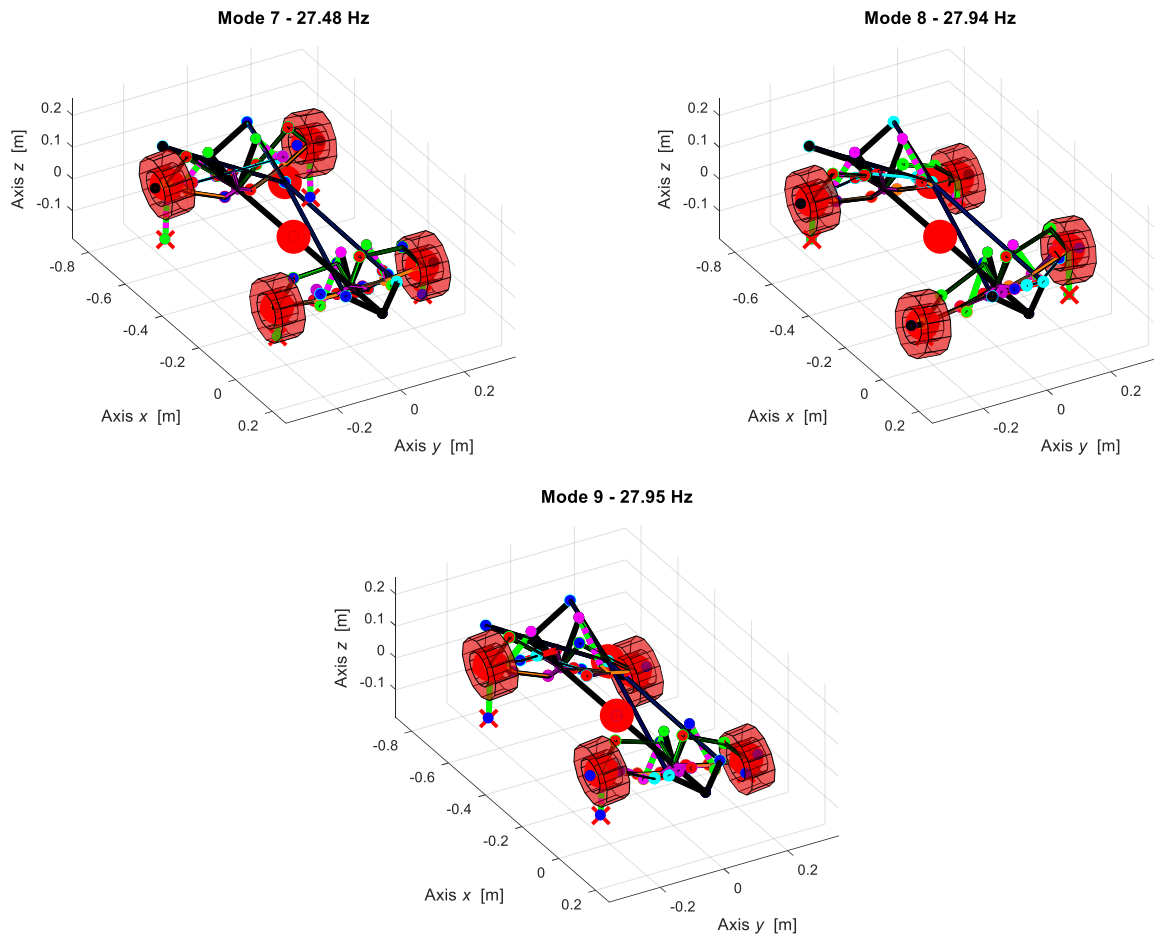


Figure 4.9.1 – Mode shapes.

The torsion modes of the anti-roll bars occur at different frequencies values for the rear and the front bar, in particular the natural frequency for the rear one is lower than the front anti-roll bars, this is due to its length which is bigger than the length of the front bar. In fact, the torsional stiffness is inversely proportional to the length, so a big length means a low stiffness and so a low natural frequency.

The considerations for the parametric analysis are the same done for to the case with the front anti-roll bars, the trend in fact is almost flat, and the torsion modes do not depend from the stiffness of the springs.

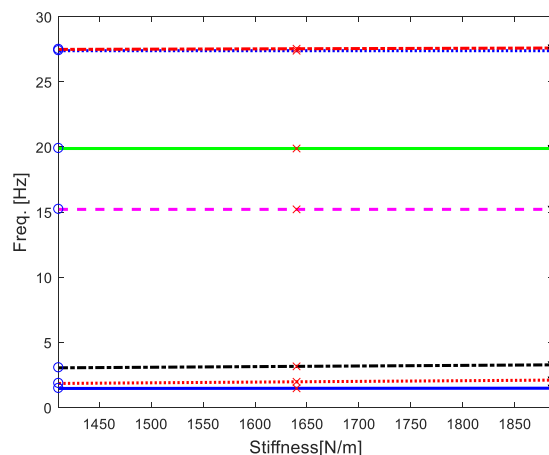


Figure 4.9.2 – Parametric analysis- fixed front blue (body case with both anti-roll bar).

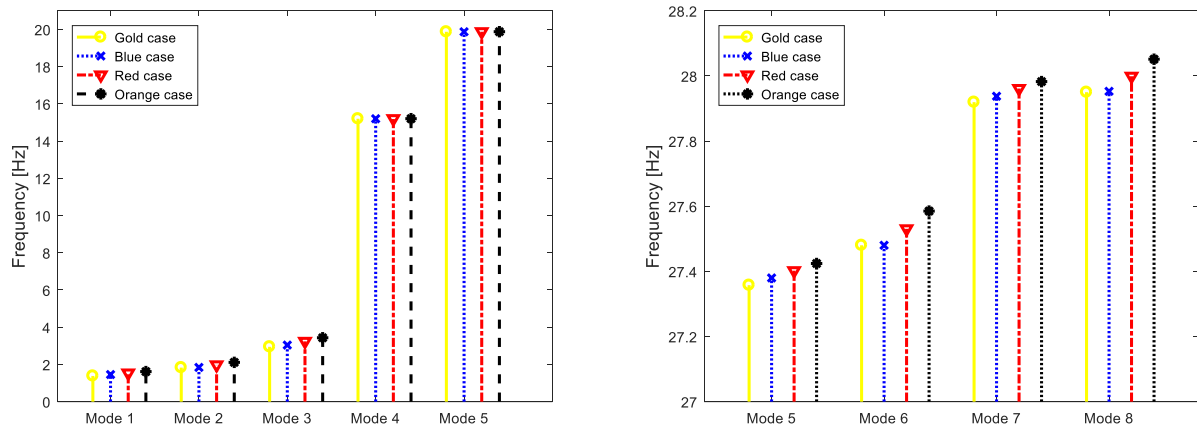


Figure 4.9.3 – Parametric analysis – comparing modes (body case with rear anti-roll).

## 5. Experimental Modal Analysis

In this chapter, the experimental modal analysis is described. The first step is building the setup for the measurements, then completing it by the addition of the acquisition system tools, and at the end acquire the data, processing them and finally making the rights considerations and modifications. At the end we can compare the experimental results with the numericals.

### 5.1 Setup for the measurement

In this paragraph the test rig built for the Experimental Modal Analysis is described. To make the construction of the setup faster and more effective, this was initially modelled in a CAD environment thanks to the software Solidworks.

The shaker must be able to stress the vehicle in different points, in particular it will press on the bottom main chassis, since its material is more appropriate than the plastic part for this kind of test. Moreover, we choose to operate from the bottom and not from the top because in the configurations where the body is present this would obstruct the passage of the shaker needle.

A sort of table is modelled to support the vehicle, this is made by aluminium beams and angular elements, on the top 4 plates are mounted and on these plates the wheels are leaned. A sort of table is also modelled for the shaker, this is to tie the shaker with rubber bands and make it float, in this way it does not receive other external forces (or at least they are minimum) and the natural frequencies of the shaker itself are very low, following the theory of experimental modal analysis. The shaker support must be able to slide inside the vehicle support to touch some points of the main chassis from underneath, modelling the setup in Solidworks allows us to figure out the overall dimensions required.

So the first step is modelling the simplified vehicle where only the main dimension are significant, such as the track, the length, the wheel thickness and diameters, the shape and the dimensions of the main chassis and its distance from the ground. Some data are taken from the previous Table 3.1.2, while others are measured in the laboratory.

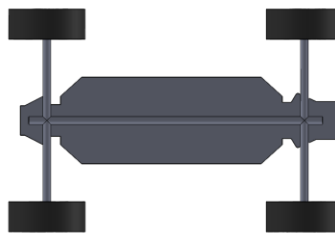


Figure 5.1.1 – Simplified Vehicle- bottom view.

The support for the vehicle is shown in Figure 5.1.2, the beams used are summarized in the Table 5.1.1.

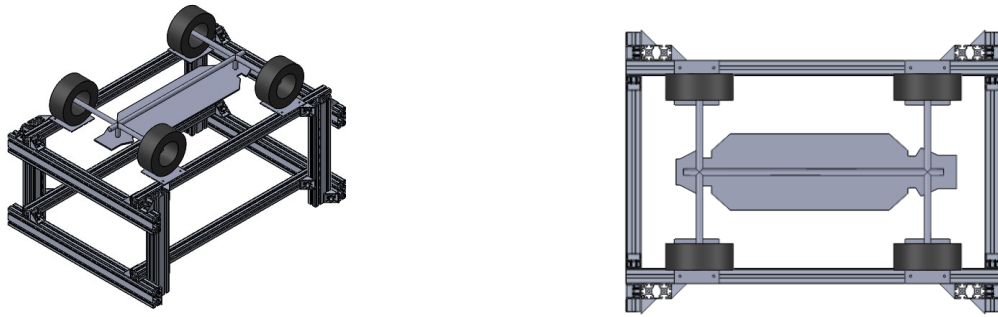


Figure 5.1.2 – Vehicle support model- isometric view (left) and top view (right).

Table 5.1.1 – Vehicle support description.

Beam description	Section	Length [cm]	Quantity [-]
Lateral	Single	100	4
Frontal	Double	75	4
Legs	Double	45	4
Angular	-	-	24

The support for the shaker is shown in Figure 5.1.3, the beams used are summarized in Table 5.1.2.

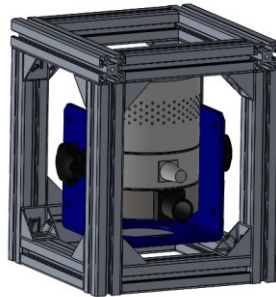


Figure 5.1.3 – Shaker support model.

Table 5.1.2 – Shaker support description.

Beam description	Section	Length [cm]	Quantity [-]
Lateral	Single	20	5
Back	Double	20	1
Top	Single	28	2
Legs	Single	30	4
Angular	-	-	16

In the following figure it is possible to see the entire setup with the shaker support inside the vehicle support.

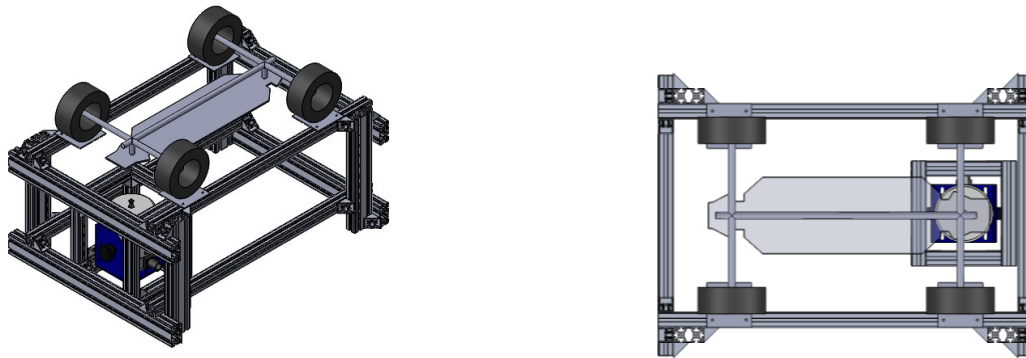


Figure 5.1.4 – Entire setup.

The stinger of the shaker is enough long to reach the main chassis. When the shaker will work, not only the vehicle will be subjected to vibrations but also its support, for this reason it can be useful to know in advance the first natural frequencies of the table, in order to discriminate them during the tests. A modal analysis is run in Solidworks, the first 4 frequencies are reported in Table 5.1.3, the mode shapes in Figure 5.1.5.

Table 5.1.3 –Natural frequencies of the vehicle support.

Mode	$f_n$ [Hz]
1	104.8
2	139
3	160
4	170

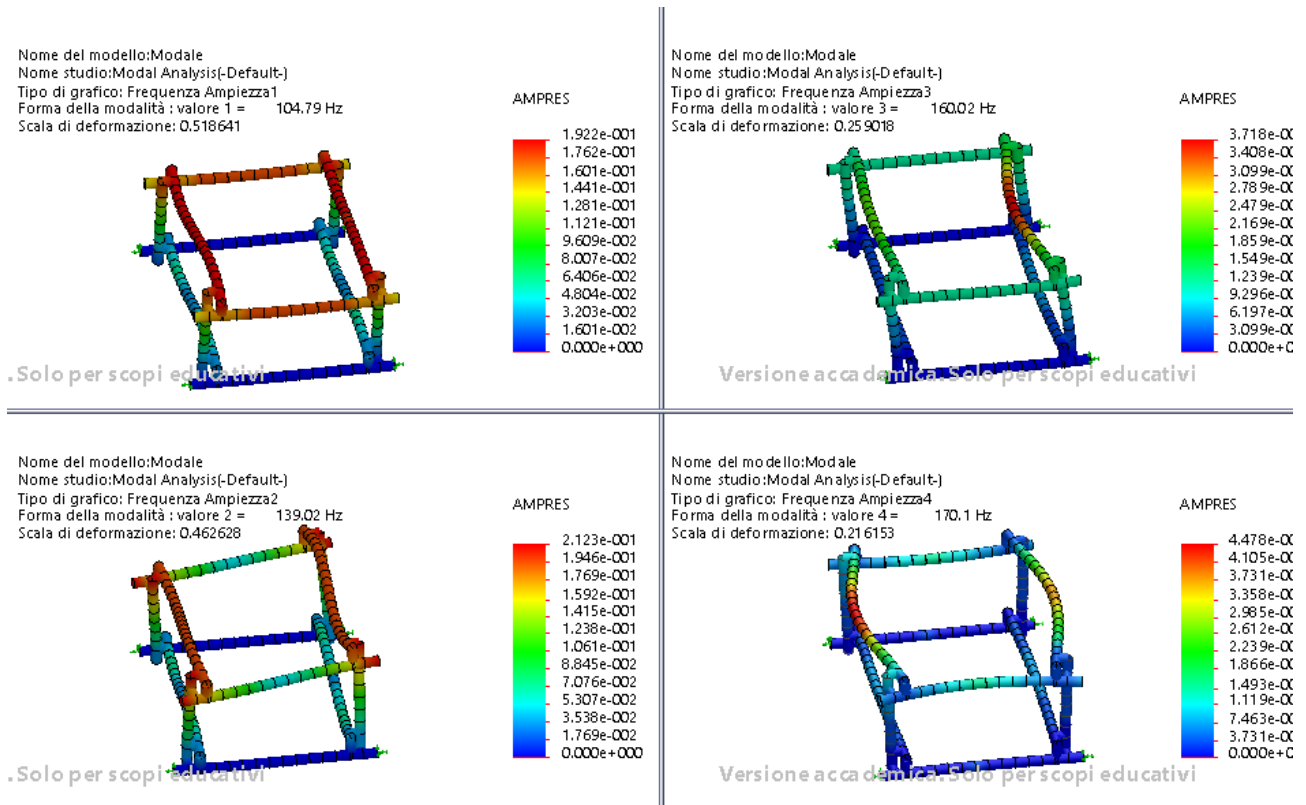


Figure 5.1.5 – Mode shapes for the vehicle support.

The next step is providing all the parts and assemble them. The aluminium beams are available in different lengths, some of these have to be cut. The plates for the wheel are made out of a scrap metal foil found in the mechanical workshop, whose thickness is 5 mm. Two more angular beams are used than the Solidworks model to avoid the movement of two legs. Special focus has been spent on the distances during the building of the structures to match all the parts.

In the Figure 5.1.6 the metal foil is shown, it has been firstly cleaned of screws and handles and then the plates are sketched on it. Then, in Figure 5.1.7 and 5.1.8 the support structures are shown.



Figure 5.1.6 – Metal foil for the wheel plates.



Figure 5.1.7 – Vehicle support.

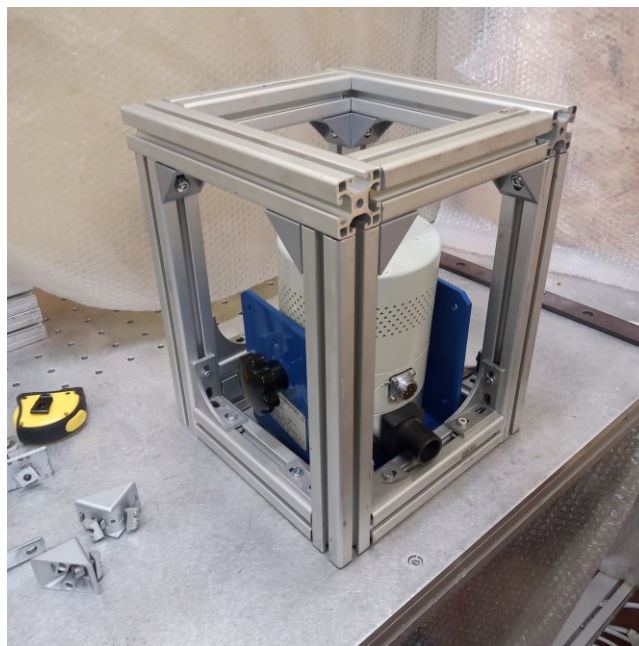


Figure 5.1.8 – Shaker support.

## 5.2 Data acquisition system

Once the supports are done, it is possible to fix the accelerometers and set all the acquisition system. The shaker is tie to the support by some elastic ropes, taking care to let it float without bending over, then the stinger is stuffed into the shaker. The shaker is positioned under the vehicle inside its support. On the chassis plate there are already two holes, one has to be enlarged, it is possible to use them to attach the load cell which is screwed to the top of the stinger. Then the accelerometers are fixed on the vehicle, they are linked to the channels of the Scadas, so as the load cell.

The acquisition system is made by:

- *Personal Computer*: where the software “TestLab17” is installed;
- *8 accelerometers and 1 load cell*: 4 accelerometers are put on the wheel-hubs on the metal parts, 4 accelerometers are put on the chassis plate placed in a symmetric position, the load cell is located on the stinger;
- *Acquisition controller Siemens Simcenter SCADAS*: this component is the core of the control system. It can receive, process, and emit signals. It is continuously in communication with the Siemens control program “LMS Testlab (vers. 2017)”. The program permit to distinguish an input signal by treats it as a reference from another one that can be trat as a response. In input it takes the signals from the accelerometers and the load cell, it is linked to the personal computer by an ethernet cable and the output cable is linked to the shaker amplifier;
- *Shaker Amplifier*: the signal of the shaker is processed by the amplifier which increase it of a value that can be decided by the user through a physical knob located in the front of the device, the maximum settable gain on the amplifier is 10;



Figure 5.2.1 – Acquisition system – real picture.

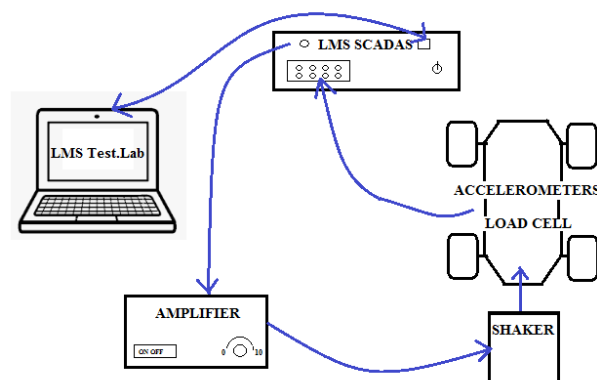


Figure 5.2.2 – Acquisition system – scheme.

In the Figure 5.2.3 the accelerometers are highlighted in red, the point highlighted in green is the first point used for the load cell, this hole was already available on the chassis, the yellow point is the other load cell possible position, this hole is made by a drilling machine.

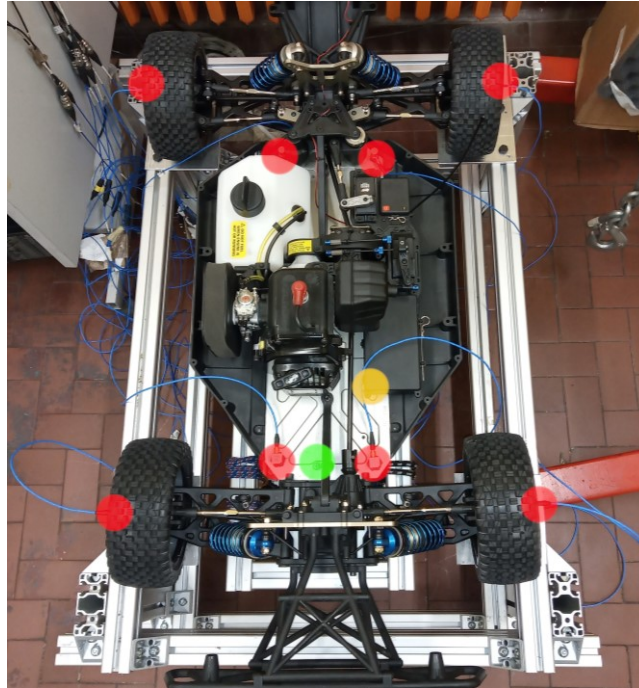


Figure 5.2.3 – Accelerometers and load cells highlight.

In Figure 5.2.4 it is possible to see a detail of the wheel, the accelerometer is fixed on the nut because it is the only metal part (proper for the vibration measurements) and the wheel is rotated so that the face on which the accelerometer rests is perpendicular to the z axis. While in Figure 5.2.5 there is a detail of the shaker stinger with the load cell.

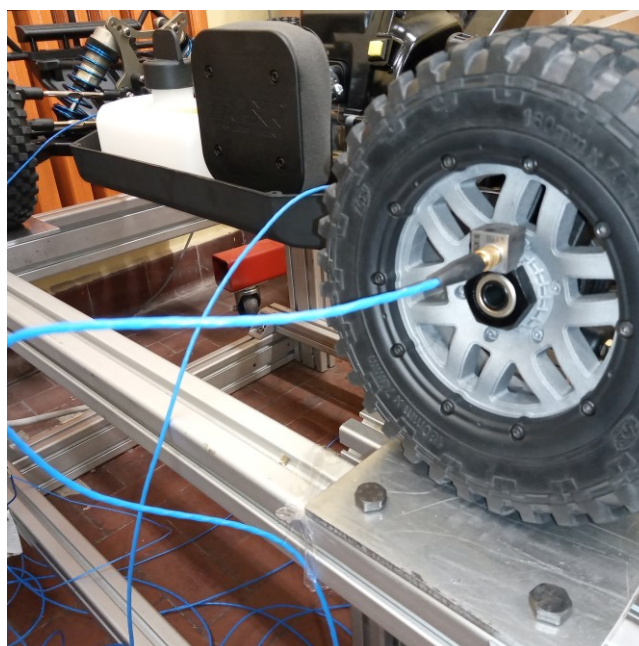


Figure 5.2.4 – Detail of rear left wheel.

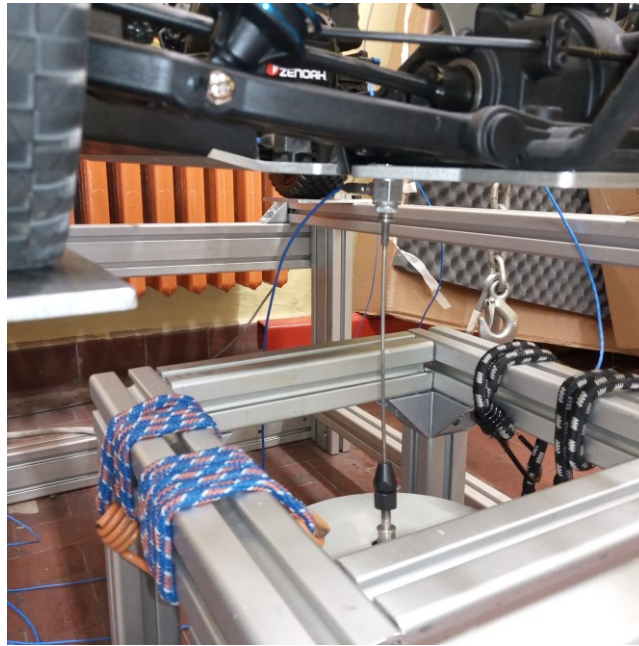


Figure 5.2.5 – Detail of the load cell.

In the Table 5.2.1, the accelerometers used are indicated and their relative channel of the SCADAS. The channel 7 is skipped because it is out of order, on the channel 10 is linked the load cell whose sensitivity is equal to 2.316 mV/N. Due to the lack of enough numbers of channels, we can get only one directional output, so only the z-axis cable of every accelerometer is linked.

Table 5.2.1 – Accelerometers.

Location		Channel	Model	Serial number	Sensitivity [mV/g]
Wheel	Front Left	1	356A24	191143	10.31
	Front Right	2	356A24	191142	10.31
	Rear Left	3	356A15	LW226919	98.6
	Rear Right	4	356A15	LW226918	102.3
Chassis	Rear Left	5	356A15	LW139287	99.3
	Rear Right	6	356A15	LW139286	99.5
	Front Right	8	352C33	LW148801	100.1
	Front Left	9	352C33	LW148802	99.5

The location of the accelerometers and the load cell is indicated into the Table 5.2.2, the reference system is the same of the vehicle, so the x-axis is the symmetry axis of the vehicle with the same travel direction, y-axis is the lateral axis and the z-axis is given by the triad, the origin is in correspondence of the front wheel center on the axis of symmetry. Then a scheme is also shown in the Figure 5.2.6. The locations of these components are useful because it is possible to insert them into the project of the software and by a simple sketch visualize the modes of the vehicle.

Table 5.2.2 – Location of accelerometers and load cells.

Point	Location	X [m]	Y [m]	Z[m]
-------	----------	-------	-------	------

1	Wheel	Rear Right	-0.305	-0.228	0
2		Front Right	+0.305	-0.228	0
3		Front Left	+0.305	+0.228	0
4		Rear Left	-0.305	+0.228	0
5	Chassis	Rear Right	-0.225	-0.065	-0.05
6		Front Right	+0.245	-0.065	-0.05
7		Front Left	+0.245	+0.065	-0.05
8		Rear Left	-0.225	+0.065	-0.05
9	Load cell	Central	-0.235	+0.015	-0.05
10		Lateral	-0.125	-0.07	-0.05

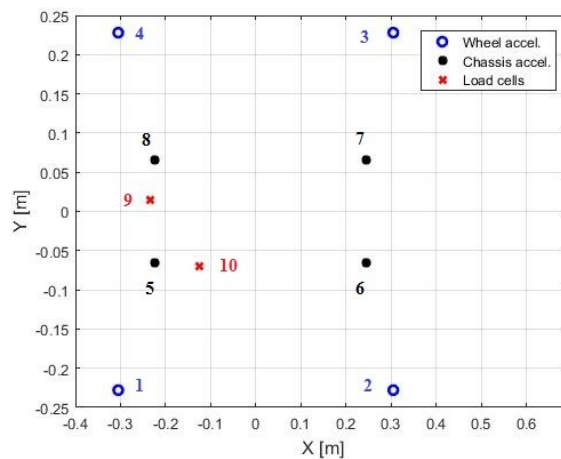


Figure 5.2.6 – Accelerometers and load cells location.

So, the first step is turn on the SCADAS, then turn on the Shaker amplifier and turn the gain from 0 V to 5 V. After it is possible to run Test.Lab and set up the project.

### 5.3 Measurements and considerations

In this paragraph all the tests conducted on the vehicle are described. At the end of each test description some considerations are done that bring to the next test.

As told in the previous paragraph, the software used to obtain the modal acquisitions and process the result is *LMS Test.Lab v.17*, specifically the modulus “MIMO Sweep & Stepped Sine Testing” in “Test.Lab Structures Acquisition” is used.

In the TestLab project, named “2020-11-17\_stepped\_losi\_5ive” there are three sections:

- Point9: the tests with the load cell located in the point 9 (almost central position) are performed;
- Point10: the tests with the load cell located in the point 10 (lateral position) are performed.
- Point10\_shaker\_fixed: the tests with new shaker setup and the load cell located in the point 10 are performed.

#### 5.3.1 Test 1: Point 9

In this test the load cell is placed in point 9 (refer to Figure 5.2.6) and the accelerometers are placed as shown in Figure 5.2.3.

The first step is building a simplified geometry of the acquisition system (section Geometry), so the nodes where the accelerometers and the possible points for the load cells are made knowing their locations (Table 5.2.2), then a simplified sketch is done linking by lines the chassis points and the wheels points and add a surface, as shown in the Figure 5.3.1.



Figure 5.3.1.1 – LMS - Simplified geometry.

Then, the signals which come from the sensors to the SCADAS have to be defined, it is done in Channel Setup section. In this case, the active channels are 9, from 1 to 10 except for the 7 which is out-of-run. The accelerometers and the load cell are not powered sensor, so ICP is the input mode. The Measured Quantity for the accelerometers is the acceleration, and for the load cell it is the Force. Channel Setup window is reported in the figure below, where the load cell is located at point 9 in this section.

PhysicalChannelId	OnOff	Reference	User channel Id	ChannelGroupId	Point	Direction	Input mode	Measured Quantity	Electrical Unit	Actual sensitivity	Transducer Type	Transducer Manu...
1	<input checked="" type="checkbox"/>	<input type="checkbox"/>		Measure	1.3	+Z	ICP	Acceleration	mV	10.31 mV/g		
2	<input checked="" type="checkbox"/>	<input type="checkbox"/>		Measure	1.2	+Z	ICP	Acceleration	mV	10.31 mV/g		
3	<input checked="" type="checkbox"/>	<input type="checkbox"/>		Measure	1.4	+Z	ICP	Acceleration	mV	98.6 mV/g		
4	<input checked="" type="checkbox"/>	<input type="checkbox"/>		Measure	1.1	+Z	ICP	Acceleration	mV	102.3 mV/g		
5	<input checked="" type="checkbox"/>	<input type="checkbox"/>		Measure	1.8	+Z	ICP	Acceleration	mV	99.3 mV/g		
6	<input checked="" type="checkbox"/>	<input type="checkbox"/>		Measure	1.5	+Z	ICP	Acceleration	mV	99.5 mV/g		
7	<input type="checkbox"/>	<input type="checkbox"/>		Measure	1.7	None	Voltage AC	Acceleration	mV	100 mV/g		
8	<input checked="" type="checkbox"/>	<input type="checkbox"/>		Measure	1.6	+Z	ICP	Acceleration	mV	100.1 mV/g		
9	<input checked="" type="checkbox"/>	<input type="checkbox"/>		Measure	1.7	+Z	ICP	Acceleration	mV	99.5 mV/g		
10	<input checked="" type="checkbox"/>	<input checked="" type="checkbox"/>		Control	1.9	+Z	ICP	Force	mV	2.316 mV/N		
11	<input type="checkbox"/>	<input type="checkbox"/>		Measure	Point11	None	Voltage AC	Acceleration	mV	100 mV/g		
12	<input type="checkbox"/>	<input type="checkbox"/>		Measure	Point12	None	Voltage AC	Acceleration	mV	100 mV/g		
13	<input type="checkbox"/>	<input type="checkbox"/>		Measure	Point13	None	Voltage AC	Acceleration	mV	100 mV/g		
14	<input type="checkbox"/>	<input type="checkbox"/>		Measure	Point14	None	Voltage AC	Acceleration	mV	100 mV/g		
15	<input type="checkbox"/>	<input type="checkbox"/>		Measure	Point15	None	Voltage AC	Acceleration	mV	100 mV/g		
16	<input type="checkbox"/>	<input type="checkbox"/>		Measure	Point16	None	Voltage AC	Acceleration	mV	100 mV/g		

Figure 5.3.1.2 – Channel Setup window

The following picture represents the MIMO Sine Setup window.

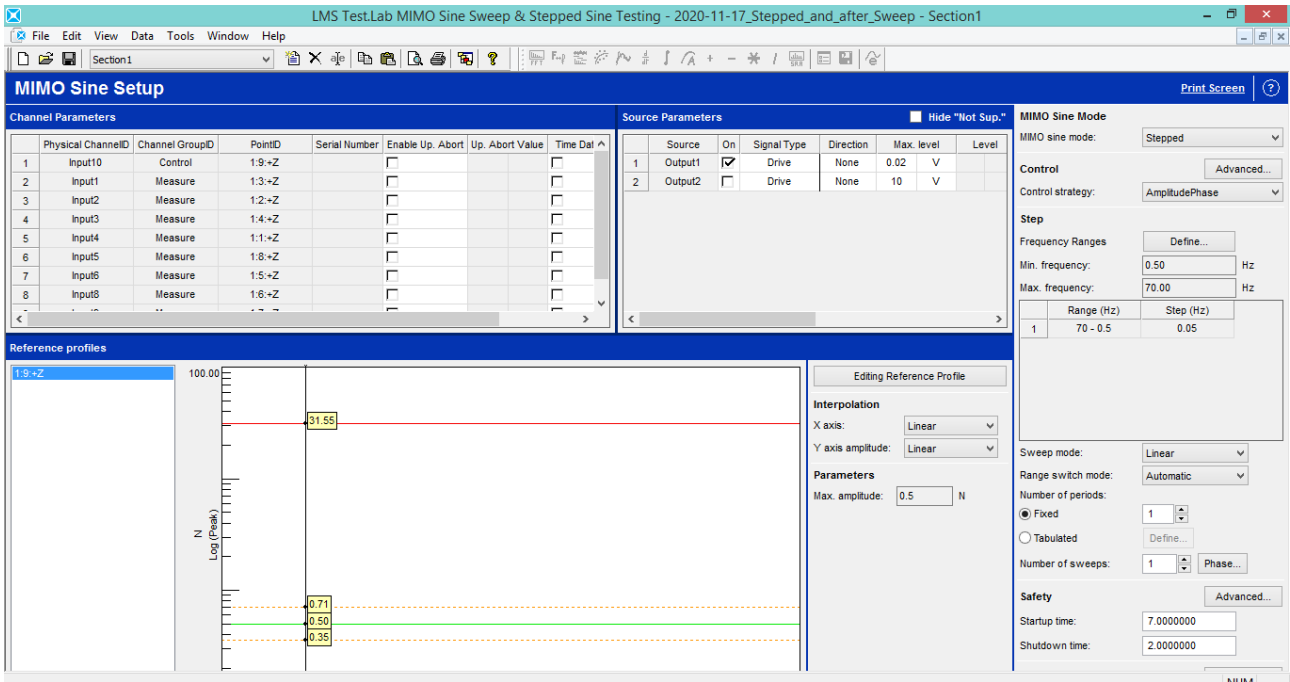


Figure 5.3.1.3 – MIMO Sine Setup window.

The MIMO sine mode can be chosen between “Swept” and “Stepped”, for the first test the “stepped mode” has been adopted. Firstly, in the right column, some parameters have to be defined:

- the control strategy
- the frequency limits in terms of Min and Max value [Hz].

In Editing Reference Profile, the frequency range [Hz] (bigger than the frequency limits) and the oscillation amplitude [N] are defined.

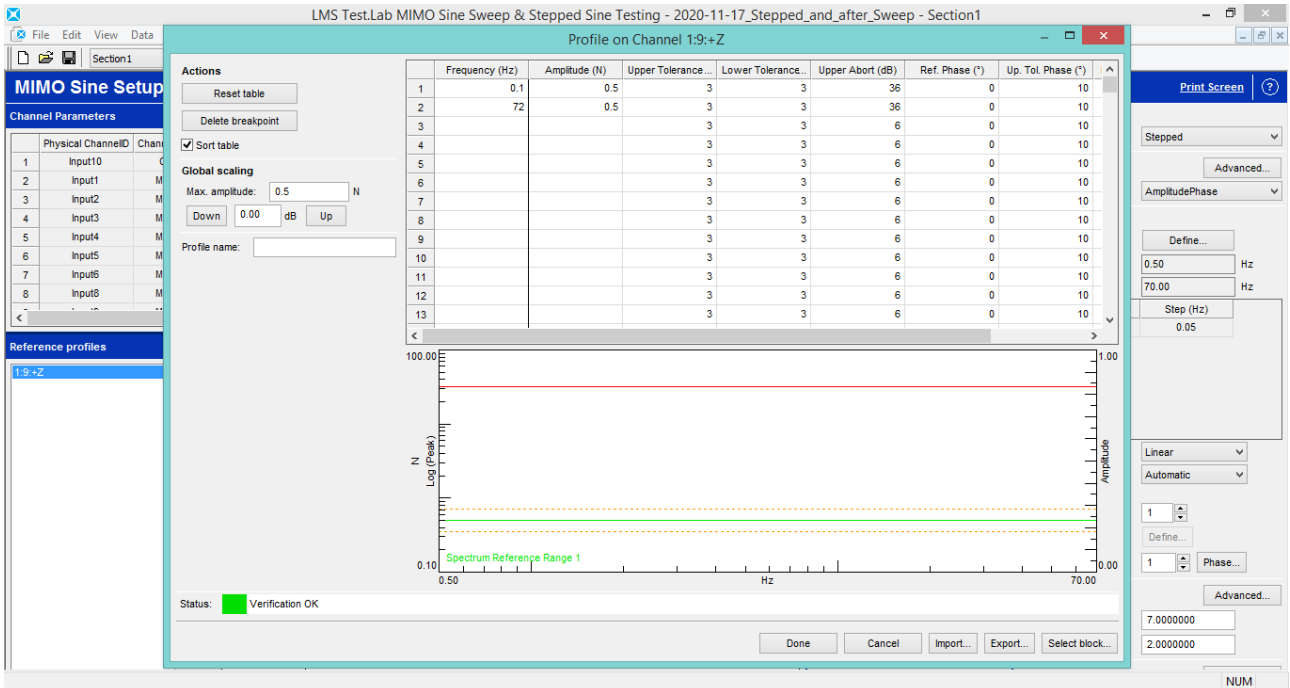


Figure 5.3.1.4 – MIMO Sine Setup Edit Reference Profile window.

Notice that a force equal to 0.5 N has been chosen, with this low value the movement of the vehicle will not be visible to unaided eye, in this way we operate in the small deformation field and the non-linearity can be neglected.

Then, in System Identification section a random input is applied to the system by the shaker in order to characterize the components and its response, in this way we are sure that the vehicle tested and the shaker are well controlled, get good and accurate results and will not get damaged.

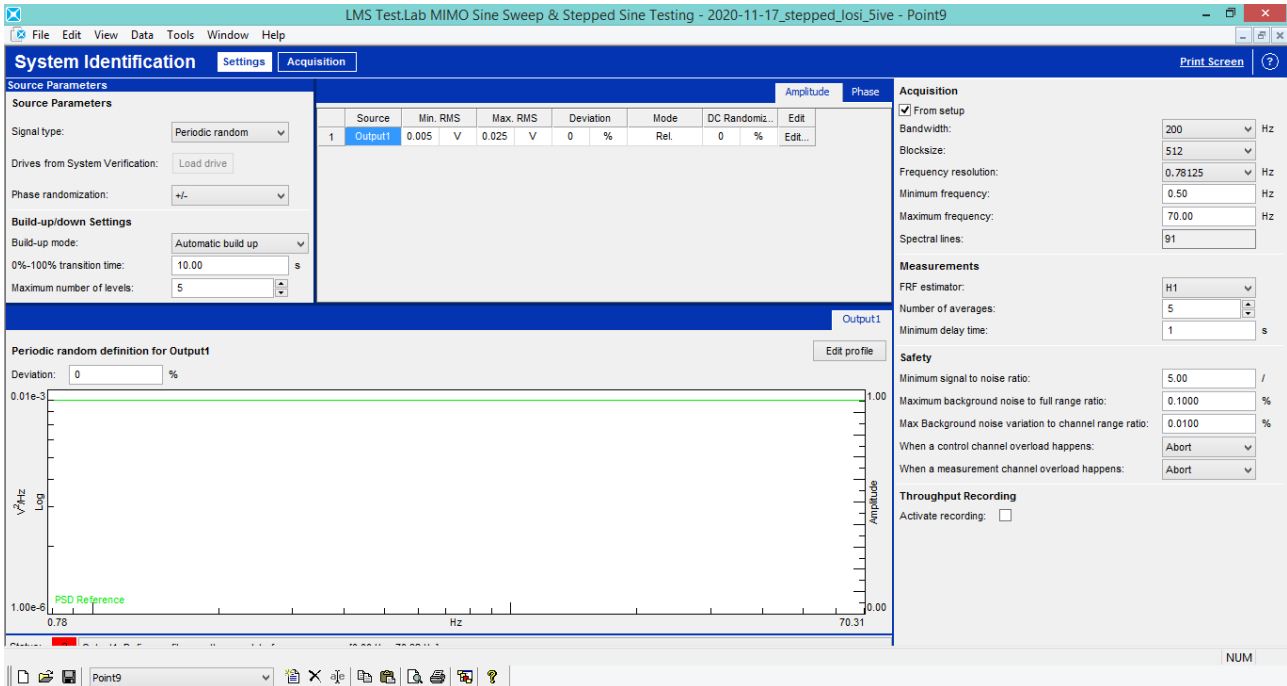


Figure 5.3.1.5 – System Identification window.

The System Identification is carried out following the path reported below.

Acquisition >> Arm >> Start

This phase lasts several minutes during which the software indicates Building up and the shaker works.

The system identification performed is verified in System Verification section.

Finally, in MIMO Sine Acquisition the test on the vehicle is performed.

The MIMO Sine Acquisition is carried out following the path reported below.

MIMO Sine Acquisition >> Arm >> Start

For each step (0.05 Hz), the software makes 5 iterations for 5 time to control the voltage that gives the imposed force. So, it goes from 70 Hz to 0.5 Hz by a step of 0.05 Hz in more iteration, moreover the time increases exponentially for lower frequencies, that makes the test really long, in fact to complete just one test around 13 hours have been spent.

Once the acquisition ended up, it is possible to save it. Then, a swept test is made to get more refined FRFs curves, giving in input the force profile got from the stepped test. Then in PolyMAX section it is possible to elaborate the data. The path is reported below:

PolyMAX >> Band >> Change Modal Data Selection >> Refresh

The sum of the FRFs functions of each accelerometer is shown in Figure 5.3.1.6.

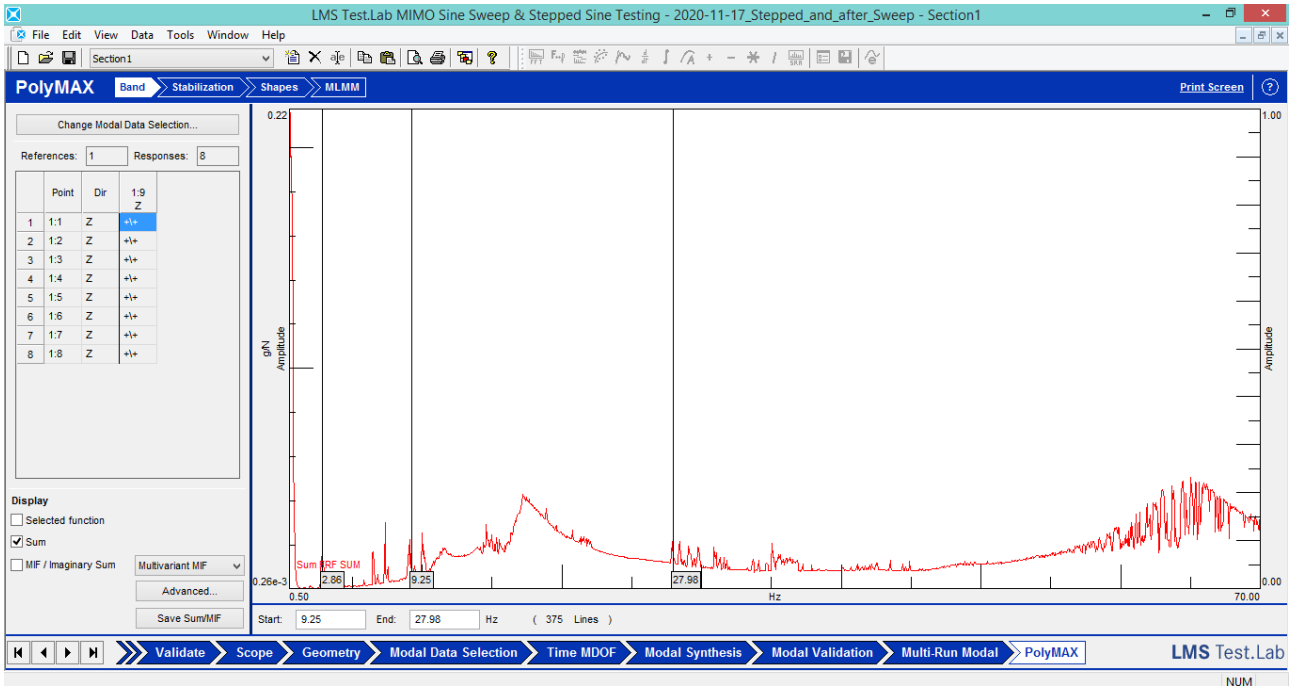


Figure 5.3.1.6 – PolyMAX Band window.

Then, following the path, the stabilization diagram is shown, it is selected the band between 0.50 and 70.00 Hz with a number of poles equal to 150.

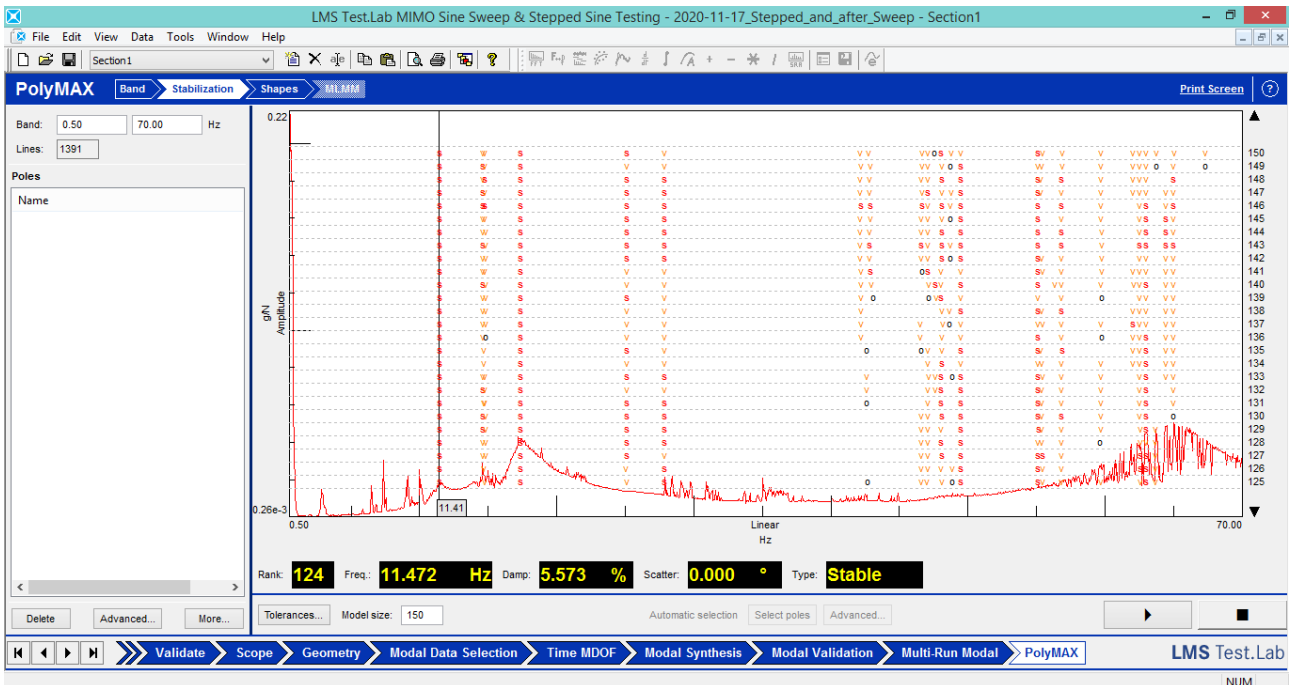


Figure 5.3.1.7 – PolyMAX Stabilization 150 poles window.

The first frequency according to this diagram is 11.4 Hz, we expected to see results at lower frequencies as obtained in the numerical model, for this reason we can try to increase the number of poles.

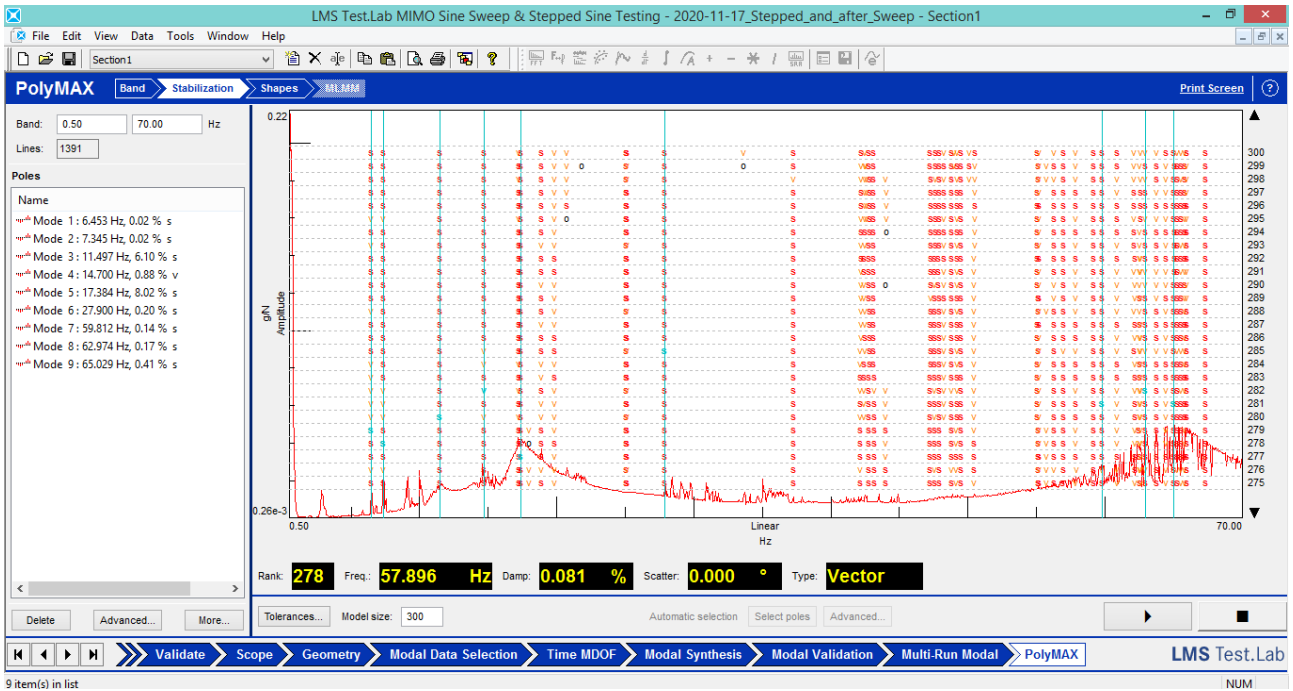


Figure 5.3.1.8 – PolyMAX Stabilization 300 poles window.

Even increasing to 300 poles, the first frequency readable on the diagram is higher than the first numerical frequency, anyway we can select the poles and in the next section of PolyMAX we can see the modal Shapes to understand if at the selected frequencies there are some relevant modes. In PolyMAX Shapes we can visualize real or complex results, the complex results are more appropriate since the vehicle is a damper system but the real shapes are easier to recognize because the nodes moves in phase, it is possible to note that only some of the selected frequencies are relevant, these and their damping ratio are reported in the Table 5.3.1.1.

Table 5.3.1.1 – Experimental Modal results – Stepped and Swept at point9 load cell.

Mode	$f_n$ [Hz]	$\xi$ [%]	Description
1	11.5	6.10	Chassis rebound
2	17.4	8.02	Chassis pitching
3	56.95	0.31	Front and rear suspension in-phase
4	59.8	0.14	Rear suspension in-phase

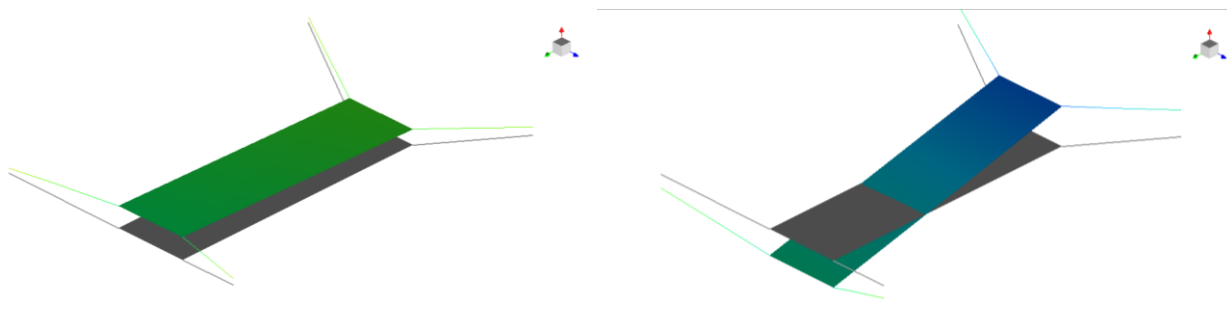


Figure 5.3.1.9 – Chassis rebound (left) and pitch (right).

The Chassis rebound and the pitching are really clear (Figure 5.3.1.9), the Chassis rolling is not so clear most probably due to the location of the load cell, in fact in this case it is located at Point 9 that is almost central, the suspension modes are visible just partially, the front and rear out-of-phase are missing, it could depend by the position of the load cell as well, or maybe they appear at frequencies out of our band investigation.

The values got experimentally are really distant from the ones got numerically, in fact the numerical frequencies for the Chassis case with both antiroll-bars were 1.57 Hz for the Chassis rebound, 2.083 Hz for the Chassis pitching and 3.91 for the Chassis rolling. For this reason, it is worth to make some investigations to find out why there is so much discrepancy.

The first hypothesis is that something went wrong building the numerical model, so we have to be sure that the numerical model is correct, for this reason we can consider a very simplified theoretical case and compare the numerical results with the theoretical ones. We consider a 4 DOF theoretical model and insert as parameters the known mass and stiffnesses, so we can get the eigenvalues from the problem using Matlab.

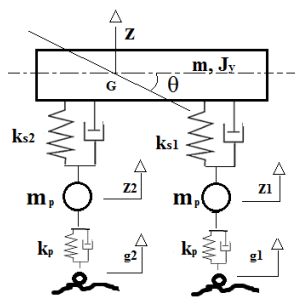


Figure 5.3.1.10 – Simplified Vehicle 4 DOFs.

The matrices of mass and stiffness are the following:

$$M = \begin{bmatrix} m & 0 & 0 & 0 \\ & J_y & 0 & 0 \\ & & m_p & 0 \\ \text{symm} & & & m_p \end{bmatrix} \quad (5.3.1.1)$$

$$K = \begin{bmatrix} k_{s1} + k_{s2} & -k_{s1}a + k_{s2}b & -k_{s1} & -k_{s2} \\ & k_{s1}a^2 + k_{s2}b^2 & k_{s2}a & -k_{s2}b \\ & & k_p + k_{s1} & 0 \\ \text{symm} & & & k_p + k_{s2} \end{bmatrix} \quad (5.3.1.2)$$

The suspension stiffness ( $k_{s1}$  and  $k_{s2}$ ) is obtained considering the inclination of the spring, as shown in Eq.3.2.9, and then the IR (Installation Ratio).

Table 5.3.1.2 – Parameters for the 4DOFs modal.

Parameter	Value	Unit	Description
$k_p$	36554	[N/m]	Tyres stiffness
$a$	0.305	[m]	Front semi-wheelbase

b	0.305	[m]	Rear semi-wheelbase
ks <sub>1</sub>	534	[N/m]	Front Blue suspensions stiffness
ks <sub>2</sub>	840.5	[N/m]	Rear Blue suspensions stiffness
m	11.95	[kg]	Sprung mass
m <sub>p</sub>	1.2475	[kg]	Unsprung mass of two wheels

The tyres and suspensions stiffness are obtained multiplying the single value twice because it is a bicycle model, the formulas to calculate the suspension stiffness from the z-component spring (Table.3.2.5) is below.

$$k_{s1} = 2 * k_z * IR \quad (5.3.1.3)$$

$$IR = \left( \frac{c}{d} \right)^2 \quad (5.3.1.4)$$

Table 5.3.1.3 – Parameters for the suspensions stiffness.

Parameter	Value	Unit	Description
IR <sub>f</sub>	0.147	[-]	Front installation ratio
IR <sub>r</sub>	0.342	[-]	Rear installation ratio
c <sub>f</sub>	0.072	[m]	Front arm spring - chassis
d <sub>f</sub>	0.188	[m]	Front arm wheel – spring
c <sub>r</sub>	0.11	[m]	Rear arm spring - chassis
d <sub>r</sub>	0.188	[m]	Rear arm wheel – spring

Thanks to the Matlab function *eig(K,M)* we get the eigenvalues and so the frequencies, reported in the following table.

Table 5.3.1.4. – Natural frequencies for 4DOFs model.

Mode	f <sub>n</sub> [Hz]	Description
1	1.62	Car rebound
2	2.20	Car pitching
3	27.44	Front wheel mode
4	27.56	Rear wheel mode

The theoretical results are really close to the numerical results, for this reason it is possible to assert that the numerical model is well done, its cinematic is correct, the results we get are rights for the parameters used.

A second hypothesis is that we have to focus the experimental analysis on the lower frequency. So the next step is making an acquisition between 0.5 and 30 Hz exciting the structure in the point 10, which is in a lateral position and so at least the rolling mode should be more clear.

### 5.3.2 Test 2: Point 10

In this paragraph the second test is described. In this case we focus the attention on the frequency range between 0.5 and 30 Hz, the load cell is located at the point 10, whose coordinate is reported in the Table 5.2.2, while the locations of the accelerometers are the same of the previous test.

The geometry already exists, so in this case the first step is create a new section of the project file, this will be named “Point10”, following this path:

## Navigator >> Create New Section

In Channel Setup we change the input 10, switching the point 10 instead of the point 9.  
The MIMO Sine Setup window is set, the values chosen are readable from the following picture.

**Channel Parameters**

Physical ChannelID	Channel GroupID	PointID	Serial Number	Enable Up. Abort	Up. Abort Value	Time Data
1	Input10	Control	1:10+Z	<input type="checkbox"/>		<input type="checkbox"/>
2	Input1	Measure	1:3+Z	<input type="checkbox"/>		<input type="checkbox"/>
3	Input2	Measure	1:2+Z	<input type="checkbox"/>		<input type="checkbox"/>
4	Input3	Measure	1:4+Z	<input type="checkbox"/>		<input type="checkbox"/>
5	Input4	Measure	1:1+Z	<input type="checkbox"/>		<input type="checkbox"/>
6	Input5	Measure	1:8+Z	<input type="checkbox"/>		<input type="checkbox"/>
7	Input6	Measure	1:5+Z	<input type="checkbox"/>		<input type="checkbox"/>
8	Input8	Measure	1:6+Z	<input type="checkbox"/>		<input type="checkbox"/>
9	Input9	Measure	1:7+Z	<input type="checkbox"/>		<input type="checkbox"/>

**Source Parameters**

Source	On	Signal Type	Direction	Max. level	Control C.		
1	Output1	<input checked="" type="checkbox"/>	Drive	None	0.05	V	1:10+Z
2	Output2	<input type="checkbox"/>	Drive	None	10	V	1:10+Z

**MIMO Sine Mode**

MIMO sine mode: Stepped

Control: Advanced...

Control strategy: Amplitude

**Step**

Frequency Ranges: Define...

Min. frequency: 0.50 Hz

Max. frequency: 30.00 Hz

Range (Hz)	Step (Hz)	
1	30 - 0.5	0.05

Sweep mode: Linear

Range switch mode: Automatic

Number of periods: Fixed 1

Number of sweeps: 1

**Safety** Advanced...

Startup time: 7.0000000

Shutdown time: 3.0000000

**Measure** Advanced...

System:  FRF

Coherence

Structure:  Autopower  FRF  THD

Crosspower  Coherence

**Throughput Recording** Advanced...

Activate recording:

**Reference profiles**

1:10+Z

Amplitude (Peak) vs. Hz

Editing Reference Profile

Interpolation: X axis: Linear, Y axis amplitude: Linear

Parameters: Max. amplitude: 0.5 N

Status: 9 Minimum control frequency is lower than High-pass 0 dB frequency of 3.70 Hz on channel 1:3+Z

Figure 5.3.2.1 – MIMO Sine Setup window - Test 2.

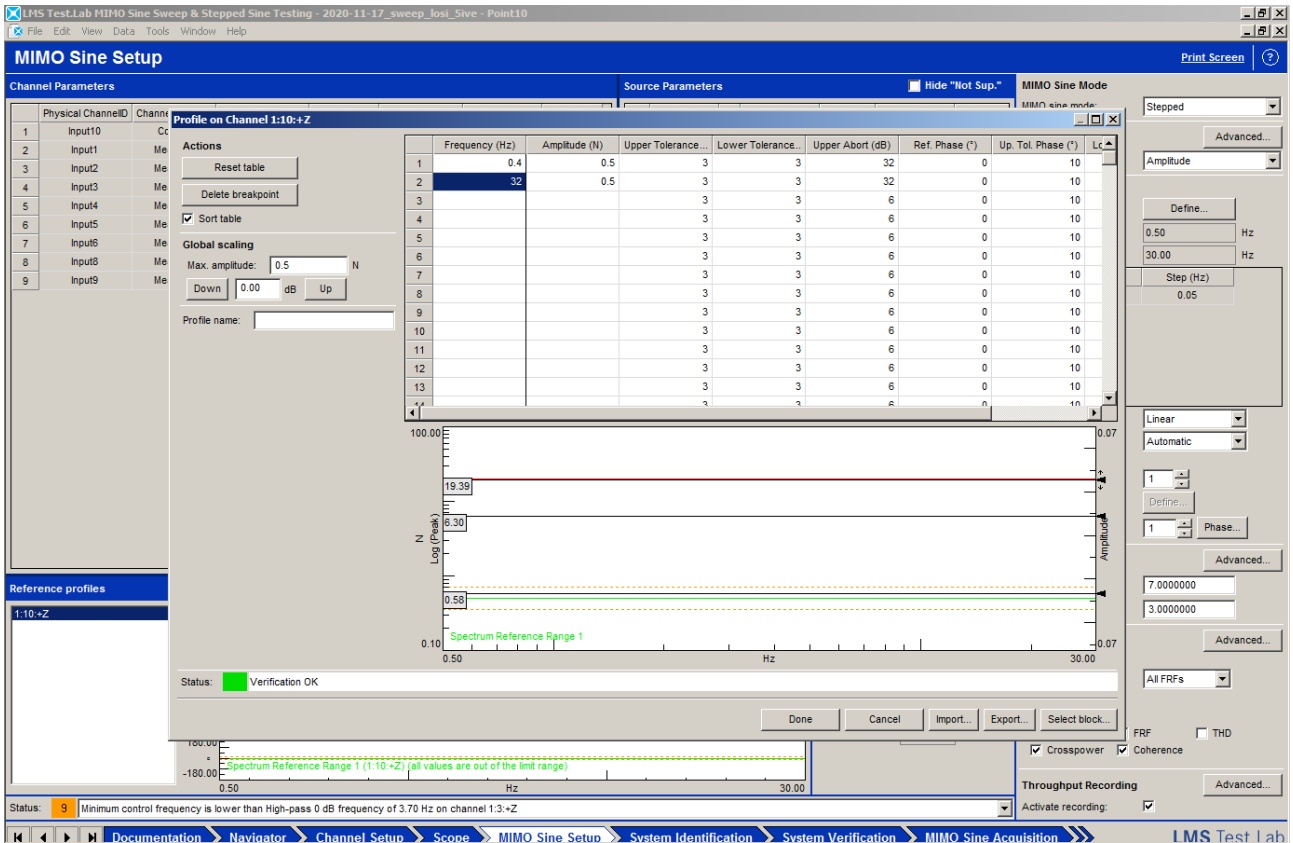


Figure 5.3.2.2 – MIMO Sine Setup window, Editing Reference Profile- Test 2.

The next step is setting the System Identification and acquiring.

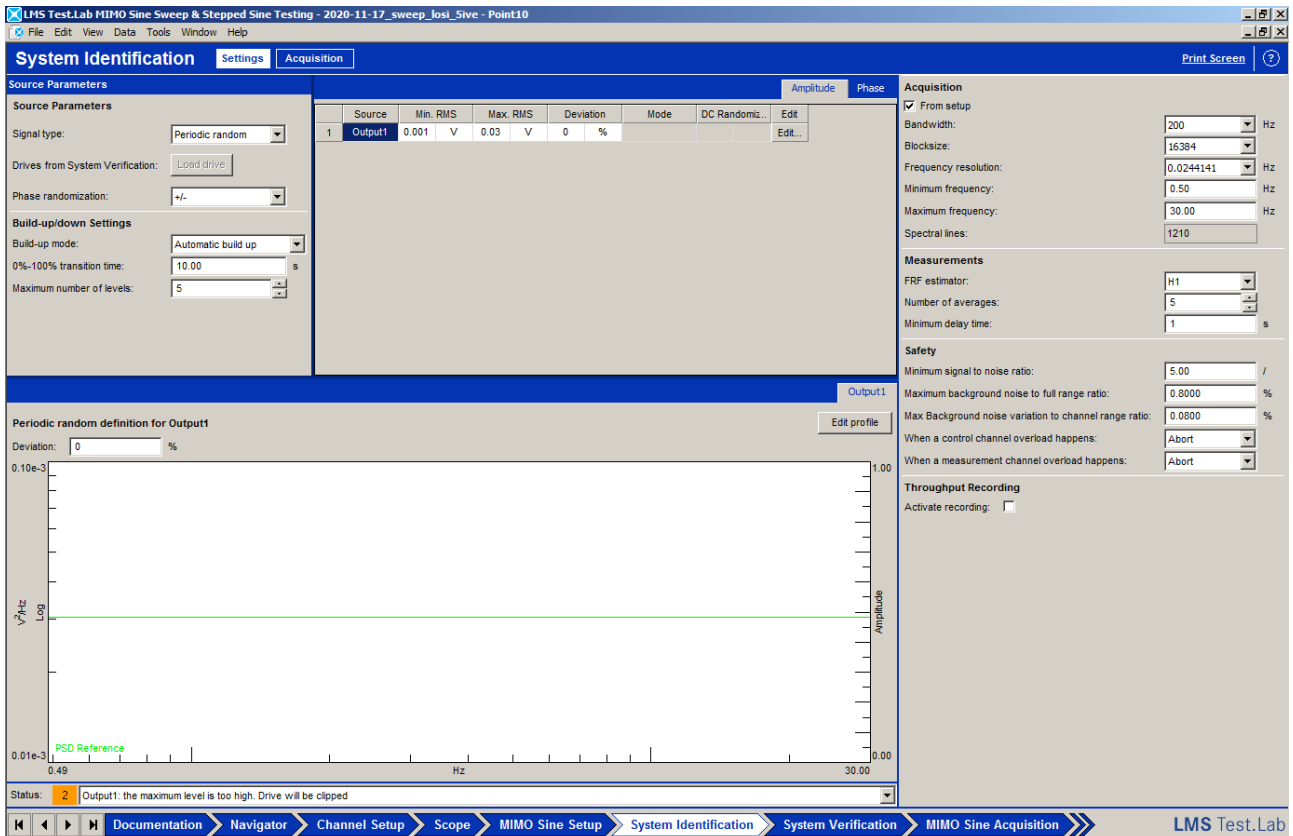


Figure 5.3.2.3 – System Identification Setting window- Test 2.

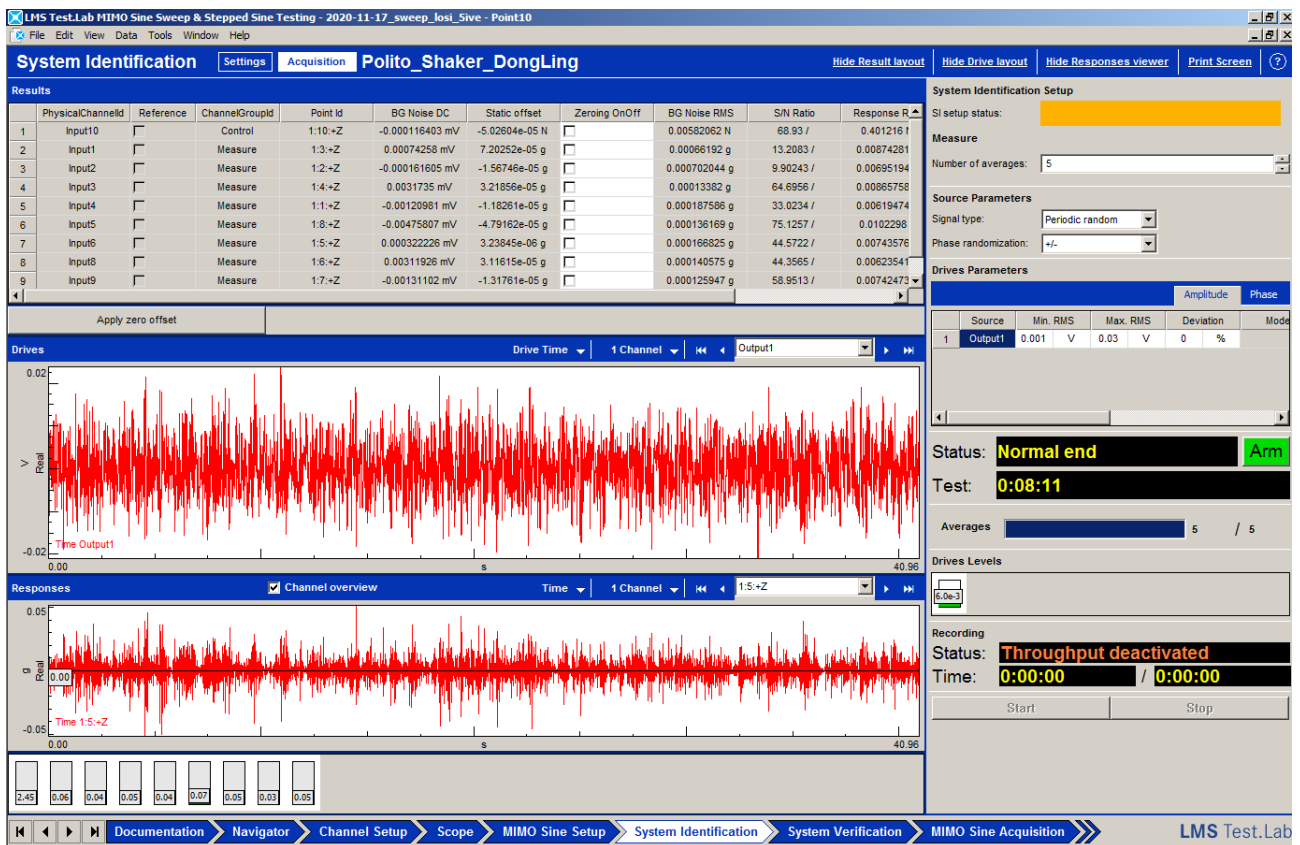


Figure 5.3.2.4 – System Identification Acquisition window- Test 2.

Then in System Verification, we can load and calculate the last system identification acquisition and clip the driver to the maximum voltage indicated.

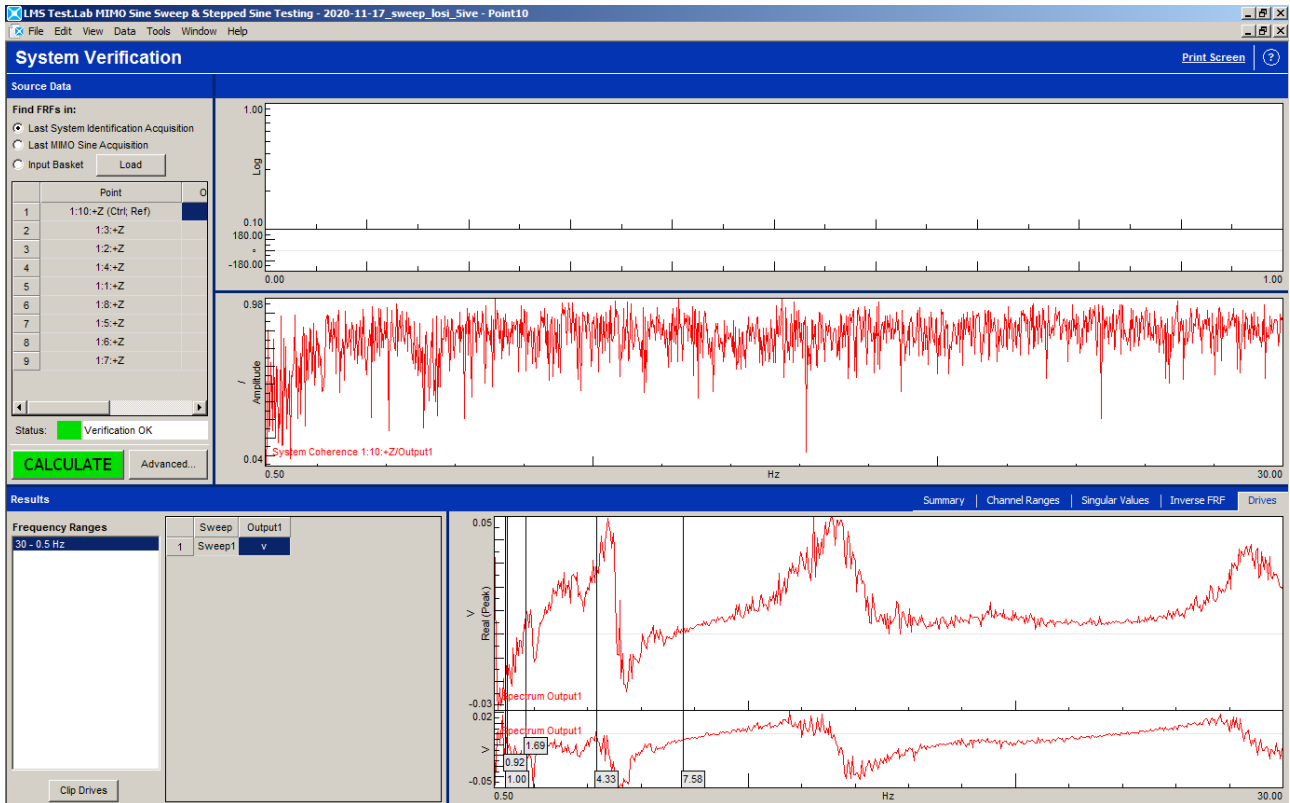


Figure 5.3.2.5 – System Verification window- Test 2.

At this point it is possible to start the acquisition following this path:

MIMO Sine Acquisition >> Arm >> Start.

Sometimes the acquisition is interrupted caused by an overload of some accelerometer, in this case it is sufficient to resume the acquisition by a slightly higher frequency value and the software correct the voltage input of the amplifier with a new iteration.

This test acquisition lasted for around 9 hours.

Then we can process the data acquired in the PolyMAX section, following the same procedure of the previous test.

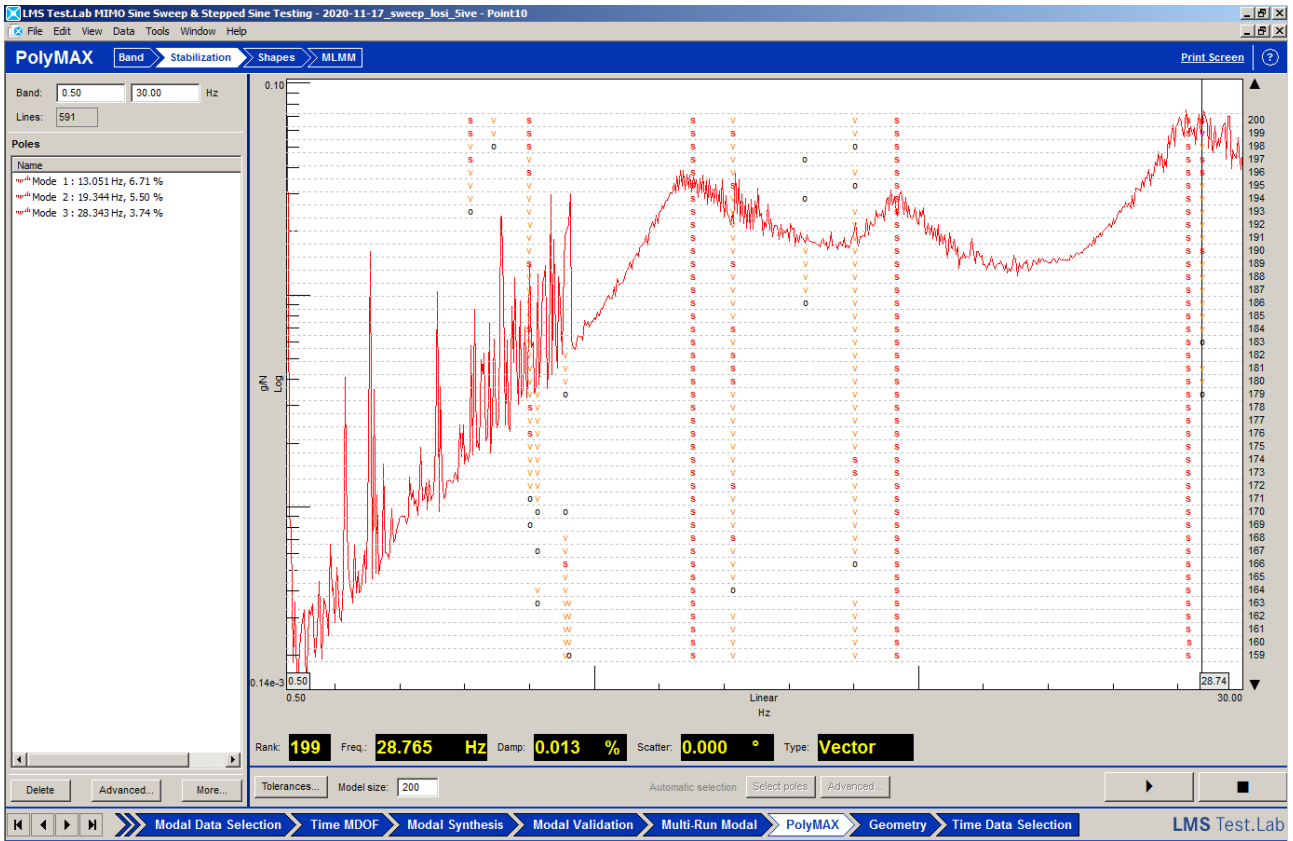


Figure 5.3.2.6 – PolyMAX Stabilitation window- Test 2.

Table 5.3.2.1 – Experimental Modal results – Stepped at point10 load cell.

Mode	$f_n$ [Hz]	$\xi$ [%]	Description
1	13.051	6.71	Chassis rebound
2	19.34	5.50	Chassis pitching
3	28.34	3.74	Chassis rolling

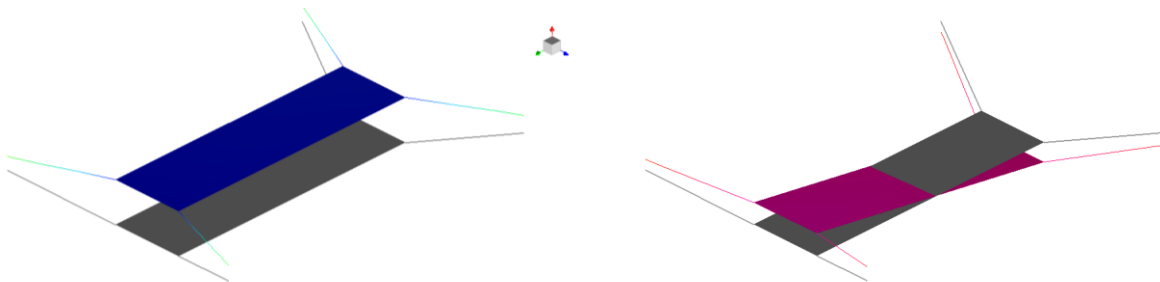


Figure 5.3.2.7 – Rebound (left) and pitch (right) mode shape Test 2.

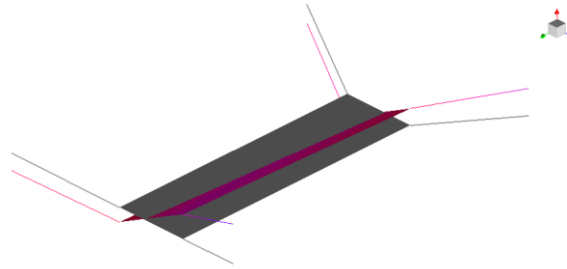


Figure 5.3.2.8 – Roll mode shape Test 2.

Also this test confirms that the first natural frequency is much higher than the one found numerically, under 10 Hz there is only a lot of noise. The modal shapes are really clear, anyway to be sure that the shapes at those frequencies are really the chassis rebound, pitch and roll we can perform another test where the accelerometers are placed in different points.

### 5.3.3 Test 3: Point 10 + new accelerometers setup

In this paragraph the third test is described. In this case the load cell is placed at the same point of the previous test, so the system is excited in the same point 10, while the accelerometers are moved to new positions. These new points are shown in magenta colour in the Figure 5.3.2.1 and in the Figure 5.3.2.2 and the coordinates are reported in the following table. They are added in the Geometry section.

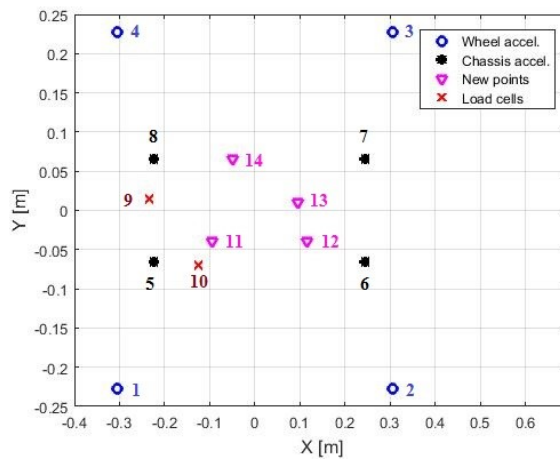


Figure 5.3.3.1 – Accelerometers and load cell setup.

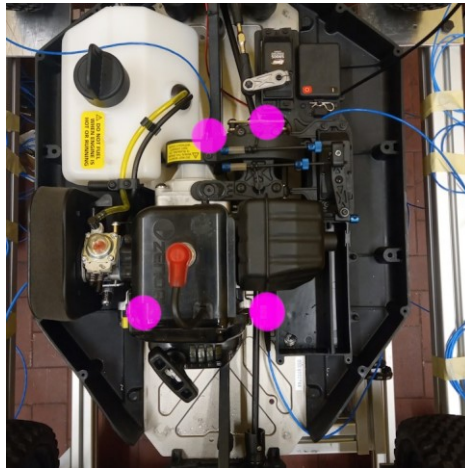


Figure 5.3.3.2– New accelerometers location.

Table 5.3.3.1 – New location of accelerometers.

Point	Location	X [m]	Y [m]	Z[m]	
11	Chassis	Rear Right	-0.095	-0.04	-0.05
12		Front Right	0.115	-0.04	-0.05
13		Front Left	0.095	0.01	-0.05
14		Rear Left	-0.05	0.066	-0.05

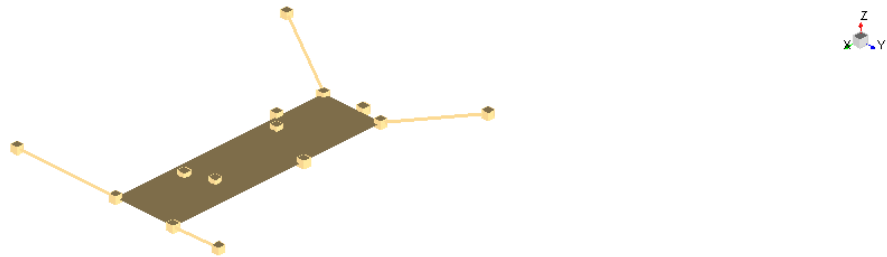


Figure 5.3.3.3– New Geometry – Test 3.

The Channel Setup section is updated switching the points 5, 6, 7, 8 with the points 11, 12, 13, 14. In System Verification section the previous acquisition is loaded so that the new acquisition should be faster, the parameters in MIMO Sine Setup are the same of the Test 2. So the MIMO Sine Acquisition is armed and the run. This acquisition lasted for around 8 hours. In Navigator section the previous acquisition (load cell at Point 10 and accelerometers in Point 5, 6, 7, 8) and the last acquisition (load cell at Point 10 and accelerometers in Point 11, 12, 13, 14) are added to the basket, so that in PolyMAX we can load both the acquisition and sum them to have a more complete view of the result, from the Stabilization diagram we can chose the frequencies corresponding to the relevant peaks.

Table 5.3.3.1 – Experimental Modal results – Test 3.

Mode	$f_n$ [Hz]	$\xi$ [%]	Description
1	12.98	6.51	Chassis rebound
2	19.30	4.88	Chassis pitching
3	28.24	3.54	Chassis rolling

This test is coherent with the Test 1 and the Test 2, and here the modal shapes are even more clear. The modal shapes are shown in the following pictures.

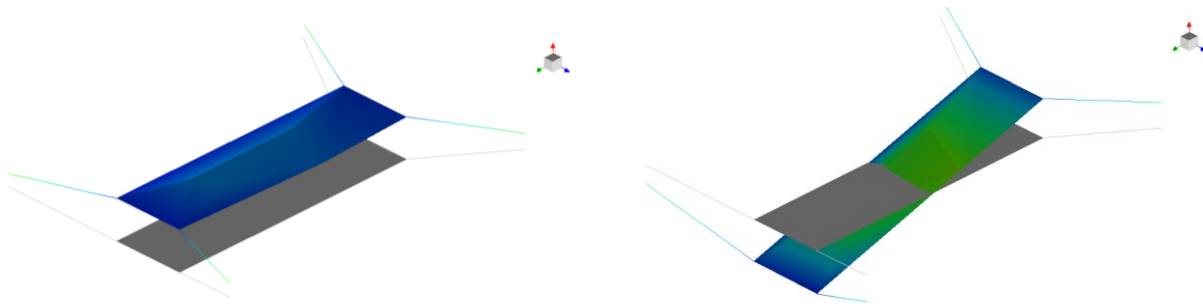


Figure 5.3.3.4 – Modal Shapes – rebound and pitch - Test 3.

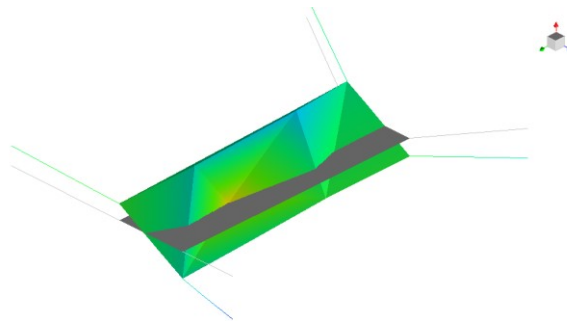


Figure 5.3.3.5 – Modal Shapes – roll - Test 3.

The FRF for one accelerometer and its synthesis is shown in the following picture.

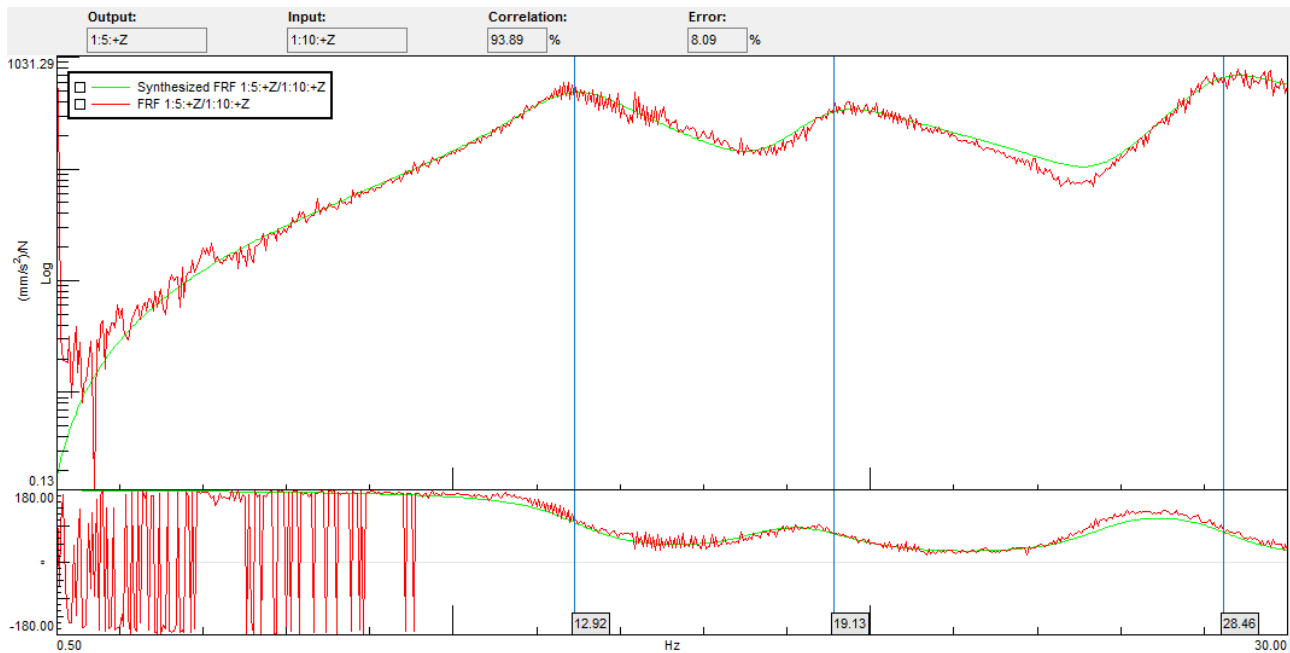


Figure 5.3.3.6 – Modal Synthesis Test 3.

Summing up, the natural frequencies got in these different tests are much higher than the natural frequencies got numerically. As demonstrate in paragraph 5.3.1, the numerical model is correct for

the stiffness parameters and the masses used, in fact the results are very close to the simply 4 dofs model. Then we focused the acquisition on a lower band frequency and excited the structure in a different point and read the response in 12 different accelerometers positions, but the results are coherent with the first test. So, we have still to investigate on the reason why there is so much discrepancy between the numerical and the experimental result.

Basically, the natural frequency depends from the stiffness and from the mass, for the mass values there are not doubts, only the inertia moments could be different from the used values but this has not a big weight on the calculation, so it is like the stiffness of the suspension system is actually much higher in the real case with respect to the values used in the model.

For these reason we want to banish the suspicion that the spring has a linear behaviour in compression, in the paragraph 2.4 the stiffness values of the spring has been measured in tension because it was easier and it was assumed the linear behaviour of the spring, now we can measure the stiffness of the spring in compression to eliminate every doubt. The verification is done for the Gold springs, using the setup shown in the following figures, the masses and the procedure used are the same used for the measurement of the paragraph 2.4 and one more mass (the glass visible in Figure 5.3.3.7, left side) that weights 5.036 kg.

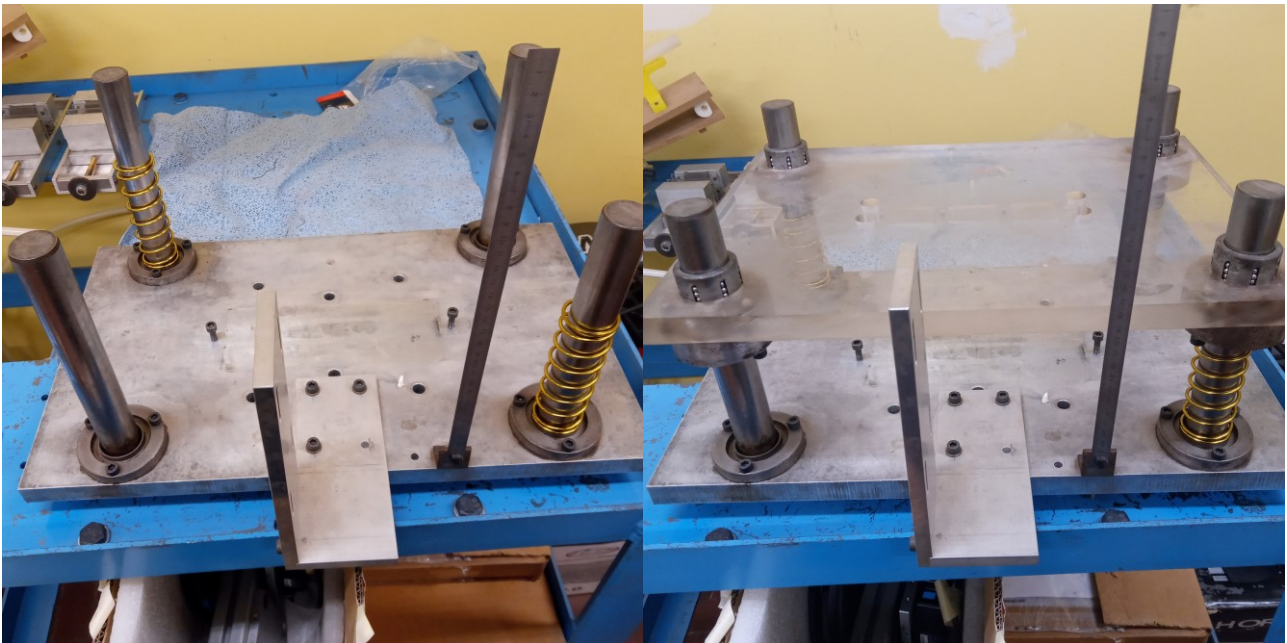


Figure 5.3.3.7 – Setup to compress the spring.



Figure 5.3.3.8 – Setup to compress the spring – measurement detail.

Then, the data are reported in a file Matlab and using the *polyfit* function we can get the characteristic of the spring, taking into account that the measure is done with two springs in parallel and so it has to be split. The characteristic in compression is compared to the one in tension on the same graph, it is shown in Figure 5.3.3.9, as it is possible to see the compression line is the natural continuation of the tension line (there is a linking part because in compression the first mass used is not zero but 5.036 kg) so we can assert that the spring have a linear behaviour.

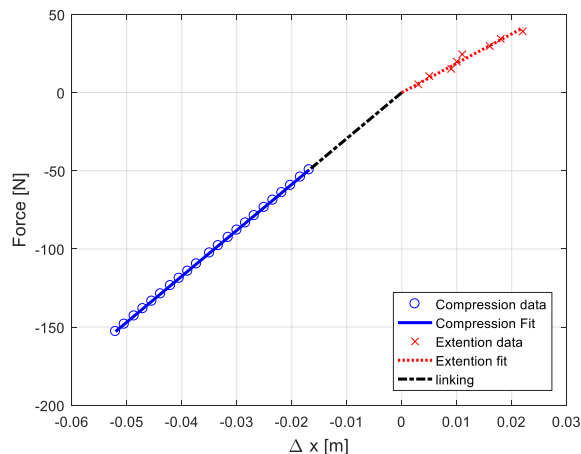


Figure 5.3.3.9 – Characteristic of the Gold spring – compression vs extension.

So, the cause of this big stiffness of the real suspensions is to be sought elsewhere, the stiffnesses of the springs are rights and the stiffness of the tyres do not influence so much the first 3 modes but only the unsprung mass modes.

The last hypothesis is that this discrepancy is due to the setup of the measurements.

#### 5.3.4 Test 4: Point 10 + shaker fixed

In the previous tests, the vehicle is excited with a force equal to 0.5 N, in this way its movement is not visible to unaided eye and so we operate in the small deformation field and the non-linearity can be neglected. The last hypothesis to explain why the real suspension stiffness results much higher than the known values is that exciting by a force of 0.5 N the frictions in the joints are not overcome and so the suspension system acts as a rigid body, the dampers do not compress and expand and so the springs do not act. So, we have to excite the vehicle with such a force that the springs expand and compress and all the movements of the suspension joints are visible to the naked eye. The setup used up to now cannot be used for this purpose because the floating shaker would move a lot, its inertia would be damage the instrumentation and moreover it could happen that the shaker moves more than the vehicle. For this reasons the setup is slightly changed: the shaker is released from its support and is fixed with a threaded screw to a very heavy metal plate, in this way the overall mass of the shaker will be very high and its very low natural frequencies will not affect the measurements.

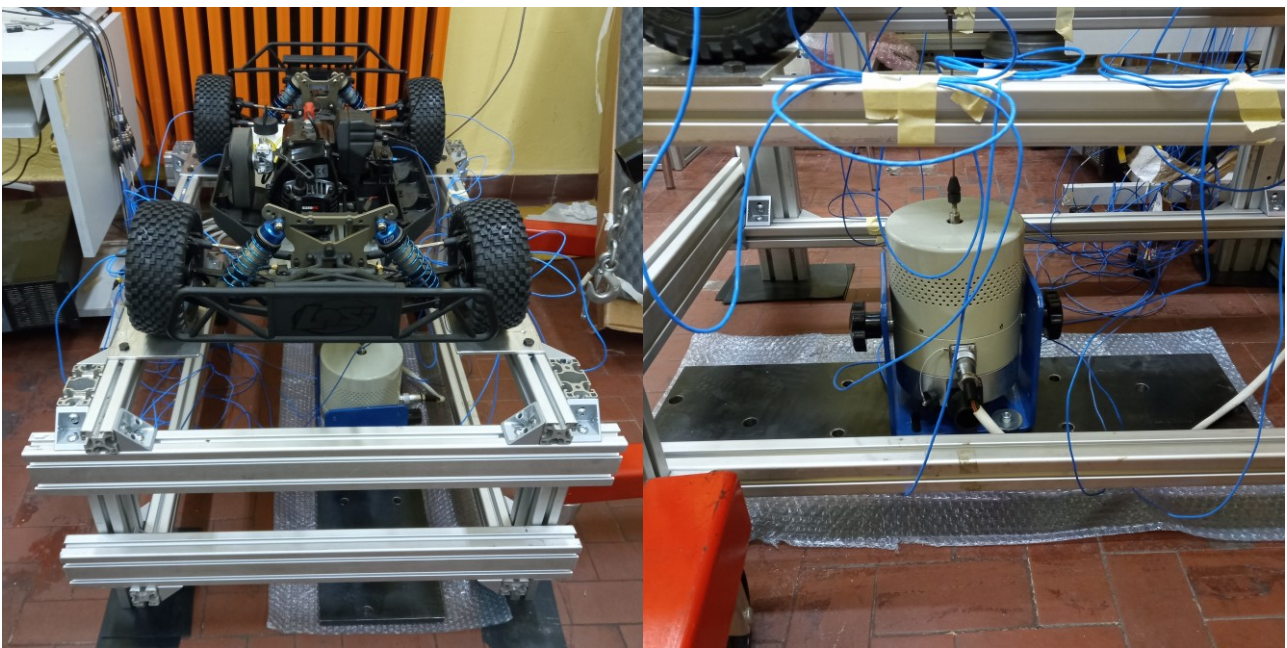


Figure 5.3.4.1 – Shaker fixed.

This test is conducted in the range 1.00 – 10 Hz so that we should see only the chassis modes. The amplitude of the exciting force, in this case is 20 N despite to the 0.5 N of the previous tests. Using the values for the various parameters shown in the following pictures, the vehicle visually moves down and up by approximately +1 and -1 cm, the suspension systems do not act anymore like rigid bodies, the low arms and the other links rotate and the dampers compress and expand; the movement of the rear suspension system is more evident than the front one, this can be explained because the exciting point is nearer to the rear than to the front part and moreover the front suspensions has the springs with the stiffness higher and there is also the steer.

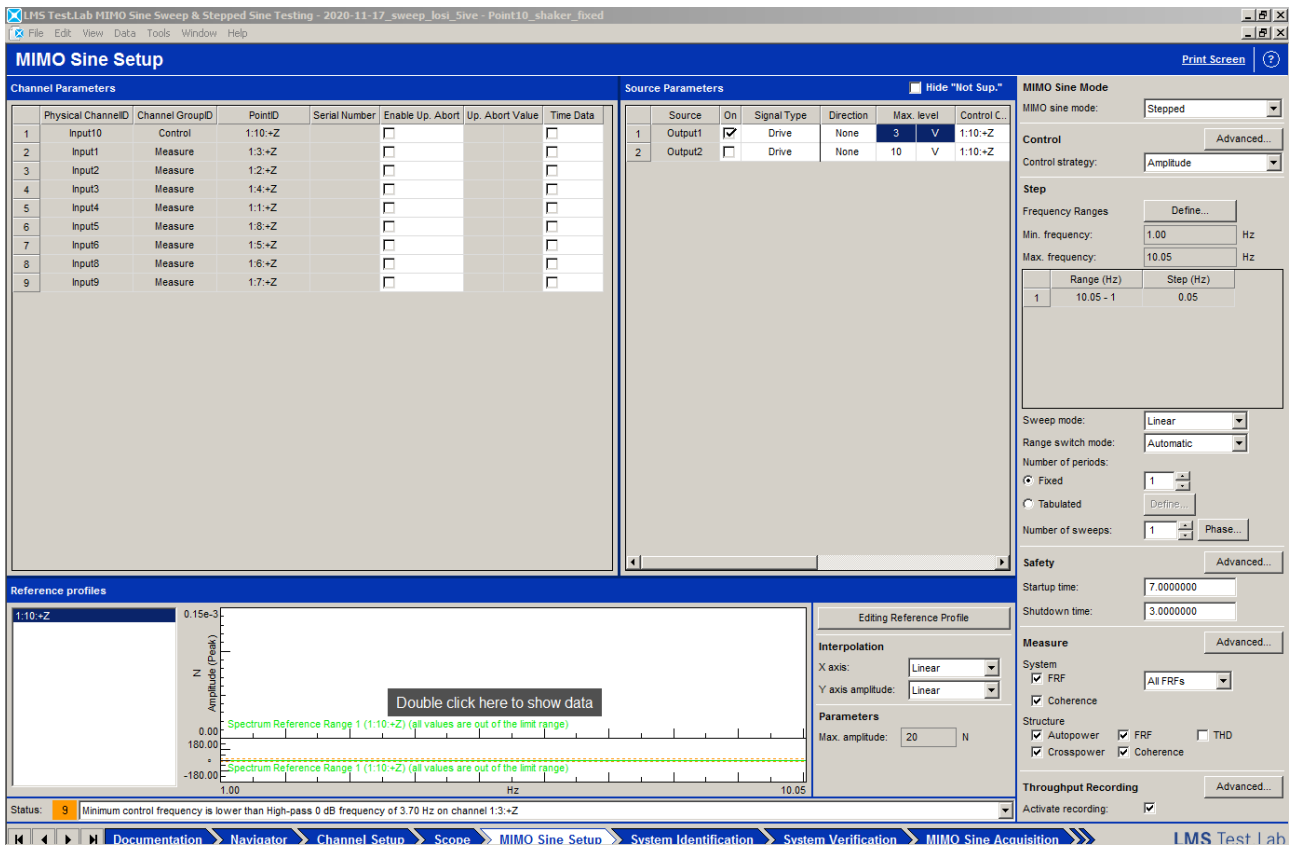


Figure 5.3.4.2 – MIMO Sine Setup window – Test 4.

A new system identification is run, the setup parameters are shown in the following picture.

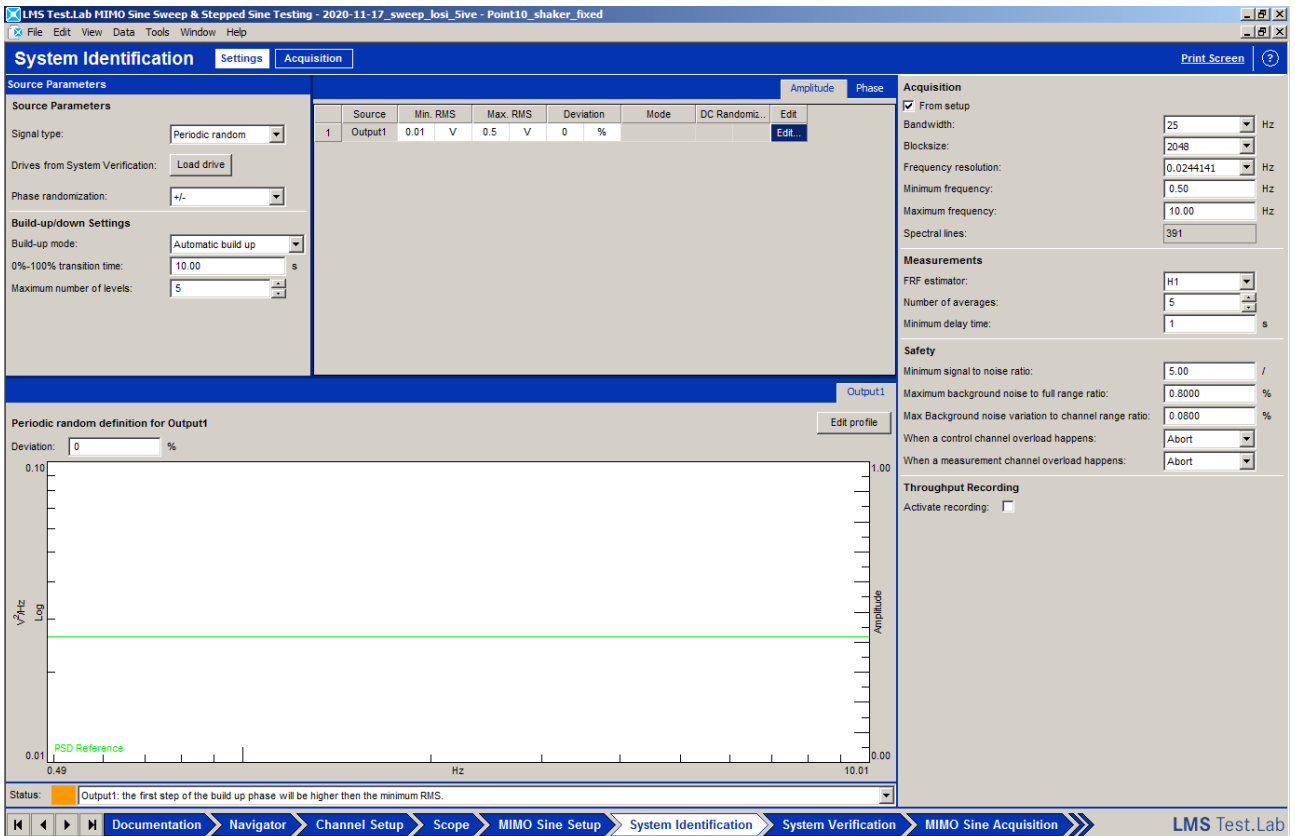


Figure 5.3.4.3 – System identification setting window – Test 4.

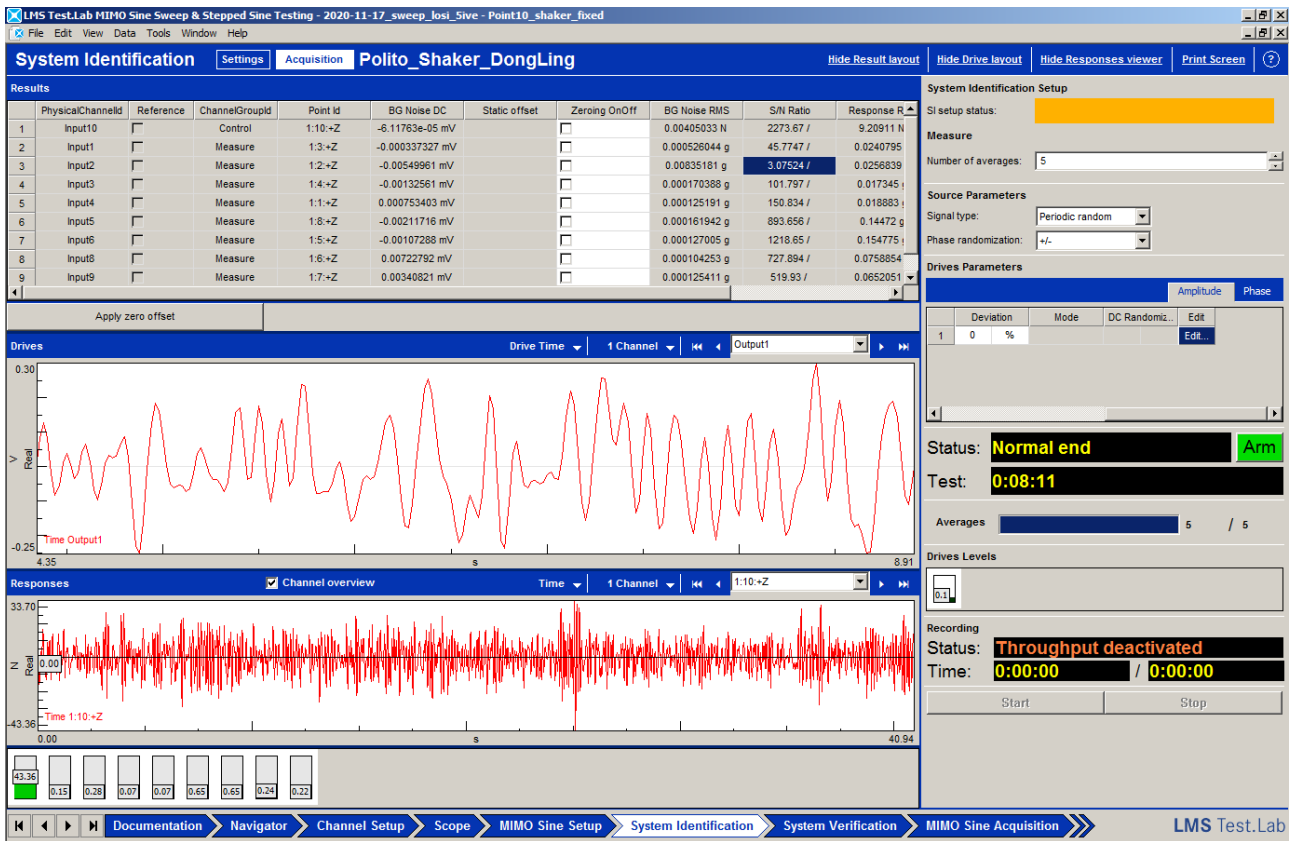


Figure 5.3.4.4 – System identification acquisition window – Test 4.

In System Verification section the last identification can be loaded and then in MIMO Sine Acquisition section the acquisition can start. The test number 4 consists in two tests:

- 1. Shaker fixed + Load cell at point 10 + accelerometers at points 5, 6, 7, 8;
- 2. Shaker fixed + Load cell at point 10 + accelerometers at points 11, 12, 13, 14.

In the following picture is shown the MIMO Sine Acquisition for the second test. It is immediately evident how the acquisition time is significantly shorter than the previous tests, in fact the two tests 4 each lasted about half an hour compared to the 8 or 13 hours of the tests in which the shaker fluctuated. For the previous tests the acquisition times were so long because the drivers to correct the shaker tension (to keep the force constant) were calculated with difficulty as the friction in the joints caused the stick and slip phenomenon, so now by overcoming the frictions the drivers are calculated more easily and there is no need for iterations, the linearity of the springs also helps this calculation.

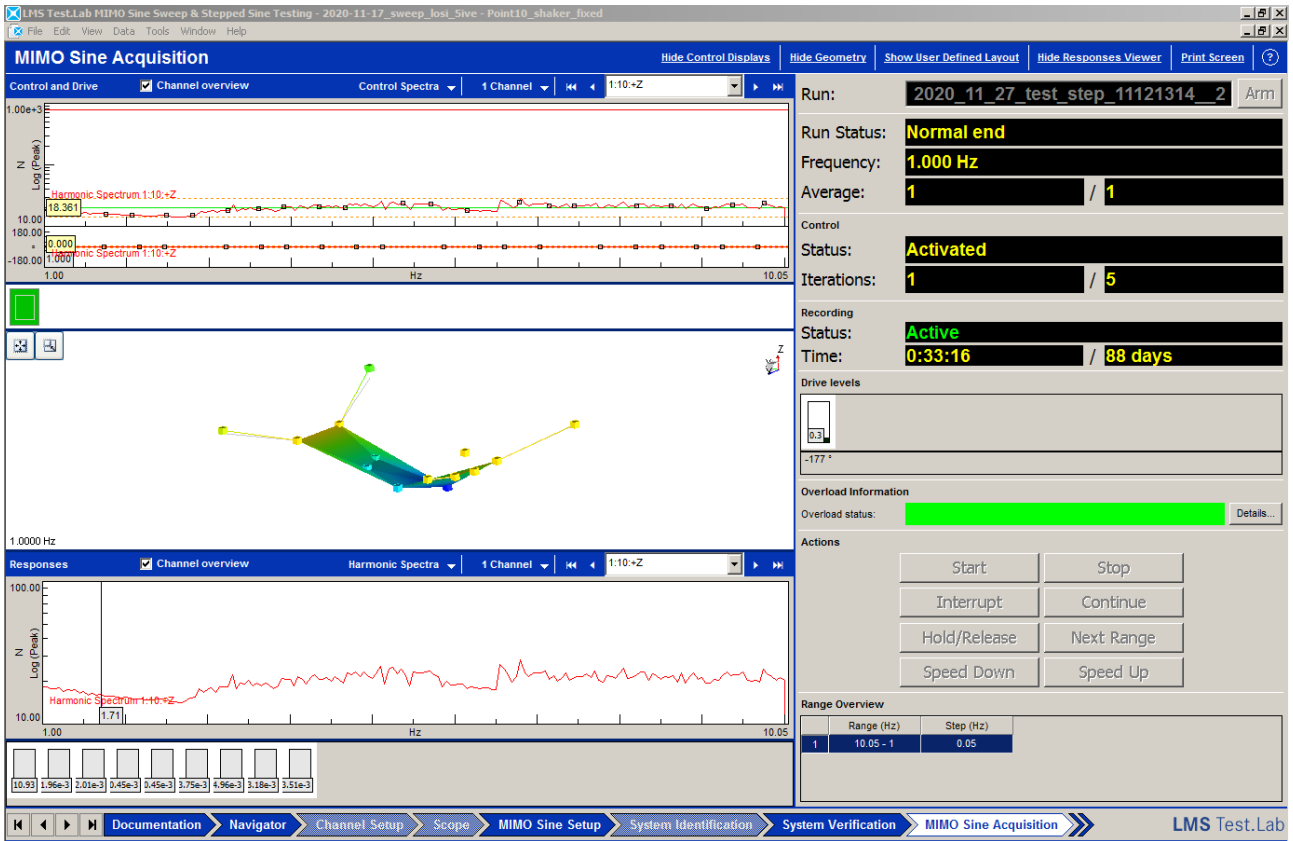


Figure 5.3.4.5 – MIMO Sine Acquisition window – Test 4.

The two tests are added to the basket in Navigator, so in PolyMAX they can both loaded and summed, in this way we see the response in 8 accelerometers points. The frequencies are selected into Stabilization diagram section, and then the modal shapes are shown.

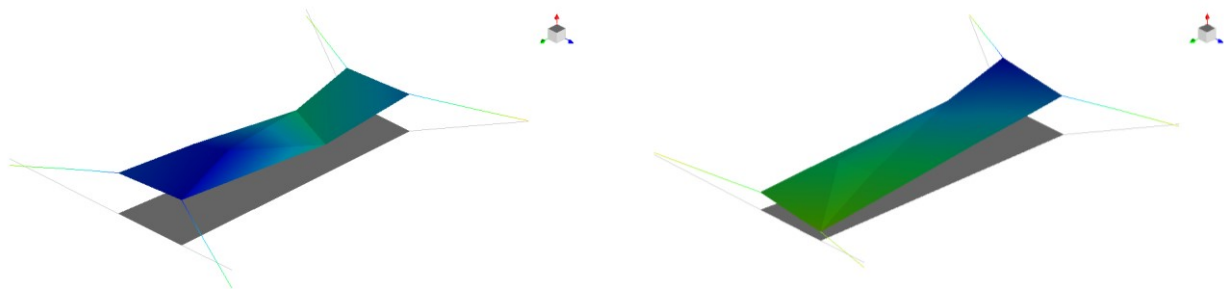


Figure 5.3.4.6 – Rebound and pitch modal shape– Test 4.

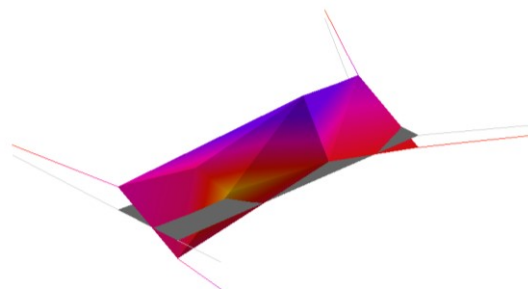


Figure 5.3.4.7 – Roll modal shape– Test 4

Table 5.3.4.1 – Experimental Modal results – Test 4.

Mode	$f_n$ [Hz]	$\xi$ [%]	Description
1	1.617	0.58	Chassis rebound
2	2.516	43.84	Chassis pitching+rebound
3	3.809	3.43	Chassis rolling

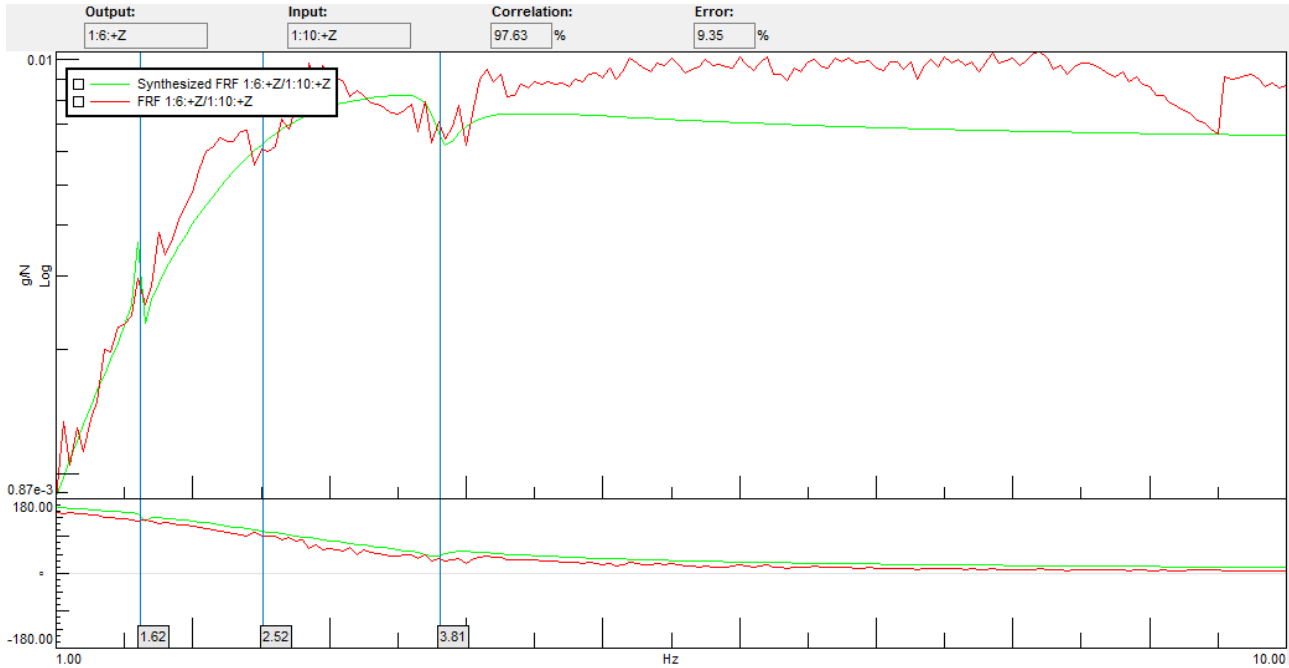


Figure 5.3.4.5 – Modal Synthesis – Test 4.

As it is possible to notice from the modal shapes and the modal synthesis the results are not as much clear as the previous tests, probably because at low frequencies there is also some noise, or maybe they would be clearer exciting the system in a different point, anyway now the frequencies are close to the numerical one, and they are reported into the Table 5.3.4.2.

Table 5.3.4.2 – Experimental vs Numerical – Test 4.

Mode	$f_n$ exp [Hz]	$f_n$ num [Hz]
1	1.617	1.580
2	2.516	2.083
3	3.809	3.910

## Conclusions

The illustrated thesis work can be concluded by summarizing the objectives, the steps followed to achieve them and the results obtained. The main goal was to create a numerical model of a radio-controlled vehicle in 1: 5 scale that would allow a series of dynamic simulations to be performed with different configurations, in particular we wanted to study the dynamics varying the springs of the suspension system. For this purpose, the first necessary step was to study the springs that are available to validate the nominal stiffnesses. The springs available are 4 pairs for the front suspension system (Gold, Blue, Red, Orange) and 3 pairs for the rear (Blue, Red, Orange). The stiffnesses were first calculated theoretically, then a numerical model was created using the Matlab LUPOS code with which the numerical stiffnesses were calculated, an experimental setup was built in the laboratory thanks to which the experimental stiffnesses were measured, finally the values of nominal, theoretical, numerical and experimental stiffnesses are compared, the relative errors were sufficiently low and so the numerical stiffnesses were validated. At this point I moved on to the realization of the numerical model of the vehicle through the LUPOS code in Matlab. The model created is a simplification of reality, it is in fact a model with lumped parameters, whose sprung mass is concentrated in the centre of gravity and the unsprung masses in the wheel centres, all the various parts have been modelled with rigid elements, except for the shock absorbers and anti-roll bars. From the execution of the numerical model it is possible to choose different vehicle configurations, for example inserting or not the body and the anti-roll bars, choosing which springs to mount and which dampers. Since only stiffness values and not damping are available, a Real Modal Analysis was performed, anyway the model was prepared to insert the damping values so it will be possible in future developments to enter these values and perform a Complex Modal Analysis . From the Modal Analysis it appears that the first 3 modes of vibration are related to the body (shaking, pitching and rolling) and occur at frequencies very close to those of a normal-scale vehicle, the analyses were performed for different vehicle configurations. Parametric analysis were subsequently performed, as the springs varied, and it resulted that the natural frequencies undergo a slight increase as the stiffness of the springs increases, but there are no significant changes. At this point, a setup was built in the laboratory to perform experimentally the Modal Analysis, the acquisition system consists of: 8 accelerometers, 1 load cell, 1 shaker, Siemens SCADAS Acquisition, Amplifier, PC with LMS.TestLab2017 software. Several tests have been carried out for the nominal vehicle configuration: exciting the system in 2 different points, exciting the system in the same point but with accelerometers in different points, varying setup for the shaker. The latest tests have shown that the experimental results are coherent with the numerical ones, however, further investigations must be made on the experimental side to obtain clearer results.

The results achieved can be a valid help for future studies, in fact we now have a numerical model that can be improved with the insertion of damping values, and we have an experimental setup with which it will be possible to perform more tests by varying configuration.

## Reference

- [1] Shaopu Yang, Yongjie Lu, Shaohua Li, *An overview on vehicle dynamics*, Springer-Verlag Berlin Heidelberg, 2013.
- [2] Garrott W.R., Heydinger G.J., Bixel R.A., *Measured Vehicle Inertial Parameters-NHTSA's Data Through November 1998*.
- [3] Previati G., Gobbi M., Mastinu G., *The Dynamics of Vehicles on Roads and Tracks-Spiryagin et al. (Eds), (Mass properties of cars-an investigation)*, pp.57-62.
- [4] Monroe springs catalogue, 2017, <https://web.tecalliance.net/tae/en/home>.
- [5] Harris William, *How Car Suspensions Work*, <https://auto.howstuffworks.com/car-suspension1.htm>.
- [6] Hitesh K. Tare, C.S. Dharankar, *Determination of damping coefficient of automotive hydraulic damper using sinusoidal testing*, 2016
- [7] Do Minh Cuong, Dinh vuong Hung, Sihong Zhu, Nguyen Thi Ngoc, *Study on the vertical stiffness and damping coefficient of tractor tire using semi-empirical model*, Journal of Science, Hue University, Vol.83, No. 5, 2013
- [8] Vella A., Report-Losi5ive\_activity\_2020-03-19, Politecnico di Torino, Torino, 19-03-2020.
- [9] Bonisoli E., *Lupos Tutorial*, Politecnico di Torino, Torino, 16-03-2020, pp. 291.
- [10] Bonisoli E., *Lupos Tutorial*, Politecnico di Torino, Torino, 16-03-2020, pp. 94-103.
- [11] Bonisoli E., *Lupos Tutorial*, Politecnico di Torino, Torino, 16-03-2020, pp. 180-190.
- [12] Bonisoli E., *Lupos Tutorial*, Politecnico di Torino, Torino, 16-03-2020, pp. 64-66.
- [13] De Giuseppe G., *Experimental setup for RC car suspensions*, Politecnico di Torino.